



HAL
open science

**Quantitative metabolism of natural and antiviral
nucleosides and nucleotides in human cells by
LC-MS/MS**

Emilie Fromentin

► **To cite this version:**

Emilie Fromentin. Quantitative metabolism of natural and antiviral nucleosides and nucleotides in human cells by LC-MS/MS. Pharmacology. AgroParisTech, 2010. English. NNT : 2010AGPT0040 . pastel-00605911

HAL Id: pastel-00605911

<https://pastel.hal.science/pastel-00605911>

Submitted on 4 Jul 2011

HAL is a multi-disciplinary open access archive for the deposit and dissemination of scientific research documents, whether they are published or not. The documents may come from teaching and research institutions in France or abroad, or from public or private research centers.

L'archive ouverte pluridisciplinaire **HAL**, est destinée au dépôt et à la diffusion de documents scientifiques de niveau recherche, publiés ou non, émanant des établissements d'enseignement et de recherche français ou étrangers, des laboratoires publics ou privés.



ParisTech

INSTITUT DES SCIENCES ET TECHNOLOGIES
PARIS INSTITUTE OF TECHNOLOGY



AgroParisTech

INSTITUT DES SCIENCES ET INDUSTRIES DU VIVANT ET DE L'ENVIRONNEMENT
PARIS INSTITUTE OF TECHNOLOGY FOR LIFE, FOOD AND ENVIRONMENTAL SCIENCES

Ecole Doctorale
ABIES

Agriculture
Agriculture
Alimentation
Food
Biologie
Biology
Environnement
Environment
Santé
Health

Doctorat ParisTech

THÈSE

pour obtenir le grade de docteur délivré par

**L'Institut des Sciences et Industries
du Vivant et de l'Environnement
(AgroParisTech)**

Spécialité : Chimie analytique et Pharmacologie

présentée et soutenue publiquement par

Emilie FROMENTIN

le 1^{er} Juin 2010

**Quantitative metabolism of natural and antiviral nucleosides and
nucleotides in human cells by LC-MS/MS**

Directeur de thèse : **Pr. Raymond F. SCHINAZI**
Enseignant responsable : **Pr. Douglas N. RUTLEDGE**

Jury : Président du jury : **Dr. Gilles GOSSELIN**

M. Luigi AGROFOGLIO, Pr., ICOA UMR-CNRS, Université d'Orléans
Mme Arlette BAILLET, Pr., Faculté de Pharmacie, Université Paris-Sud11
M. Thierry BELTRAN, Dr., SANOFI-AVENTIS
M. Gilles GOSSELIN, Dr., CNRS, Laboratoires IDENIX Sarl.

Rapporteur
Rapporteur
Examineur
Examineur

AgroParisTech
Laboratoire de Chimie Analytique
6, rue Claude Bernard, 75005 Paris, France



**Quantitative metabolism of natural and
antiviral nucleosides and nucleotides in
human cells by LC-MS/MS**

**This work was performed at the Emory University
School of Medicine and Veterans Affairs Medical Center
and was supported by Emory University, CFAR and NIH
funding.**



Acknowledgments

I would like to thank Professor Rutledge and Mme Launay for accepting my application to the ABIES doctoral school and for supporting this collaboration between AgroParisTech and Emory University.

I would like to express my deepest gratitude to the thesis committee members who kindly accepted our invitation to evaluate the research presented in this dissertation and the oral presentation.

Dr Raymond. F. Schinazi has trusted my work and me since October 2006, when he offered me a position in his laboratory. Thanks to his scientific advices, help and patience I have been able to learn day after day the basics not only in nucleoside analytical chemistry, but also in virology, toxicology and cell biology. I would like to thank him for encouraging me to explore new areas, such as pharmacology and pharmacokinetics. He supported my ideas and contributed tremendously to my scientific growth. This thesis represents a great team effort, which could not have been born without Dr Schinazi's supervision. Importantly, I would like to thank Dr Schinazi for allowing me to attend numerous International and local conferences since I joined the laboratory in order to broaden my horizons.

Working in the pharmacology team has been a tremendous experience. I would like to thank Aleksandr Obikhod for teaching me chromatography, mass spectrometry, cell culture and for his help on instruments maintenance. We have worked together on several projects and established a functional teamwork. Selwyn Hurwitz taught me pharmacokinetics and encouraged me to be critical with the interpretation of my experiments. His advices were very important for my scientific training. Christina Gavegnano has taught me cell culture as well as helped me with the understanding of the basic virology and immunology of HIV infection. She trusted me with the analysis of her precious macrophages, which represented weeks of work. I also would like to thank her for her contagious enthusiasm, which cheered me up more than once. I would also like to thank Ghazia Asif and especially Judy Matthew for their help. I am especially grateful for Claire de la Calle who has been a great student during the summer 2009.

Importantly, I am thankful to the virology team, Mervi Detori, Kim Rapp, Sadie Solomon and Cathy Montero for providing me with cells when I needed and for their precious teamwork. I would also like to thank all the biologists and chemists at RFS Pharma, LLC for their encouragement, support and friendship.

Carol Jeffcoat has been a great support during these four years. She created an enjoyable atmosphere in the laboratory, for everyone to feel comfortable.

I could not thank enough Brenda Hernandez-Santiago for making me feel so welcome in her house for my first year in Atlanta. She not only trusted me scientifically, with work that we published together, but she also personally made my arrival to this new country extremely comfortable and enjoyable. The year that we shared together was a privileged experience to me and I will never forget it.

I would like to thank Dr Schinazi, Judy Mathew, Selwyn Hurwitz and Franck Amblard for their careful reading of this dissertation and for making the suggestions and corrections that were necessary to clarify and improve this manuscript.

I would like to thank Barbara Stoll, the chair of the pediatrics department, Dr Schinazi and Emory University for giving the financial support that was necessary to accomplish this work.

I met during those 4 years in Atlanta extraordinary people who have changed the way I see the world. Merci Maïra pour ton soutien quotidien et ta joie de vivre. I specially would like to thank Ivana, Meta, Adriana, Niko, Fedá, Helder, Omar, Jessica, Thandi, Leda, Matthew, Tami... Je n'oublierai pas la French team Ethel, Franck, Véro, Vincent, Ugo pour les fameux diners à la française et randonnées en Géorgie. Votre amitié m'a rendue plus forte et m'a accompagné tout au long de cette merveilleuse expérience. Gracias, obrigado, thank you, merci.

Cette longue histoire ne serait pas arrivée sans l'aide de Thierry Beltran qui a non seulement été à l'origine de cette opportunité d'emploi aux Etats-Unis mais aussi de cette thèse. Il avait déjà compris durant mon stage de fin d'études d'ingénieur que j'aurai la volonté et l'enthousiasme nécessaire pour poursuivre une formation doctorale et m'a aidé à le réaliser.

Si cette décision de quitter mon pays pour aller travailler aux Etats-Unis fut riche, elle ne fut pas sans peine. Quitter ma famille pendant ces quatre années a représenté pour moi un sacrifice important. Mais le soutien qu'ils m'ont apporté dans cette décision initiale ainsi que dans la transformation de cette expérience en doctorat a été crucial. Même si mes choix vous ont parfois un peu dépassés, je vous suis reconnaissante à tous les trois, Angélique, papa, maman pour la confiance que vous m'avez accordée et tout l'amour que vous m'avez donné.

David, porque estuviste a mi lado todo el tiempo, haciendo mejores mis días. Porque me diste la confianza para progresar y porque tuviste la paciencia para enseñarme los intrincados caminos de la ciencia. Porque cambiaste mi vida a un mundo sin nubes, por esto es que quiero decirte gracias.

“Chronologiquement, aucune connaissance ne précède en nous l’expérience et c’est avec elle que toutes commencent.” (Emmanuel Kant)

To remember those who have fought.



“In June of 1987, a small group of strangers gathered in a San Francisco storefront to document the lives they feared history would neglect. Their goal was to create a memorial for those who had died of AIDS, and to thereby help people understand the devastating impact of the disease. This meeting of devoted friends and lovers served as the foundation of the NAMES Project AIDS Memorial Quilt. The Quilt was conceived in November of 1985 by long-time San Francisco gay rights activist Cleve Jones, who helped organize the annual candlelight march honoring Harvey Milk and Mayor George Moscone. At the end of the 1985 march, Jones and others stood on ladders taping placards bearing the names of friends and loved ones who had died of AIDS to the walls of the San Francisco Federal Building. The wall of names looked like a patchwork quilt. On October 11, 1987, The Quilt included 1,920 panels and was displayed for the first time on the National Mall in Washington, D.C. during the *National March on Washington for Lesbian and Gay Rights*. The Quilt returned to Washington, D.C. in October of 1988, when 8,288 panels were displayed on the Ellipse in front of the White House. The entire Quilt was again displayed on the National Mall in 1992 and 1996, when it contained approximately 37,440 individual panels. The Quilt was nominated for a Nobel Peace Prize in 1989, and is today the largest community art project in the world. The Quilt has been the subject of countless books, films, scholarly papers, articles, and theatrical, artistic and musical performances. In 2001 The NAMES Project Foundation headquarters and The AIDS Memorial Quilt moved from San Francisco to Atlanta, GA, and today displays continue being held across the country every day, new panels continue to be accepted and incorporated into The Quilt, and a new, solid financial foundation continues to be built beneath The Quilt, guaranteeing its ongoing work and securing its future.”

List of publications related to this work (2007-2010)

Manuscripts

In preparation

1. Study of 9- β -D-(1,3-dioxolan-4-yl)guanine phosphorylation alone and in combination with other nucleosides analogs in human peripheral blood mononuclear cells. Emilie Fromentin, Claire De La Calle, Mervi Detorio, Aleksandr Obikhod, Selwyn J. Hurwitz, Raymond F. Schinazi.
2. Cellular Pharmacology and Potency of HIV-1 Nucleoside Analogues in Primary Human Macrophages: Implications for HIV-1 Eradication. Christina Gavegnano, Emilie Fromentin, Leda Bassit, Mervi Detorio, and Raymond F. Schinazi.
3. *In vivo* and *in vitro* studies supporting the use of reduced dose regimens for d4T. Selwyn J. Hurwitz, Emilie Fromentin, Raymond F. Schinazi.
4. Biochemical Simulation of Human Immunodeficiency Virus Type 1 Reverse Transcription with Physiological Nucleotide Pools found in Macrophages and CD4⁺ T cells. Edward M. Kennedy, Christina Gavegnano, Laura Nguyen, Rebecca Slater, Amanda Lucas, Emilie Fromentin, Raymond F. Schinazi and Baek Kim.

Published

1. Simultaneous quantification of intracellular and antiretroviral nucleosides and nucleotides by liquid chromatography-tandem mass spectrometry. Emilie Fromentin, Christina Gavegnan, Aleksandr Obikhod, Raymond F. Schinazi. Anal Chem. 2010 Mar 1;82(5):1982-9.
2. Lack of pharmacokinetic interaction between amdoxovir and reduced and standard dose zidovudine in HIV-1 infected individuals. Selwyn J. Hurwitz, Ghazia Asif, Emilie Fromentin, Phillip M. Tharnish, Raymond F. Schinazi. Antimicrob Agents Chemother. 2010 Mar;54(3):1248-55.
3. Synthesis and evaluation of 3'-azido-2',3'-dideoxypurine nucleosides as inhibitors of human immunodeficiency virus. Hong-wang Zhang, Steven J. Coats, Lavanya Bondada, Franck Amblard, Mervi Detorio, Emilie Fromentin, Sarah Solomon, Aleksandr Obikhod, Tony Whitaker, Nicolas Sluis-Cremer, John W. Mellors, Raymond F. Schinazi. Bioorg Med Chem Lett. 2010 Jan 1;20(1):60-4.
4. Simultaneous quantification of 9-(β -D-1,3-dioxolan-4-yl)guanine, amdoxovir and zidovudine in human plasma by liquid chromatography-tandem mass spectrometric assay. Emilie Fromentin, Ghazia Asif, Aleksandr Obikhod, Selwyn J. Hurwitz, Raymond F. Schinazi. J Chromatogr B Analyt Technol Biomed Life Sci. 2009 Nov 1;877(29):3482-8.
5. Synthesis, antiviral activity, and stability of nucleoside analogs containing tricyclic bases. Franck Amblard, Emilie Fromentin, Mervi Detorio, Alexander Obikhod, Kimberly L. Rapp, Tamara R. McBrayer, Tony Whitaker, Steven J. Coats and Raymond F. Schinazi. Eur J Med Chem. 2009 Oct;44(10):3845-51.
6. Acyclovir is activated into a HIV-1 reverse transcriptase inhibitor in herpesvirus-infected human tissues. Andrea Lisco, Christophe Vanpouille, Egor P. Tchesnokov, Jean-Charles Grivel, Angélique Biancotto, Beda Brichacek, Julie Elliott, Emilie Fromentin, Robin Shattock, Peter Anton, Robert Gorelick, Jan Balzarini, Christopher McGuigan, Marco Derudas, Matthias Götte, Raymond F. Schinazi and Leonid Margolis. Cell Host Microbe. 2008 Sep 11;4(3):260-70.
7. Short communication cellular pharmacology of 9-(β -D-1,3-dioxolan-4-yl) guanine and its lack of drug interactions with zidovudine in primary human lymphocytes. Brenda I Hernandez-Santiago, Aleksandr Obikhod, Emilie Fromentin, Selwyn J Hurwitz, Raymond F Schinazi. Antivir Chem Chemother. 2007;18(6):343-6.

Conference Communications

- 1- Elevated rNTP incorporation by HIV-1 RT with dNTP/rNTP pools found in human macrophages. Edward Kennedy, Raymond Schinazi, Christina Gavegnano, Emilie Fromentin, Baek Kim. Palm Springs Symposium on HIV/AIDS, CA. March 11-13, 2010.
- 2- Synthesis of 2'-C-methyl purine modified nucleosides as a potential anti-HCV agents. H-W Zhang, SJ Coats, L Zhou, M Detorio, T Whitaker, T McBrayer, PM Tharnish, A Obikhod, E Fromentin, and RF Schinazi. HEP DART, Hawaii, Dec 6-10 2009. Global antiviral journal, volume 5 supplement 1, p92.
- 3- Novel purine dioxolane protides are potent inhibitors of hepatitis B virus. L Bassit, L Bondada, A Obikhod, E Fromentin, SJ Coats, and RF Schinazi. HEP DART, Hawaii, Dec 6-10, 2009. Global antiviral journal, volume 5 supplement 1, p91.
- 4- Anti-HIV-1 nucleoside analogue triphosphate levels are significantly lower in primary human macrophages than in lymphocytes. C Gavegnano, E Fromentin and RF Schinazi. 4th HIV-1 Persistence Workshop, St. Martin, French West Indies. Dec 8-11, 2009. Global antiviral journal, volume 5 supplement 2, p43.
- 5- HIV-1 nucleoside analogue triphosphate levels are significantly lower in primary human macrophages than in human lymphocytes. Christina Gavegnano, Emilie Fromentin and Raymond F. Schinazi. XVIII International Drug Resistance Workshop, Fort Meyers, FL. June 9-13, 2009. Global antiviral journal, volume 4, supplement 1, p77.
- 6- Metabolism of highly active and selective 3'-azido-2',3'-dideoxypurine nucleosides in primary human lymphocytes and MT-2 cells. Aleksandr Obikhod, Emilie Fromentin, Mervi Detorio, Steven J. Coats, Nicolas Sluis-Cremer, and John W. Mellors, and Raymond F. Schinazi. HIV DART, Rio Grande, Puerto Rico - Dec 9-12, 2008. Global antiviral journal, volume 4, supplement 1, p79.
- 7- Cellular pharmacology of HIV-1 nucleoside analogues in primary human macrophages compared to human lymphocytes. Christina Gavegnano, Emilie Fromentin and Raymond F. Schinazi. Georgia Life Sciences Summit, Atlanta, GA. Sept 24, 2008.
- 8- Synthesis and antiviral activity of tricyclic 3,9-dihydro-9-oxo-5H-imidazo[1,2-A]purine nucleosides: toward new nucleoside prodrugs. F Amblard, E Fromentin, A Obikhod, TR McBrayer, KL Rapp, M Detorio, T Whitaker, SJ Coats, RF Schinazi. Georgia Life Sciences Summit, Atlanta, GA. Sept 24, 2008.
- 9- Potent activity and lack of pharmacokinetic interaction between amdoxovir when co-administered with low dose zidovudine. Selwyn J. Hurwitz, Emilie Fromentin, Ghazia Asif, Phillip Tharnish, Judy Mathew, Nancy M. Kivel, Carlos Zala, Claudia Ochoa, Robert Murphy, and Raymond F. Schinazi. XVII International AIDS Society, Mexico City, Mexico, Aug 3-8, 2008.
- 10- A common anti-herpetic drug acyclovir is converted into a nucleoside reverse transcriptase inhibitor that suppresses HIV-1 in herpesvirus infected human tissues. A. Lisco, C. Vanpouille, E. Tchesnokov, J.-C. Grivel, A. Biancotto, B. Brichacek, J. Elliott, E. Fromentin, R. Shattock, P. Anton, R. Gorelick, M. Derudas, J. Balzarini, C. McGuigan, M. Götte, R. Schinazi, L. Margolis. XVII International AIDS Society, Mexico City, Mexico, Aug 3-8, 2008.
- 11- Pharmacokinetics and potent anti-HIV-1 activity of amdoxovir plus zidovudine in a randomized double-blind placebo-controlled study. Robert Murphy, Carlos Zala, Claudia Ochoa, Phillip Tharnish, Judy Mathew, Emilie Fromentin, Ghazia Asif, Selwyn J. Hurwitz, Nancy M. Kivel, Raymond F. Schinazi. 15th CROI, Boston, MA. Feb 3-6, 2008. Abstract 794.
- 12- Simultaneous quantification of (-)- β -D-dioxolane guanosine (DXG), its prodrug amdoxovir, and zidovudine in human plasma by LC-MS/MS. Emilie Fromentin, Ghazia Asif and Raymond F. Schinazi. LCMS Montreux Symposium, Hilton Head, SC. October 10-12, 2007.

Abbreviations

Biological terms

AIDS: Acquired Immunodeficiency Syndrome
AUC: Area under the curve *versus* time
CI: Synergistic index
Cl: Drug clearance
CNT: Concentrative Na⁺ or H⁺-dependent nucleoside transporter
C_{max}: Maximal concentration
C_{min}: Minimal concentration
DEC: Dead end complex
DNA: Deoxyribonucleic acid
dNTP: 2'-deoxyribonucleoside-5'-triphosphate
EC₅₀: 50% effective concentration
ENT: Equilibrative nucleoside transporter
F: Bioavailability
FBS: Fetal bovine serum
FDA: Food and Drug Administration
HAART: Highly active antiretroviral treatment
t_{1/2}: Half-life
HIV: Human immunodeficiency virus
HBV: Hepatitis B virus
IC₅₀: 50% inhibitory concentration
IL-2: Interleukin-2
K_i: HIV-1 RT inhibition constant against a DNA/RNA primer/template
K_m: Apparent binding constant
MRP: Multidrug resistance protein
Mt: Mitochondrial
OAT-OCT: Organic anions or cations transporter
PBM cells: Peripheral blood mononuclear cells
PBS: Phosphate-buffered saline
PHA: Phytohemagglutinin
PK: Pharmacokinetics
RNA: Ribonucleic Acid
rNTP: Ribonucleoside-5'-triphosphate
RT: Reverse transcriptase
SIV: Simian immunodeficiency virus
TAMs: Thymidine analogue mutations
T_{max}: Time at C_{max}
Vd: Volume of distribution
WHO: world health organization

Drugs and metabolites

FI/EI: Fusion/Entry inhibitor
INI: Integrase inhibitor
NRTI: Nucleoside reverse transcriptase inhibitor
NRTI-MP: Nucleoside reverse transcriptase inhibitor monophosphate
NRTI-DP: Nucleoside reverse transcriptase inhibitor diphosphate

NRTI-TP: Nucleoside reverse transcriptase inhibitor triphosphate
NtRTI: Nucleotide reverse transcriptase inhibitor
NNRTI: Non-nucleoside reverse transcriptase inhibitor
PI: Protease inhibitor
ABC: Abacavir, (1*S*,4*R*)-4-[2-amino-6-(cyclopropylamino)-9H-purin-9-yl]-2-cyclopentene-1-methanol succinate
CBV-TP: Carbovir-triphosphate, (-)-carbovir-triphosphate, 2-amino-9-[(1*R*,4*S*)-4-(hydroxymethyl)cyclopent-2-en-1-yl]-3H-purin-6-one -5'-triphosphate
DAPD: Amdoxovir, (-)-β-D-(2*R*,4*R*)-1,3-dioxolane-2,6-diaminopurine
DPD: 2,6-diaminopurine-2'-deoxyribose
ddATP: 2',3'-dideoxyadenosine triphosphate
ddC: Zalcitabine, 2',3'-dideoxycytidine
ddI: Videx, 2',3'-dideoxyinosine
DXG: 9-β-D-(1,3-dioxolan-4-yl)guanine
d4T: Stavudine, 3'-deoxythymidine
(-)-FTC: Emtricitabine, (-)-β-3'-thia-2',3'-dideoxy-5-fluorocytidine
PMPA, TFV: Tenofovir, (R)-9-(2-phosphonylmethoxypropyl)adenine
RBV: Ribavirin, 1-β-D-ribofuranosyl-1,2,4-triazole-3-carboxamide
TDF: Tenofovir disoproxil fumarate
ZDV: Zidovudine, 3'-Azido-3'-deoxythymidine
3TC: Lamivudine, (-)-β-3'-thia-2',3'-dideoxycytidine

Liquid chromatography and mass spectrometry:

CRM: Charge Residue Model
ESI: Electrospray Ionization
HA: Hexylamine
IEM: Ion Evaporation Method
IS: Internal Standard
LC: Liquid chromatography
MS: Mass spectrometry
m/z: mass to charge
N,N-DHMA: N,N-dimethylhexylamine

Enzymes

ADA: Adenosine deaminase, EC:3.5.4.4
AMPDA: Adenylate deaminase, EC:3.5.4.6
AMPK: Adenylate kinase, EC:2.7.4.3
APRT: Adenine phosphoribosyl-transferase, EC:2.4.2.7
ADSS/L: Adenylosuccinate synthase/lysase EC:6.3.4.4/EC:4.3.2.2
Ca-NT: Calcium activated nucleotidase, EC:3.6.1.6
CDA: Cytidine deaminase, EC:3.5.4.5
CMPK: Cytidine monophosphate (UMP-CMP) kinase 2, mitochondrial, EC:2.7.4.14
CTPS: CTP synthase, EC:6.3.4.2
dCK: 2'-deoxycytidine kinase, EC 2.7.1.74
dGK: 2'-deoxyguanosine kinase, EC:2.7.1.113
dCMPDA: dioxycytidine monophosphate deaminase, EC:3.5.4.12
EDP : Ectonucleoside triphosphate diphosphohydrolase, EC:3.6.1.5
GDA: Guanine deaminase, EC:3.5.4.3
GMPK: Guanylate kinase, EC:2.7.4.8

GMPS: Guanylate synthase, EC:6.3.5.2
HPRT: Hypoxanthine phosphoribosyl-transferase, EC:2.4.2.8
IMPDH: Inosinate dehydrogenase, EC:1.1.1.205
NDPK : Nucleoside diphosphate kinase, EC:2.7.4.6
PNP: Purine nucleoside phosphorylase, EC:2.4.2.1
RNR : Ribonucleotide reductase, EC:1.17.4.1
TK1 or TK2: Thymidine kinase 1 or 2, EC:2.7.1.21
TMPK: Thymidylate kinase, EC:2.7.4.9
TMPS: Thymidylate synthetase, EC:2.1.1.45
TP: Thymidine phosphorylase, EC:2.4.2.4
UCK: Uridine-cytidine kinase, EC:2.7.1.48
UP: Uridine phosphorylase, EC:2.4.2.3
UTG: UDP-glucuronyltransferase, EC 2.4.1.17
XDH: Xanthine dehydrogenase, EC:1.17.1.4
5'-NT : High K_m 5'-nucleotidase, cytosolic II, EC:3.1.3.5

Endogenous nucleobase, nucleosides and nucleotides

A, Ade: Adenine, Ado: adenosine, dAdo: 2'-deoxyadenosine
AMP: Adenylate, adenosine monophosphate
ADP: Adenosine diphosphate
ATP: Adenosine triphosphate
C, Cyt: Cytosine, Cyd: cytidine, dCyd: 2'-deoxycytidine
CMP: Cytidylate, cytidine monophosphate
CDP: Cytidine diphosphate
CTP: Cytidine triphosphate
G, Gua: Guanine, Guo: guanosine, dGuo: 2'-deoxyguanosine
GMP: Guanylate, guanosine monophosphate
GDP: Guanosine diphosphate
GTP: Guanosine triphosphate
IMP: Inosinate, inosine monophosphate
OMP: Orotate
PPi: Pyrophosphate
PRPP: Phosphoribosyl pyrophosphate
RMP: α -D-ribose-5-phosphate
T, Thy: Thymine, Thd: Thymidine
TMP: Thymidylate, thymidine monophosphate
TDP: Thymidine diphosphate
TTP: Thymidine triphosphate
U, Ura: Uracil, Urd: Uridine, dUrd: 2'-deoxyuridine
UMP: Uridine monophosphate
UDP: Uridine diphosphate
UTP: Uridine triphosphate
3PG: 3-phosphoglycerate

Table of Content

1	Introduction	8
1.1	The Laboratory of Biochemical Pharmacology, LOBP	8
1.2	Human Immunodeficiency Virus (HIV)	10
1.2.1	Discovery and characterization of HIV	10
1.2.2	Epidemiology of HIV	10
1.2.3	Virology of HIV	11
1.2.4	HIV progression and persistence	15
1.3	Antiretroviral treatment	17
1.3.1	Nucleoside Reverse Transcriptase Inhibitors (NRTI)	18
1.3.2	Metabolism and mechanism of action of NRTI	22
1.3.3	Drug combination and treatment limitations	29
1.4	Endogenous nucleotide pool	33
1.4.1	Endogenous nucleotide synthesis	34
1.4.2	Interactions between NRTI and endogenous nucleotide pool	36
1.4.3	Imbalances in the endogenous nucleotide pool can cause toxicity	38
1.4.4	Endogenous nucleotide pool vary with cell type and activation	40
1.5	Detection and quantification of natural and synthetic nucleos(t)ides	43
1.5.1	Chemical properties of nucleosides and nucleotides	43
1.5.2	Electrospray ionization tandem mass spectrometry	44
1.5.3	High Pressure Liquid Chromatography (HPLC)	48
1.5.4	Quantification of nucleosides and nucleotides by LC-MS/MS	51
2	Objectives	53
3	Material and methods	54
3.1	Chemicals and Reagents	54
3.2	Isolation, differentiation and culture of cells	55
3.2.1	PBM cells isolation and stimulation	55
3.2.2	Differentiation of PBM cells in macrophages	55
3.3	Cellular pharmacology studies	56
3.3.1	Studies in PBM cells and in macrophages	56
3.3.2	DXG phosphorylation studies in human PBM cells	56
3.3.3	DXG/ZDV combinations	57
3.3.4	DXG/3TC and DXG/(-)-FTC combinations	57
3.3.5	DXG decay	57
3.4	Collection of samples for clinical trial	58
3.5	Preparation of clinical samples	59
3.5.1	Intracellular extraction	59
3.5.2	Plasma extraction	59
3.6	LC-MS/MS	60
3.6.1	Ultimate 3000 and TSQ Quantum Ultra	60
3.6.2	LC-MS/MS for nucleotides	60
3.6.3	LC-MS/MS for nucleosides	64
3.7	Statistical analysis	70

4	CHAPTER 1: Quantification of nucleosides and nucleotides in activated and unactivated human primary PBM cells and macrophages	71
4.1	Simultaneous quantification of intracellular natural and antiretroviral nucleosides and nucleotides by liquid chromatography tandem mass spectrometry.....	71
4.1.1	Column and temperature selection.....	73
4.1.2	Ion-pair method development.....	74
4.1.3	Method sensitivity and partial validation.	78
4.2	Application: Measurement of NRTI-TP and endogenous nucleotides in PBM cells and in macrophages	83
4.2.1	Method cross-validation by comparison to previous published results.....	83
4.2.2	The levels of NRTI-TP are lower in macrophages than in PBM cells.....	83
4.3	Conclusions	88
5	CHAPTER 2: Study of DXG phosphorylation and endogenous nucleotide pool in human peripheral blood mononuclear cells	89
5.1	DXG phosphorylation is limited by competition with all guanine nucleosides.....	90
5.2	Lack of interaction between ZDV and DXG for phosphorylation in PBM cells but decreased endogenous dNTP levels.....	92
5.3	Lack of interaction between 3TC or (-)-FTC and DXG for phosphorylation in PBM cells	95
5.4	DXG phosphorylation is strongly inhibited by guanine nucleosides but not by other NRTI	96
5.5	Do NRTI affect the endogenous nucleotide pool?	99
5.6	Conclusions	100
6	CHAPTER 3: Quantification of nucleosides in human plasma by LC-MS/MS as part of a clinical study for DAPD combination with reduced dose of ZDV	101
6.1	Simultaneous quantification of 9-(β-D-1,3-dioxolan-4-yl)guanine, amdoxovir and zidovudine in human plasma by LC-MS/MS assay.....	101
6.1.1	LC-MS/MS characteristics.....	102
6.1.2	Calibrations curves and limit of quantification.....	104
6.1.3	Validation results.....	105
6.1.4	Discussion of the analytical advances by the present method.....	107
6.2	Application: Pharmacokinetics of DAPD plus ZDV	109
6.2.1	Non-compartmental PK analysis.....	109
6.2.2	Evidence for the lack of interaction between DAPD and ZDV	110
6.3	Conclusions	111
7	Conclusions and perspectives.....	112
8	References	115

1 Introduction

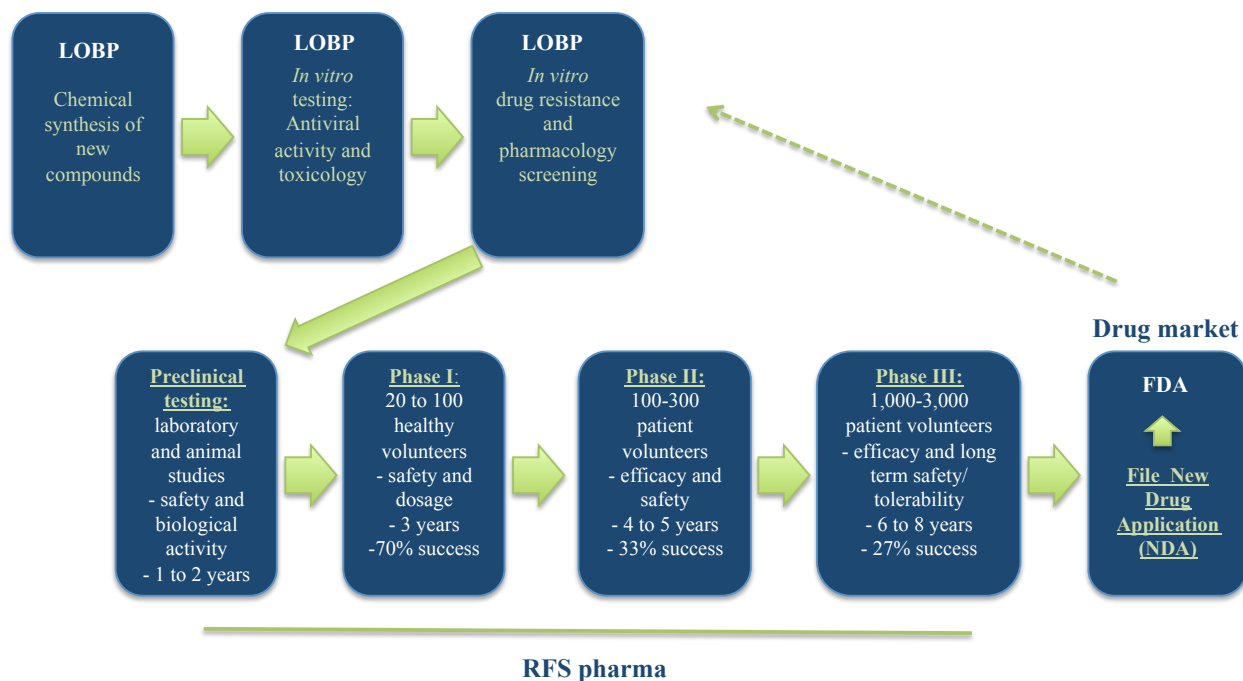
1.1 The Laboratory of Biochemical Pharmacology, LOBP

The research presented in this dissertation was performed in the Laboratory of Biochemical Pharmacology (LOBP) at the Veterans Affairs Medical Center/Emory University. LOBP is a drug discovery and preclinical drug development laboratory directed by Dr. Raymond F. Schinazi. The objective of the laboratory is to discover and develop new drugs for the treatment of human immunodeficiency virus-1 (HIV-1) and hepatitis infections, focusing on nucleoside analogues. Work performed at LOBP is independent from a biotech company in Tucker, GA, called RFS Pharma, LLC (RFSP; also founded by Dr. Raymond F. Schinazi, www.rfspharma.com, last consulted on March 24th 2010). RFSP has in-licensed a series of anti-HIV drugs including Amdoxovir[™] (AMDX, DAPD) from Emory University and the University of Georgia Research Foundation.

LOBP is organized around five cross-functional teams that work together to complete the preclinical process of drug discovery (**Figure 01**). The organic chemists design and synthesize new antiviral compounds. The virology group evaluates the potency of these compounds *in vitro* using peripheral blood mononuclear (PBM) cells infected with various strains of HIV, including resistant mutations. Toxicity is initially assessed against a panel of cells grown in culture, subsequently tested in animal models provided the compound has favorable therapeutic window and pharmacology profile *in vitro*. Pharmacology studies are undertaken to understand the metabolism of potential nucleosides, intracellular phosphorylation to active triphosphate, which is responsible for viral inhibition and the activity at the enzyme level. Pharmacokinetic (PK) studies are performed first in mice and rats and later in rhesus monkeys, to assess the absorption,

distribution, metabolism and elimination of these agents in animals. These results contribute towards predicting a starting dose for clinical testing in humans. The pharmacology team is comprised of cellular biologists, bioanalytical chemists, pharmacological and pharmacodynamic modelists, pharmacometricians and clinicians. Part of the accomplishments on amdoxovir, which is currently in phase II clinical development will be presented in this dissertation along with *in vitro* studies of approved anti HIV drugs. Accumulation of safety and efficacy data on drugs post marketing can provide useful information for new drug design.

Figure 01: Schematic of the drug development process.



Adaptated from <http://www.medscape.com>

1.2 Human Immunodeficiency Virus (HIV)

1.2.1 Discovery and characterization of HIV

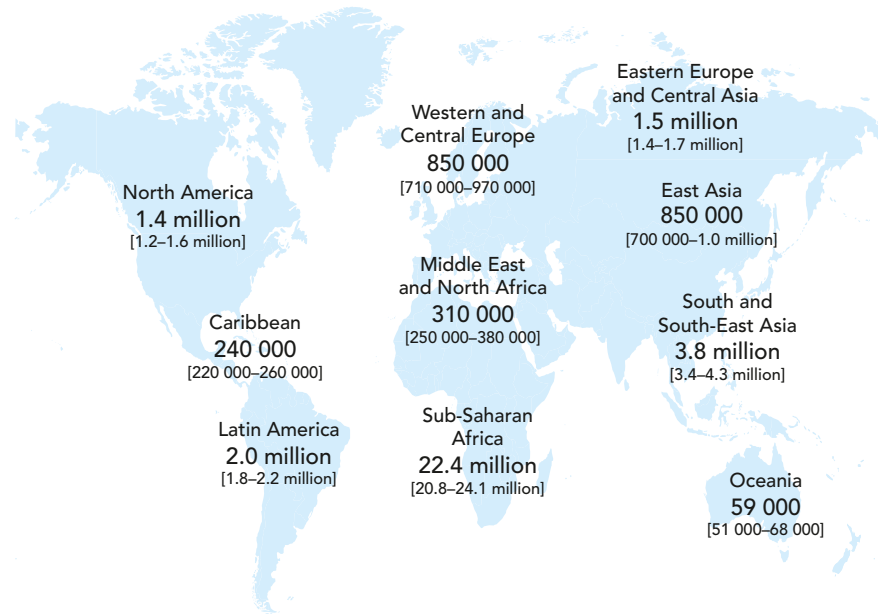
In the summer of 1981, clinicians in New York and California reported cases of men who were diagnosed with *Pneumocystis carinii* pneumonia, a rare opportunistic infection¹ or with the rare skin cancer Kaposi's sarcoma.² This condition, characterized by low CD4⁺ T cell counts, lymphadenopathy and infection by opportunistic diseases, was soon named Acquired Immunodeficiency Syndrome (AIDS). The transmission of this infectious microorganism was suggested to occur through sexual activity or blood.³ In 1983 the virus was isolated from infected patients by two different teams: Gallo and Montagnier. Gallo showed that this virus morphology was similar to human T cell leukemia and other type-C retroviruses.⁴ Montagnier characterized the retroviral activity using [³H]-uridine and named it lymphadenopathy-associated virus.⁵ Later, phylogenetic studies and replication cycle analysis showed that the AIDS virus was related to members of the lentivirus genus of the *retroviridae* family of viruses, and was named human immunodeficiency virus (HIV).^{6,7}

The natural ancestor of HIV is likely simian immunodeficiency virus (SIV), which infects naturally chimpanzees in west central Africa. A common ancestor would have appeared in the 1920's, and spread as the main cities such as Congo-Kinshasa were expanding.^{8,9}

1.2.2 Epidemiology of HIV

In 2008, there were an estimated total of 33.4 million (31.1-35.8 million) people who were living with HIV in the world (**Figure 02**), with about 2.7 million of newly infected adults and children and 2 million deaths. The number people living with the virus has increased by 40% since 1990. The number of deaths due to AIDS has decreased by about 10% since 2004 and the new infections are 30% less frequent than in the mid 90's.¹⁰

Figure 02: Adults and children estimated to be living with HIV in 2008.¹⁰



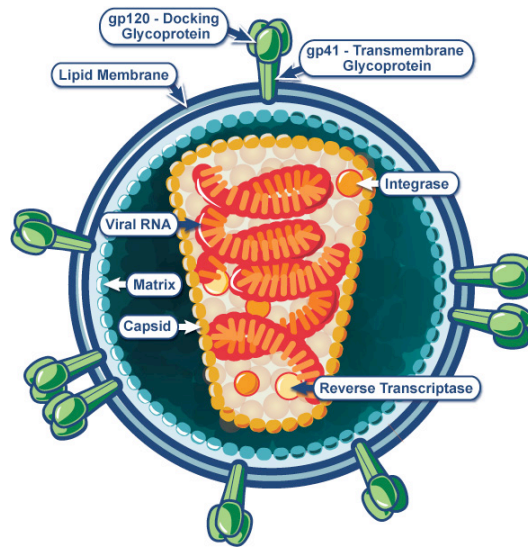
The epidemic is evolving with HIV prevention strategies, availability of drugs and improved access to treatment having a positive impact on disease burden. However, because the incidence of new infections continues to increase in limited resource countries, HIV/AIDS remains a global health priority. Since no vaccine is available, the treatments need to be improved and universalized.¹⁰

1.2.3 Virology of HIV

1.2.3.1 Features of HIV replication cycle

Lentiviruses comprise a separate genus of the family *retroviridae*; they cause immune deficiencies, disorders of the hematopoietic and central nervous system, and have a larger genome than those of simple retroviruses.¹¹ The genome of HIV-1 consists of two identical 9.2 kb single stranded RNA molecules within the virion, which codes for 15 proteins, whereas the persistent form of the HIV-1 genome is a proviral double-stranded DNA within infected cells **(Figure 03 and 04).**¹²

Figure 03: Structure of HIV virions. ¹²



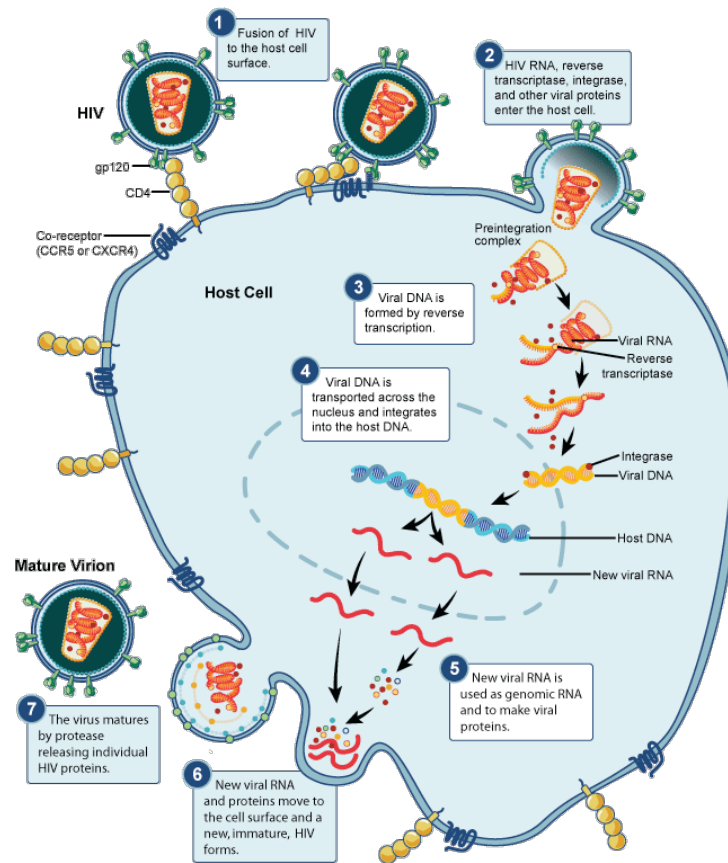
Source: <http://www3.niaid.nih.gov/topics/HIVAIDS/Understanding/Biology/hivVirionLargeImage.htm>

HIV virions have spherical morphology and consist of a lipid bilayer membrane that surrounds a dense truncated cone-shaped nucleocapsid, which contains the genomic RNA molecules, the viral proteases (not represented), reverse transcriptase, integrase.¹²

Three coding regions of the genome are the *env*, *pol* and *gag* genes, producing structural polyproteins that are common to all retroviruses. The *env* gene encodes the envelope proteins that are necessary for viral fusion to the host cells. It encodes two glycoproteins, gp41 anchors the structure of the viral envelope and gp 120 binds to the CD4 molecule on the surface of CD4⁺ T cells.¹³ This binding exposes a secondary site for binding to a chemokine co-receptor on the host cell, CCR5 or CXCR4.⁶

Pol and *gag* genes exert control over host-cell machinery by encoding a gag-pol precursor protein that is subsequently cleaved by proteases to generate various essential proteins, including: structural nucleocapsid, capsid and matrix proteins, as well as the viral enzymes: protease, reverse transcriptase (RT) and integrase (**Figure 04**).⁶

Figure 04: Steps in the HIV Replication Cycle.



Source: <http://www3.niaid.nih.gov/topics/HIVAIDS/Understanding/Biology/hivReplicationCycle.htm>

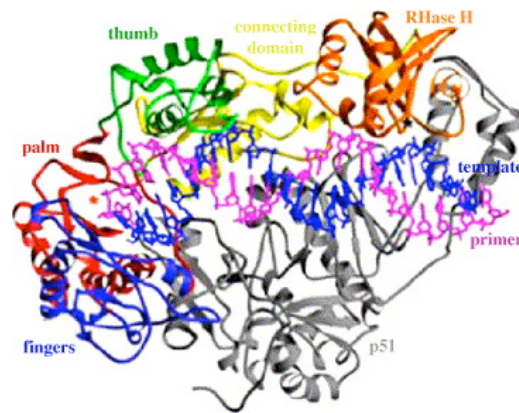
Lentiviral genomes encode for auxiliary proteins, *tat* and *rev*, which perform regulatory functions. The long terminal repeats promote transcriptional activators (NF- κ B or NFAT), which activate T-cells.¹¹

Finally, four accessory proteins, *Nef*, *Vif*, *Vpr* and *Vpu* (or *Vpx* for HIV-2) modulate viral replication. They are not necessary for viral reproduction in immortalized cell lines, but are necessary for viral replication *in vivo*¹¹ since they may protect the virus against cellular restriction factors.¹⁴

1.2.3.2 Reverse transcription and genome integration

The viral RT uses both RNA and DNA as templates to copy the single-stranded HIV-1 RNA genome to either a double-stranded DNA genome or a RNA-DNA heteroduplex.^{15, 16} RT from retroviruses has two catalytic activities: DNA polymerization and associated RNase H activity (RNA/DNA heteroduplex RNA degradation). The enzyme is a heterodimer formed by a regulator subunit of p51 (in grey **Figure 05**) and a catalytic subunit of p66 (coloured **Figure 05**).¹⁷ The p66 subunit resembles a right hand, where the subdomains are designated fingers, palm and thumb (**Figure 05**). The palm acts as a clamp to position the template-primer to the catalytic motif.¹⁸⁻²⁰

Figure 05: Crystal structure of the HIV-1 RT enzyme coupled with primer (backbone structure in pink) and template (backbone in blue).¹²



One major property of the HIV-1 RT is its high rate of base-substitution, addition and deletion errors in the HIV-1 genome. The error rate in the HIV-1 genome has been reported as 1 in 2,000 to 5,000 nucleotides *in vitro*,^{21, 22} and 3.4×10^{-5} mutation per base pair per cycle *in vivo*.²³⁻²⁵ The induced nucleotide mismatches are inherited as replication continues.²⁶ This high rate of mutation can be attributed to the lack of HIV-1 RT 3'→5' exonucleolytic proofreading capacity,²⁷ the fluctuations in the nucleotide pool levels,²⁸ the incorporation of dUTP²⁹ and the G→A hypermutations.³⁰ This hypermutability of new virions leads to the emergence of a

complex mixture of “quasispecies”, which are related but genetically distinct forms of HIV-1 in infected individuals, which renders treatment challenging.²⁷

Following reverse transcription, the double stranded DNA viral copy is integrated into the host cell’s genome, by the viral integrase. The viral genome is then transcribed and translated into protein products by the viral protease, which generates a new batch of proteins that will form the new virion (**Figure 04**).³¹

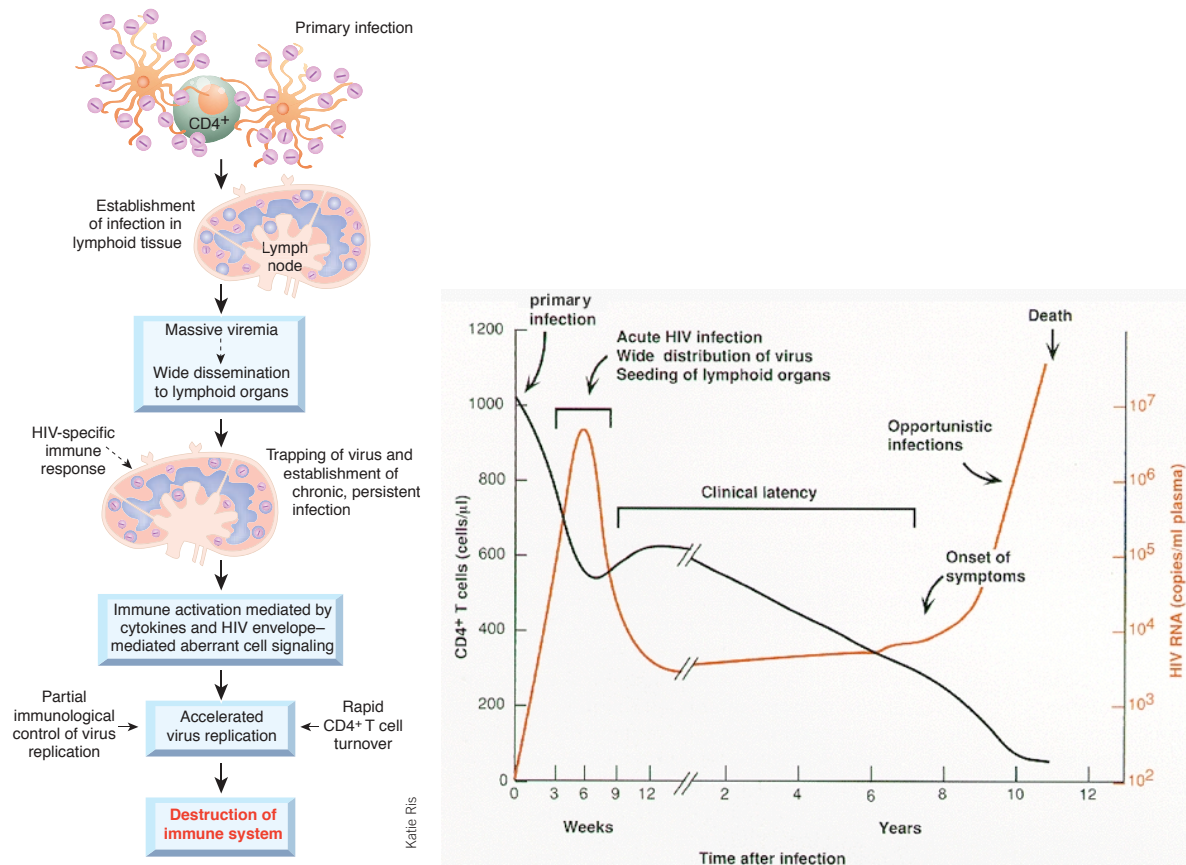
1.2.4 HIV progression and persistence

1.2.4.1 *The course of HIV infection*

HIV infection is characterized by an acute and a chronic phase. During the acute phase of infection, HIV viral replication is widespread and extensive in lymphoid and intestinal tissues. CCR5⁺ CD4⁺ T cells are the initial targets and are rapidly depleted. They are located in mucosal surfaces of the intestinal, respiratory and reproductive tract.³² Subsequent targets are CD4⁺ T cells bearing CXCR4⁺ co-receptor in peripheral blood, lymph nodes, and spleen.^{33, 34} This phase of profound depletion is followed by a phase of CD4⁺ T cell renewal. However, the restoration of memory CD4⁺ T creates additional targets for HIV-1 leading to exhaustion of the immune system.³⁴ The HIV infected individuals enter a phase of clinical latency characterized by a slow, continuous decrease in CD4⁺ T cells and maintenance of CD8⁺ T cells. The HIV infection becomes chronic (**Figure 06**).³³

During progression to AIDS, both CD4⁺ and CD8⁺ T cell counts drop dramatically. The increased viral replication in the lymph nodes eventually lead to their destruction and the patient becomes susceptible to opportunistic infections that ultimately cause death (**Figure 06**).¹¹

Figure 06: Pathogenic events in untreated HIV mediated disease.^{7,35}



1.2.4.2 HIV latency

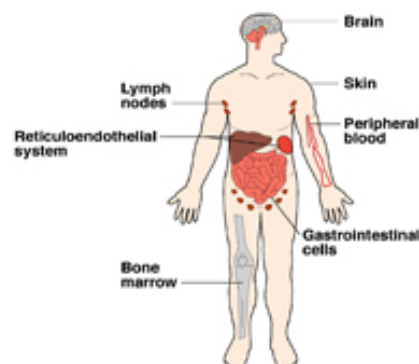
The latent reservoirs are established early during the infection by infected cells, which do not divide or produce virions (little production of HIV mRNA). One infected $CD4^+$ T cell in a million reverts back to a resting state.³⁶ Macrophages also exhibit the co-receptor CCR5 causing susceptibility to infection by HIV-1 but might be less susceptible to viral cytopathicity.³⁷ Even though monocytes and macrophages produce ~ 10 to 60-fold fewer virus particles per cell than $CD4^+$ T cells during each infectious cycle, they can secrete virus over a longer period and contribute to the viral burden³⁸ sufficiently to be considered a reservoir.³⁷ Macrophages and dendritic cells also play an important role in virus dissemination to $CD4^+$ T cells.^{31, 33}

To date, HIV-1 latency established in resting memory CD4⁺ T cells,³⁹ macrophages^{31, 38,}^{40, 41} or mononuclear cells⁴² represents a major barrier to virus eradication.⁴³ Highly active antiretroviral treatment (HAART) is capable of suppressing HIV, even to undetectable levels in the blood, but they cannot eliminate the virus hiding in these latent reservoirs. Studying the mechanism of viral persistence to existing HAART remains a focus of research, and may lead to the development of new strategies to purge these viral reservoirs.⁴⁴

1.2.4.3 *Predominant sites of HIV infection in vivo*

In addition to the sites of infection mentioned previously, CNS/brain is targeted by HIV-1 primarily mediated by infected macrophages and is responsible for CNS dysfunction in infected individuals (**Figure 07**).⁴⁵

Figure 07: HIV can hide in the brain, lymph nodes, skin, peripheral blood, reticuloendothelial system, bone marrow, and gastrointestinal cells.



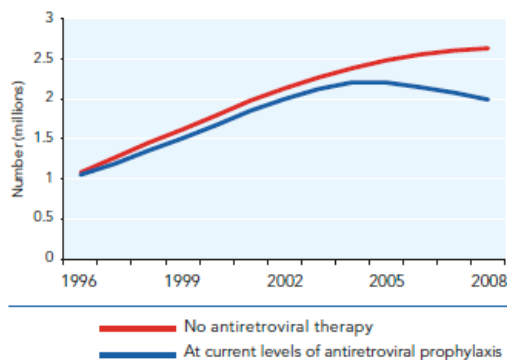
Source: <http://www3.niaid.nih.gov/topics/HIVAIDS/Understanding/Biology/hidesImmuneSystem.htm>

1.3 Antiretroviral treatment

Modern drug discovery has transformed HIV-1 infection into a treatable chronic infectious disease.⁴⁶ Before the availability of drugs, patients diagnosed with AIDS would die within one-two years.⁴⁷ Antiretroviral treatments were developed in order to decrease HIV-1

replication, and prevent the decline of CD4⁺ T cells by targeting several steps in the virus replication. Increased access to treatment and care has raised the life expectancy of HIV-1 infected individuals to over five years in resource-limited countries, and even longer in high-income countries (**Figure 08**).¹⁰

Figure 08: AIDS related death with and without antiretroviral therapy in the world.¹⁰



To date, the US Food and Drug Administration (FDA) has formally approved 24 drugs for the treatment of HIV infections. However, not all are used widely due to cytotoxicity and poor response. These antiretroviral agents can be classified in 5 categories according to the step of the HIV replicative cycle they target (**Figure 04**): nucleoside reverse transcriptase inhibitors (NRTI), non-nucleoside reverse transcriptase inhibitors (NNRTI), protease (maturation) inhibitors (PI), integrase inhibitors (INI) and fusion/entry inhibitors (FI/EI).⁴⁸

1.3.1 Nucleoside Reverse Transcriptase Inhibitors (NRTI)

The replication of HIV-1 is dependent on a viral reverse transcriptase enzyme not expressed by mammalian cells, thus, making it an attractive therapeutic drug target. The first antiretroviral agent was zidovudine (ZDV, AZT), and since then many more potent and safer NRTI have been developed, and this class of drug remains the backbone of modern HAART regimens especially because of its high genetic barrier to resistance.⁴⁹ The LOBP focuses on the development of new NRTI including the recently developed NRTI amdoxovir™, which will be

cited throughout this dissertation. Please refer to **Figure 9** for structures of FDA approved NRTI that will be described below.

1.3.1.1 FDA approved NRTI

The first HIV inhibitor 3'-azido-3'-deoxythymidine (Zidovudine, ZDV, AZT), was approved by the FDA for anti-HIV usage in 1987. ZDV showed antiviral activity in cell lines at concentrations as low as 50-500 nM.⁵⁰ Soon after the approval of ZDV, a panel of dideoxynucleosides was evaluated⁵¹ and 2',3'-dideoxyinosine (ddI)⁵² and 2',3'-dideoxycytidine (ddC)⁵³ were approved by the FDA in 1991 and 1992, respectively; ddC is no longer marketed because of its toxicity.⁴⁸ Modifications of 2',3'-deoxythymidine to form an unsaturated derivative, namely 2',3'-didehydro-3'-deoxythymidine led to the development of stavudine (d4T).⁵⁴

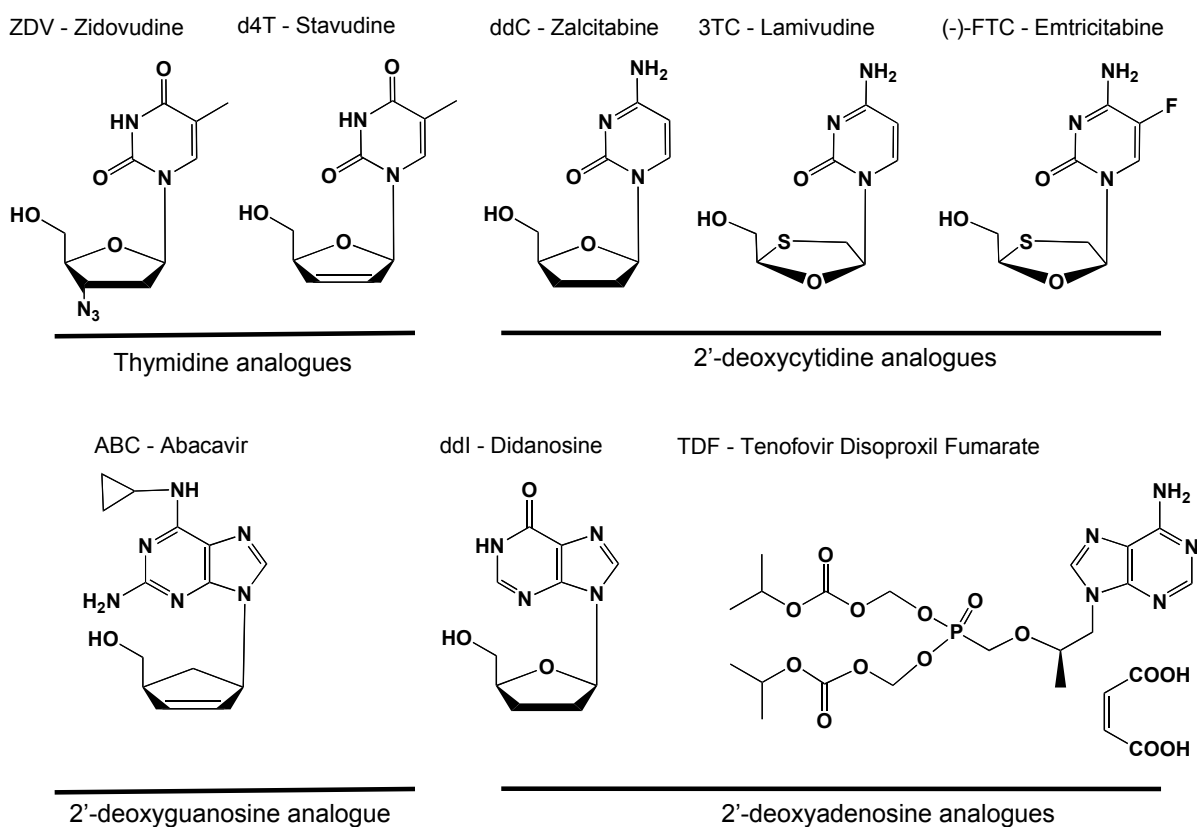
The first four nucleosides approved were D-enantiomers, which is the configuration of natural nucleosides. However, it was also discovered that certain L-nucleosides, such as lamivudine, (3TC) or emtricitabine [(-)-FTC], were more potent and less toxic than the (+) isomer.⁵⁵ (-)-FTC may offer improved activity compared to 3TC, due to better affinity of (-)-FTC-TP for the HIV-1 RT, probably due to tighter hydrogen bonding with the the 5-fluorine.⁵⁶ Furthermore, the 5-fluorine moiety on the base increases its lipophilicity and may increase penetration of the nucleoside analogue into the CNS, which is an important reservoir for HIV-1.

Abacavir (ABC) was the first guanosine analogue approved. The carbocyclic sugar moiety decreases the lability of the glycosidic bond cleavage that is typical of 2',3'-dideoxynucleosides.⁵⁷

The acyclic nucleotide reverse transcriptase inhibitor tenofovir disoproxil fumarate (TDF DF) is a salt of (*R*)-9-(2-phosphonylmethoxypropyl)adenine (PMPA) and was approved in 2001

by the FDA. This drug was formulated as the disoproxil fumarate salt to mask the two negative charges on the phosphonate moiety, which limits the gastrointestinal absorption of PMPA.⁵⁸ The vast majority of the drug is observed as PMPA in the systemic circulation. TDF was initially suggested for pre- and post-exposure prophylaxis and is now marketed as a fixed dose combination with (-)-FTC (Truvada[®]) and a triple coformulation with (-)-FTC and efavirenz (Atripla[®]).⁵⁹

Figure 09: Structures of the currently FDA approved NRTI.

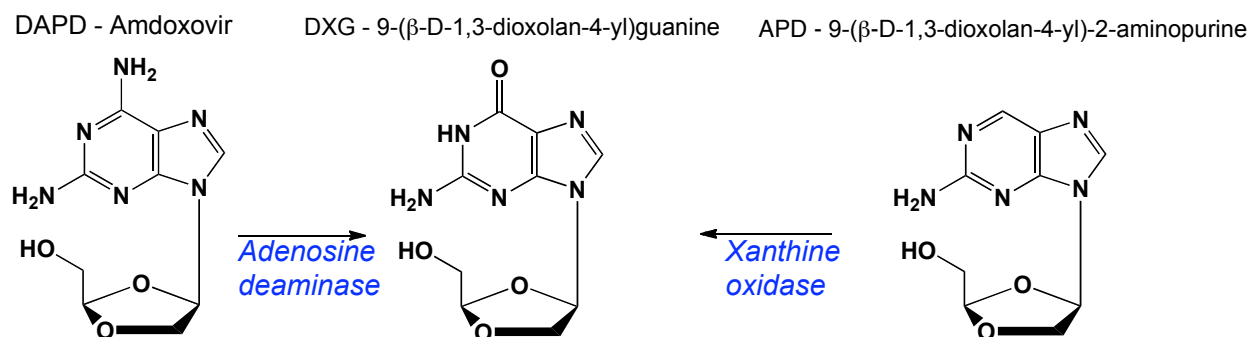


1.3.1.2 Amdoxovir

DXG [9-(β -D-1,3-dioxolan-4-yl)guanine] (**Figure 10**), is a guanosine nucleoside with a potent and selective activity against HIV-1, HIV-2 and hepatitis B virus (HBV). Since DXG is poorly soluble, a prodrug, amdoxovir, [(-)- β -D-2,6-diaminopurine dioxolane or DAPD] (**Figure 10**) was designed and resulted in improved oral bioavailability. DAPD is deaminated by the

ubiquitous adenosine deaminase (ADA) to DXG, before undergoing intracellular phosphorylation.⁶⁰ DXG-TP has a K_i of 20 nM *versus* HIV-1 RT making it one of the most potent inhibitors of this enzyme. DAPD is currently in phase II clinical testing for the treatment of HIV-1 infection, and has been safely administered to 206 individuals⁶¹ (www.rfspharma.com, accessed on March 24th, 2010).

Figure 10: Conversion of DAPD to DXG by adenosine deaminase.



Following oral administration of DAPD to woodchucks or rhesus monkeys, plasma concentrations of DXG are significantly higher than DAPD. These data suggest that DAPD is rapidly absorbed and converted into DXG *in vivo*. None of the currently approved NRTI contains a dioxolane sugar motif. In addition, DXG does not cause cellular toxicity up to 500 μM in primary cells and in cell lines. Together, these preliminary results make DXG an attractive molecule for future drug development.⁶²

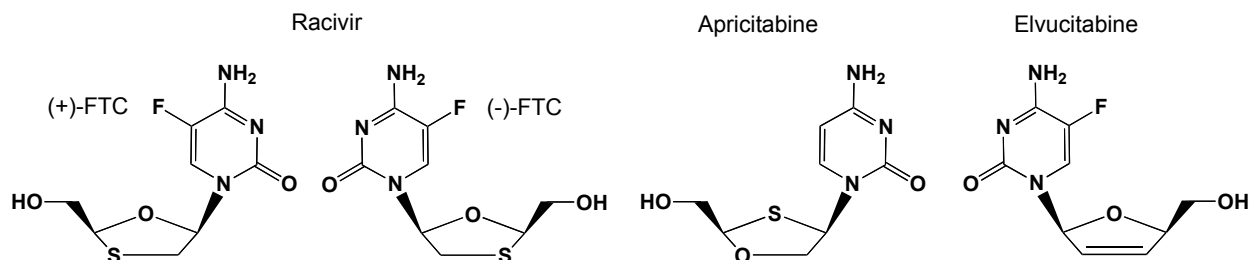
The major toxicity of amdoxovir in extensive animal toxicology studies was obstructive nephropathy at high doses, secondary to the precipitation of DAPD/DXG in the renal tubules. This was probably due to the poor aqueous solubility of DXG, similar to that observed for the related nucleoside analogues acyclovir. In a 52-week study, five cynomolgus monkeys, receiving DAPD 800 or 1200 mg/kg per day, developed obstructive nephropathy and associated uremia after 26 weeks of treatment, which was reversible after early identification and discontinuation of

medication. In addition, islet cell atrophy and hyperglycemia occurred, and lens opacities were observed,⁶³ which were thought to be secondary to hyperglycemia, and not a direct effect of DAPD. No individuals enrolled in clinical trials of DAPD have developed any renal abnormalities attributable to the drug.^{64, 65} Consequently, various prodrugs have been designed to improve DXG solubility and its pharmacological profile.⁶⁶ APD [(-)-β-D-2-aminopurine-dioxolane] (**Figure 10**) is an alternative prodrug of DXG in preclinical development at LOBP. Although preclinical studies are promising, APD is yet to undergo clinical testing.⁶⁷

1.3.1.3 Other NRTI in development

There are currently, 3 other NRTI undergoing clinical evaluation, (-)-2'-deoxy-3'-oxa-4'-thiocytidine (apricitabine) developed by Avexa, Ltd., (±)-β-2',3'-dideoxy-5-fluoro-3'-thiacytidine (racivir) by Pharmasset, Inc. and (-)-β-2',3'-didehydro-2',3'-dideoxy-5-fluorocytidine (elvucitabine) by Achillion Pharmaceuticals, Inc (**Figure 11**).⁶⁸

Figure 11: Structures of other NRTI in development

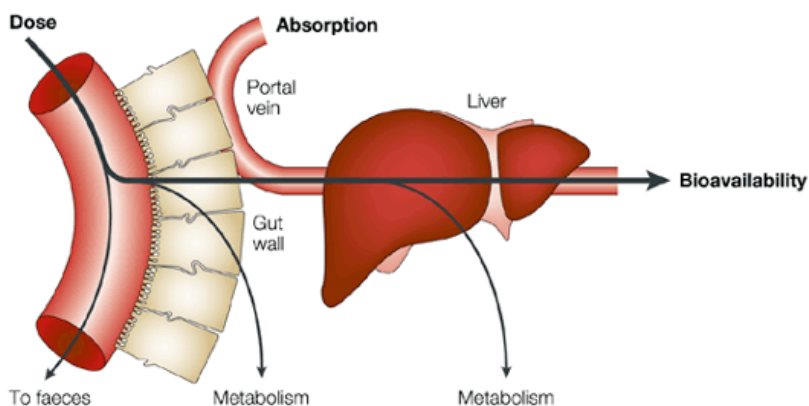


1.3.2 Metabolism and mechanism of action of NRTI

1.3.2.1 Plasma pharmacokinetics

Following oral absorption, generally a nucleoside is absorbed in the gastro-intestinal tract and rapidly through the gut wall *via* a facilitative (non-ATP dependent) nucleoside transporter into the hepatic circulation. After passing through the liver, where some metabolism can occur the remaining drug enters the systemic circulation (**Figure 12**).

Figure 12: Drug metabolism during the absorption process.⁶⁹



Nature Reviews | Drug Discovery

The extent of the drug distribution to tissues and organs depends on its physico-chemical properties and the expression of nucleoside transporters on their surface. Nucleosides are relatively hydrophilic and generally do not bind to plasma proteins and are not extensively metabolized by the cytochrome CYP450 enzymes, with the exception of ZDV and ABC.^{70, 71}

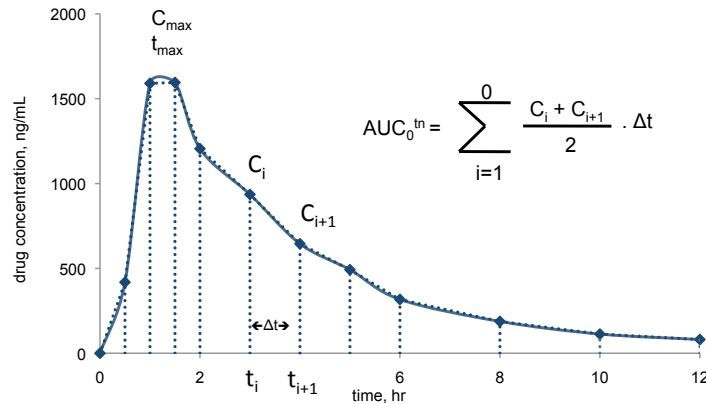
Pharmacokinetic studies are performed in order to quantify the drug adsorption, distribution, metabolism and excretion (ADME) characteristics, mainly using drug concentration *versus* time profiles measured in blood plasma and urine, since these compartments are easily sampled. Drug concentrations are usually measured in plasma, which correlated with the proportion of drug in equilibrium with target cells, rather than in whole blood.

Since HIV infected individuals are often given several drugs in combinations, the appropriate clinical trials should be designed to detect potential drug-drug interactions and evaluate the pharmacokinetics for each drug alone and in the combination to be used in the clinic.

1.3.2.2 Non-compartmental analysis

Non-compartmental pharmacokinetic analysis is a descriptive regression analysis, which does not include any assumption regarding tissue compartments, providing a detailed modeling of absorption or distribution processes of the drug or metabolites. The area under a plot of the plasma concentration *versus* time curve (AUC) is a measure of drug exposure, and is often correlated with drug efficacy and toxicity. For single dose measurements, the component of the AUC between dose and the last data point (AUC_{obs}) is calculated using a modification of the trapezoidal rule (**Figure 13**).

Figure 13: Graphical representation of the trapezoidal rule.



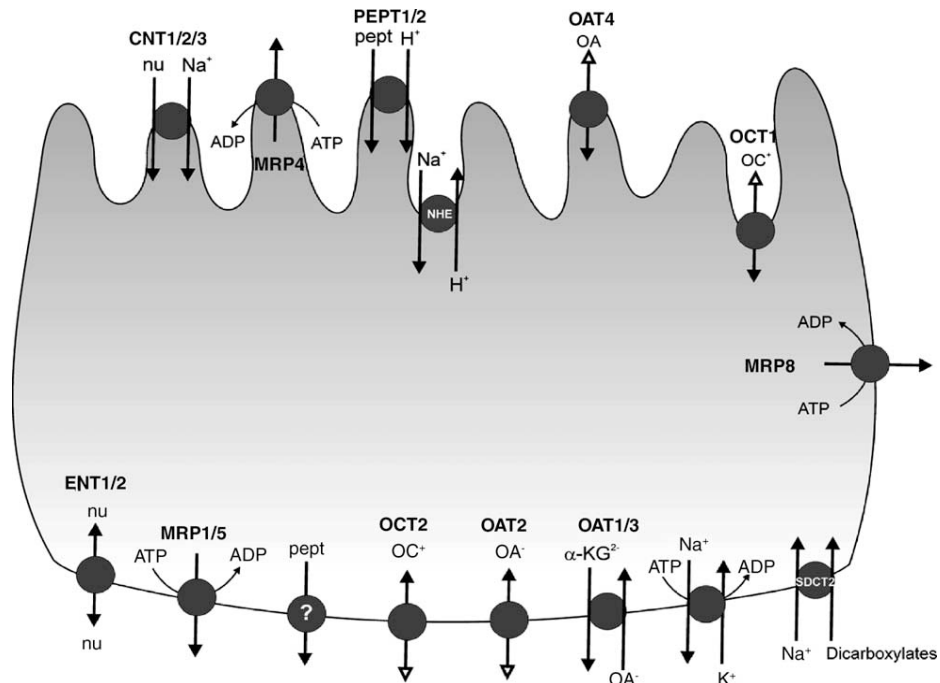
The remaining portion of the AUC between the last point measured and infinity (AUC_{extrap}), is extrapolated assuming exponential decay. The total AUC (AUC_{tot}) is then $AUC_{obs} + AUC_{extrap}$.

With repeated dosing, equilibrium is reached when the AUC between doses (AUC_{τ}) are reproducible. At equilibrium the amount of drug entering and leaving the plasma are equal. It follows that AUC_{tot} from the first dose is equal to AUC_{τ} at steady-state. Maximal plasma concentrations (C_{max}) are of interest, since drug exposure may correlate with toxicity. C_{min} represents minimal drug concentrations between doses, when the tissues of the person are most susceptible to infection.

1.3.2.3 Cell penetration

Nucleosides have to access the cytoplasm to exert an effect on the viral RT target. Nucleosides are generally hydrophilic and do not enter lipid bilayers easily. They enter lymphocytes and other cells through facilitative nucleoside transporters on their surface.⁷² These transmembrane proteins include equilibrative nucleoside transporters (ENT), concentrative Na⁺ or H⁺-dependent nucleoside transporters (CNT) and organic anions or cations transporter (OAT-OCT) (**Figure 14**).⁷³ Multidrug resistance protein (MRP) belongs to the ATP-binding cassette family of active transporters and plays a role in the efflux of several nucleotides, including the monophosphate of ZDV and 3TC.⁷⁴ Some NRTI, particularly (-)-FTC have shown to be a substrate as well as an inhibitor of MRP proteins, which could lead to intracellular accumulation of other NRTI in combination.^{75, 76}

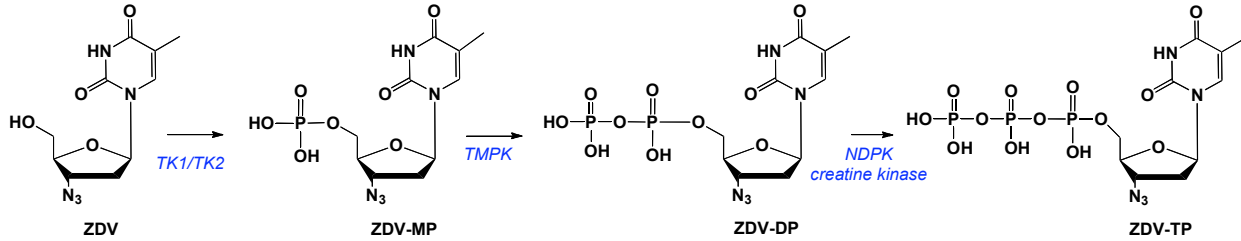
Figure 14: Schematic representation of the major transporters implicated in the uptake and efflux of NRTI. (Note: the expression of transporters might vary from one cell type to the other, all are represented on the same cell for simplification)



1.3.2.4 Activation of NRTI

After crossing the cellular membrane, NRTI are phosphorylated by the kinases of the salvage pathway (**Figure 15 and 16**).^{77, 78}

Figure 15: An example of NRTI phosphorylation: ZDV phosphorylation.



The kinases catalyzing the phosphorylation of the nucleoside analogues are the salvage kinases that catalyze the phosphorylation of respective endogenous 2'-deoxyadenosine, 2'-deoxyguanosine, 2'-deoxycytidine or thymidine analogues (**Figure 16**).

Figure 16: Phosphorylation pathways of NRTI,⁷⁹ namely 2'-deoxyadenosine, 2'-deoxyguanosine,⁸⁰ 2'-deoxycytidine⁸¹⁻⁸⁵ or thymidine analogues.⁸⁶⁻⁸⁹ Reverse dephosphorylation reactions are catalyzed by 5'-nucleotidases [phosphatases] (not displayed here).

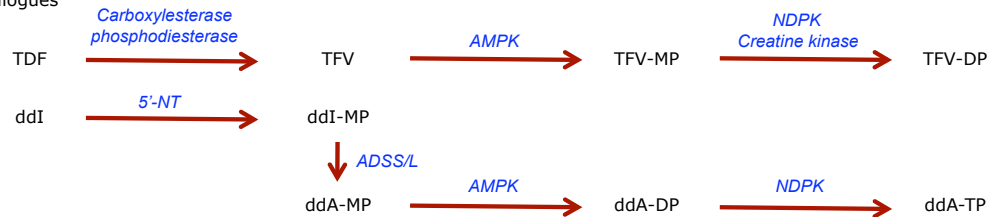
Thymidine analogues



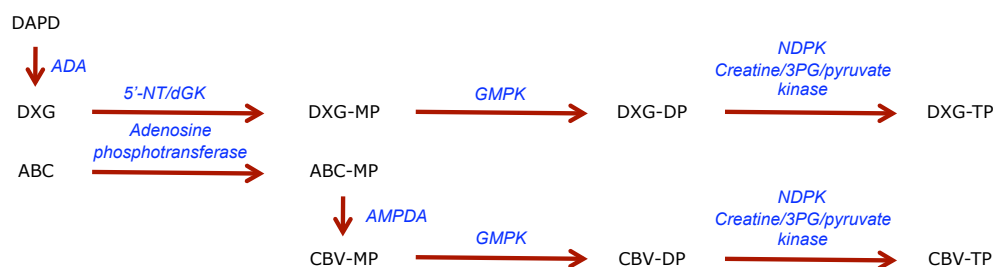
2'-deoxycytidine analogues



2'-deoxyadenosine analogues



2'-deoxyguanosine analogues



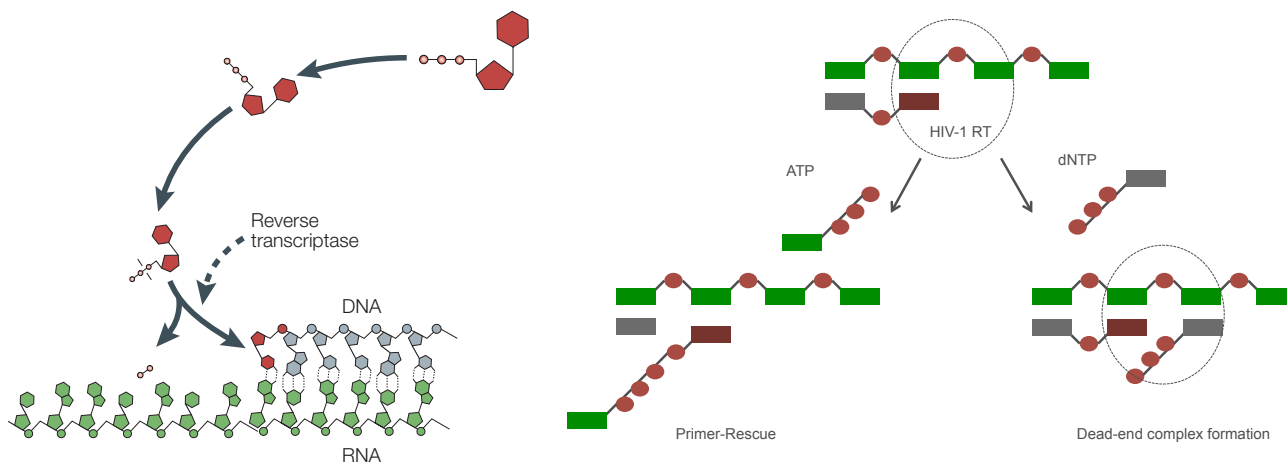
The rate limiting phosphorylation step of many NRTI including DXG, d4T and ddI is the first one.^{79, 80} However, in the case of ZDV, the second phosphorylation step, catalyzed by thymidylate kinase is rate limiting.⁹⁰⁻⁹² The last phosphorylation step is usually non-specific and non-rate limiting, since nucleoside diphosphate kinase (NDPK) has a high affinity for many nucleotide diphosphates. However, creatine kinase and 3-phosphoglycerate (3PG) kinase can also catalyze this reaction for NRTI-DP in the D- and L-enantiomeric ribose conformation, respectively.⁸⁵ Thus, in the case of 3TC, the last phosphorylation step can be limiting.

Following deamination of DAPD (see § 1.3.1.2, Figures 10 and 16), the conversion of DXG to DXG-MP is mainly catalyzed by the high K_m 5'-nucleotidase (5'-NT) and to a lesser extent by 2'-deoxyguanosine kinase (dGK), followed by phosphorylation of DXG-MP to DXG-DP by the sole enzyme, guanylate kinase (GMP). The third phosphorylation step may be catalyzed by creatine kinase, NDPK and to a lesser extent by 3PG-kinase and pyruvate kinase. DXG-TP levels in CEM cells were about 15 fmol/10⁶ cells after a 24 hr incubation with DXG at 5 μ M.⁸⁰ DXG-TP demonstrates a ~ 9 hr decay half-life in primary lymphocytes derived from a study in humans.⁹³

1.3.2.5 Reverse transcriptase inhibition

The antiviral efficacy of NRTI-TP depends on competition with the corresponding endogenous nucleotides for recognition, binding and incorporation by the HIV-1-RT.⁷⁸

Figure 17: Schematic representation of interaction between HIV-1 RT and the chain terminated primer/template.^{94, 95}



After incorporation by the HIV-1 RT, the NRTI-MP can have two different fates. It could either cause a chain termination by incorporation of the next endogenous nucleotide followed by the formation of a dead end complex (DEC), or it could be excised from the elongating DNA strand (**Figure 17**). Once the NRTI has been incorporated to the template, the polymerase still has the ability to translocate to the next position and incorporate the next incoming endogenous dNTP. However, the polymerase will be unable to catalyze the phosphodiester bond synthesis because the NRTI lacks its 3'-hydroxyl group on the sugar moiety, resulting in a DEC that has been crystallized.⁹⁶ When the conditions are not favorable to the DEC formation, excision occurs, either through ATP or pyrophosphate (PPi). Not all the NRTI are efficiently excised; ZDV is more prone to excision than others, resulting in resistant mutants.⁹⁷

Enzymatically, it is possible to evaluate the HIV-1 RT inhibition constant (K_i) against a DNA/RNA primer/template, using the following equation: $K_i = IC_{50(NRTI-TP)} / (1 + [dNTP] / K_{m(dNTP)})$; where $IC_{50(NRTI-TP)}$ is the experimental measure for dNMP incorporation inhibition, $[dNTP]$ is the concentration of the natural endogenous dNTP, and $K_{m(dNTP)}$ is the

apparent binding constant for the natural dNTP.⁹⁸

1.3.3 Drug combination and treatment limitations

1.3.3.1 Brief overview of the other classes of highly active antiretroviral therapy (HAART) drugs approved

NNRTI also inhibits the HIV-1 RT, by binding to an allosteric site located at a short distance from the catalytic site of the enzyme, where NRTI binds. To date, 4 NNRTI have been approved by the FDA.⁴⁸ PI bind with a viral protease required for the cleavage of the *gag* and *gag-pol* precursors to structural and functional proteins, resulting in inhibition of the maturation of viral particle formation. There are currently 10 approved PI on the market. Other classes of antiretroviral agents approved by the FDA include the CCR5 binding antagonist, maraviroc and the integrase strand transfer inhibitor, raltegravir.⁶⁸

1.3.3.2 Synergism of drug combinations

ZDV was initially used as monotherapy. However, its antiviral effect was enhanced when used in combination with other antiretroviral agents.⁹⁹⁻¹⁰¹ Drug combinations are usually formulated in order to maximize antiviral efficacy or to reduce the dose. Ideally, constituents in a drug regimen should produce antiviral efficacies, which are at least additive and preferably synergistic; they should never be antagonistic. The antiviral activity of drugs in combination is initially characterized *in vitro*. This analysis typically involves measurement of the 50% effective concentration (EC₅₀) of the individual drugs or in combination using different ratios of the individual drugs. An isobologram is generated from the dose response curve of the drugs and a combination index is calculated. A combination index (CI) > 1 reflects antagonism, = 1 additivity and < 1 synergism.^{62, 102}

Previous results indicated antiviral synergy when DXG is combined with 3TC (CI = 0.8 at the EC₅₀) and with ZDV (CI = 0.6 at the EC₅₀).^{62, 103} The mechanism of NRTI synergism may be explained by additional properties acquired by each individual drug when used in combination. The NRTI may be active against different drug resistant HIV-1 mutants, and the use of drugs with complementary resistance profiles may decrease the rate of emergence of resistant viral populations. One NRTI may enhance the formation of DEC by the other NRTI.^{102, 104} In addition, one NRTI may increase the levels of active triphosphate of the other, *via* metabolic interactions. This has been reported in the case of TDF in combination with (-)-FTC or with ddI.^{105, 106} Generally, NRTI with the same metabolic pathway such as ZDV with d4T or 3TC with (-)-FTC are not combined to avoid direct interaction.^{107, 108} This is particularly valid for the first two phosphorylation steps. Since 3TC, ZDV and DXG do not use the same kinases (**Figure 17**), it is not likely that DXG in combination with 3TC or ZDV would interact at the phosphorylation level. Nonetheless, the incorporation of NRTI-TP by HIV-1 RT is influenced by the competition with the corresponding endogenous dNTP^{49, 109, 110} and by the incorporation of the following dNTP by HIV-1 RT.^{94, 111, 112} *Thus, a decrease in the levels of the competing endogenous dNTP could explain the synergism observed between nucleosides. This hypothesis has been studied in this dissertation.*

1.3.3.3 HIV NRTI resistance

Resistance to multiple NRTI has been associated with amino-acid substitutions at the nucleoside-binding site of the enzyme of HIV-1 RT. When these mutations arise in the active site of the enzyme, a change in the RT conformation occurs resulting in reduced effectiveness of these inhibitors. There are two main mechanisms of NRTI resistance: drug discrimination and drug excision.¹¹³ Variations in the level of drug are associated with the selection of specific

mutations. Clinically, drug adherence might be the main cause of drug resistance selection that can lead to HAART failure. In this context, more than 50 RT mutations are associated with NRTI resistance, with the most common reported in **Table 01**.¹¹³

Table 01: Most common mutations in the RT gene associated with resistance to NRTI, residues involved in drug discrimination are depicted in purple and drug excision in green.^{114, 115}

NRTI	Mutations
ABC	K65R, L74V, Y115F, M184V
ddI	K65R, L74V
(-)-FTC	K65R, M184V
3TC	K65R, M184V
d4T	M41L, K65R, D67N, K70R, L210W, T215Y/F, K219Q/E
TFV	K65R, K70E
ZDV	M41L, D67N, K70R, L210W, T215Y/F, K219Q/E

The emergence of drug-resistant mutants has complicated the management of HIV infected subjects, but the availability of a wide range of drugs in the treatment armamentarium provides greater flexibility and the possibility of having a normal life span.

1.3.3.4 Resistance selection and therapy guidelines

The world health organization (WHO) and the United-States department of health and human services (DHHS) have established guidelines that are used by the clinicians to identify the appropriate treatment for the management of HIV infection. Initiation of treatment is recommended when the patients' CD4⁺ T cell count is either less than 350 or less than 500 cell/ μ L for WHO and DHHS, respectively. For initial treatment, the preferred regimen is two NRTI in combination with a NNRTI or a PI. In the event of drug resistance, it is recommended to switch for another agent within the same class. When viral failure is detected, a class switching is recommended.

When defining a new NRTI backbone regimen, it is important for the two drugs to have different or bidirectional resistance profile.

In the case of DAPD, the resistance develops slowly *in vitro*, and is associated with mutations at K65R or L74V.^{60, 116, 117} An *in vitro* selection study conducted in our laboratory in HIV-infected primary human lymphocytes demonstrated that ZDV alone selected for a mixture of K70K/R mutations at week 25, and DAPD alone selected for a mixture of K65R or L74V mutations at week 20. When DAPD and ZDV were used in combination, no drug resistant mutations were detected through week 28.¹¹⁸ Therefore, the inclusion of ZDV as a “resistant repellent” in combination with DAPD may prevent or delay the emergence of these mutations.¹¹⁹ These results obtained in our laboratory were consistent with the current understanding that thymidine analogue mutations (TAMs) and the K65R mutations antagonize each other through reduced drug discrimination and excision process, respectively.^{60, 113} In addition, HIV drug resistant mutants susceptible to DXG include viruses containing M184V/I (primary mutation to evolve from majority of first line therapies) and the 69SS double insert.^{62, 103, 120} This drug resistance profile, suggests that DAPD/DXG could be administered in combination with ZDV as second line therapy.^{65, 98}

1.3.3.5 *NRTI toxicity*

The pharmacological measure of toxicity is the therapeutic index, and is defined as the ratio between the cytotoxic concentration (CC_{50}) to the median antiviral concentration (EC_{50}).¹²¹ Antiretroviral drugs were designed to target viral enzymes that are not present in mammalian cells and generally have a high therapeutic index. Thus, an ideal NRTI would have a high affinity for HIV-1 RT and a low affinity for mammalian polymerases.¹²² The most recent drugs, particularly 3TC, (-)-FTC and TDF showed a high therapeutic index.

The earlier antiretroviral drug regimens had high pill burden with twenty (or more) pills per day. Fortunately, treatment has improved steadily with the advent of newer generation of

drugs with longer half-lives resulting in increased dosing convenience, improved potency and tolerability, and increased compliance to therapy. For instance, in July 2006 the all-in-one once a day tablet Atripla[®] became available.⁴⁸ However, it is important to keep in mind that combination therapy might also exhibit side effects. Some HAART combinations are associated with rare but potentially fatal metabolic toxicities, such as lactic acidosis, hepatocellular failure (ZDV, d4T, ddI), lipodystrophy (d4T), pancreatitis (ddI, d4T, or 3TC in children), peripheral neuropathy (ddI, d4T, 3TC).^{122, 123} Other rare side effects include diabetes mellitus (ddI) and myopathy (ddI, ZDV).¹²² ZDV phosphates also cause bone marrow suppression leading to anemia and granulocytopenia.¹²⁴⁻¹²⁷ ABC and its metabolites in plasma have been associated with hypersensitivity. This reaction was mediated by an innate immune defense and was observed in approximately 5% of patients.¹²⁸⁻¹³⁰ ABC has also been associated with increased risks for myocardial infarction.¹¹⁵

Most of these symptoms have been associated with mitochondrial (mt) toxicity.¹³¹⁻¹³³ Other toxicities could arise from the imbalances in endogenous natural nucleotide pools, producing mutations in regulatory genes, inducing chromosomal aberrations, sister chromatid exchange or shortened telomeres, in cultured cells.¹³⁶

1.4 Endogenous nucleotide pool

The endogenous nucleotides interfere with NRTI for phosphorylation and for incorporation by the viral reverse transcriptase. Imbalances in the endogenous nucleotide pool have been associated with both self-synergism of drugs and with DNA mutations.^{77, 134, 135} However, the endogenous nucleotide pool tends to be regulated, maintaining homeostasis thereby preventing metabolic disorders.¹³⁶ Thus it is important to assess the variations of the

endogenous nucleotide pool in cells treated with NRTI. Mechanistically, it is possible that NRTI could directly inhibit the expression of the metabolizing enzymes or perturb allosteric regulations of enzymes responsible for regulating cellular dNTP pools.^{108, 137}

1.4.1 Endogenous nucleotide synthesis

1.4.1.1 *De novo and salvage pathways*

For purines, the *de novo* pathway consists of the synthesis of inosine monophosphate (IMP) from amphibolic intermediates: 11 enzyme-catalyzed reactions convert α -D-ribose-5-phosphate (RMP) to IMP, which plays a central role for the overall purine nucleotide synthesis (**Figure 18**). For pyrimidines, six enzymes, multifunctional proteins, catalyze the *de novo* synthesis. Uridine monophosphate (UMP) here plays a central role in this pathway (**Figure 18**).

Mammals have four deoxyribonucleoside kinases, the cytoplasmic thymidine kinase 1 (TK1) and 2'-deoxycytidine kinase (dCK) and the mitochondrial TK2 and 2'-deoxyguanosine kinase (dGK), which control the salvage synthesis of degraded 2'-deoxyribonucleotides from 2'-deoxyribonucleosides. Bases can also be recycled, adenine or hypoxanthine phosphoribosyl transferase (APRT or HPRT, respectively) catalyzes the transfer: purine (base) + phosphoribosyl pyrophosphate (PRPP) \rightarrow purine monophosphate + PPi.¹³⁸ Salvage reactions require less energy than the *de novo* synthesis.¹³⁶

and since RBV inhibits the conversion of IMP to XMP (**Figure 18**),^{141, 142} it would be expected to result in an increased buildup of the respective NRTI-TP, thereby enhancing anti-HIV potency.^{80, 140, 143, 144} However, combination of RBV with ABC, PMPA (TFV), ZDV, d4T, 3TC and (-)-FTC were antagonistic in MT-2 cells.¹⁴⁵ This antagonism could be explained by a direct competition at the level of phosphorylating enzymes (**Figure 16**) between RBV and ABC PMPA.¹⁴⁶ An increase in TTP and dCTP following RBV treatment might explain antagonistic effect with ZDV, 3TC, (-)-FTC and d4T.¹⁰⁹ It is possible that the NRTI might compete with endogenous nucleosides for phosphorylation by the same kinases and also NRTI-TP with endogenous dNTP for incorporation by the reverse transcriptase.

Although the combinations of NRTI with such antimetabolites have been interesting for elucidating phosphorylation pathways and the interplay between endogenous cellular nucleotide, this approach did not boost NRTI efficacy in humans, and was limited by side effects.^{109, 147}

A similar approach was used to determine which endogenous nucleosides limit DXG phosphorylation.

1.4.2.2 NRTI modify endogenous nucleotide pool size

Nucleoside analogues, by their resemblance to natural nucleosides might affect the endogenous nucleotide pool. The most studied NRTI with respect to influencing natural nucleotide pool was ZDV. Incubation of ZDV for 24 hr significantly decreased TTP and dGTP levels while increasing dATP and dCTP levels in H9 cells^{77, 148} and in PBM cells.¹⁴⁹ Depleted TTP levels following ZDV exposure was also reported in the perfused rat heart, in U937 and raji cell lines.^{150, 151} CEM cells incubated with super-clinical concentrations of ZDV (1,000 μ M) demonstrated reduced dATP, dGTP and TTP level and increased dCTP levels.¹⁵² The effect of ZDV on TTP levels was explained by crystal structure analysis of the TMPK, which

demonstrated that ZDV-MP inhibited its own as well as TMP phosphorylation.^{90, 91} Other NRTI studied including ddC, d4T, 3TC, ddI and ddG also decreased the formation of the corresponding dNTP in PBM cells.¹⁴⁹ However other NRTI like, 3TC, (-)-FTC, PMPA, ABC and CBV did not influence dNTP levels in CEM cells.^{152, 153}

As a consequence, dNTP pool variations may be of clinical relevance for drug combinations. For instance, ZDV was synergistic with ddI, possibly through a decrease in the dATP pool, resulting in an increase in the ddATP/dATP ratio, which could improve the probability of ddATP incorporation by HIV-1 RT. ZDV did not increase ddATP levels directly.^{154, 155}

Since the treatment with ZDV correlates with changes in dNTP pool levels in certain cell lines, we have assessed this effect in primary human PBM cells and in combination with DXG.

1.4.3 Imbalances in the endogenous nucleotide pool can cause toxicity

1.4.3.1 Mitochondrial toxicity

A direct mtDNA and mtRNAs depletion can be caused directly by the NRTI phosphate or by nucleos(t)ide pool imbalances.¹⁵⁶ For instance, a decrease in dGTP levels was associated with a decrease in respiratory chain activity,¹⁵⁷ in ATP levels, and in pyrimidine synthesis and phosphorylation.¹⁵⁸

The mechanism of ZDV associated mt toxicity is still under investigation. Early studies proved that ZDV-MP is responsible for mitochondrial toxicity.¹⁵⁹ However, the mechanism by which ZDV-MP would reach the mitochondria is yet to be elucidated, since mitochondrial TK2 has a poor affinity for ZDV¹⁶⁰ and the mitochondrial transporters do not use dNMP forms as substrates.¹⁶¹ More recent studies associated mitochondrial toxicity with the decrease in TTP levels.¹⁵¹ In addition, ZDV toxicity was reversed by uridine supplementation in hepatocytes and

in mice.¹⁶²⁻¹⁶⁴ However, the role of TTP in mitochondrial toxicity was not confirmed in adipocytes.¹⁶⁵

1.4.3.2 Genotoxicity, mutagenesis

Alterations of the equilibrium of natural nucleotide dNTP may have dramatic genetic consequences for mammalian cells including the induction of mutations, the sensitization to DNA damaging agents, and the production of gross chromosomal abnormalities. Even subtle alteration in the dCTP/TTP balance causes mutation rates to increase.^{135, 166}

Depletion of TTP, decrease in dGTP levels and accumulation of dUTP levels produce DNA breaks in particular, during the S phase. Disturbed pool diminishes the effectiveness of the 3'→5' proofreading endonuclease and increases incorporation of uracil into the DNA.¹³⁴ However, ZDV treatment results in an increase in the retroviral mutation rates by a mechanism, which does not involve alterations in dNTP pools.²⁸

1.4.3.3 2'-deoxyguanosine lymphocyte toxicity

2'-Deoxyguanosine (dGuo) is a cytotoxic compound, which has demonstrated toxicity in B and T cancer cells lines *via* the accumulation of dGTP, which induces apoptosis.¹⁶⁷ These toxic effects are reversed by the addition of adenine or adenosine. Interestingly dGuo and Guo exposure did not demonstrate cytotoxicity against activated PBM cells up to 500 μM for 24 hr.¹⁶⁸

Since imbalances in the endogenous nucleotide pool, including guanine nucleotides may be prognostic factors for toxicities, we developed an assay capable of measuring natural nucleoside triphosphate levels in human primary cells.

1.4.4 Endogenous nucleotide pool vary with cell type and activation

1.4.4.1 Cell type

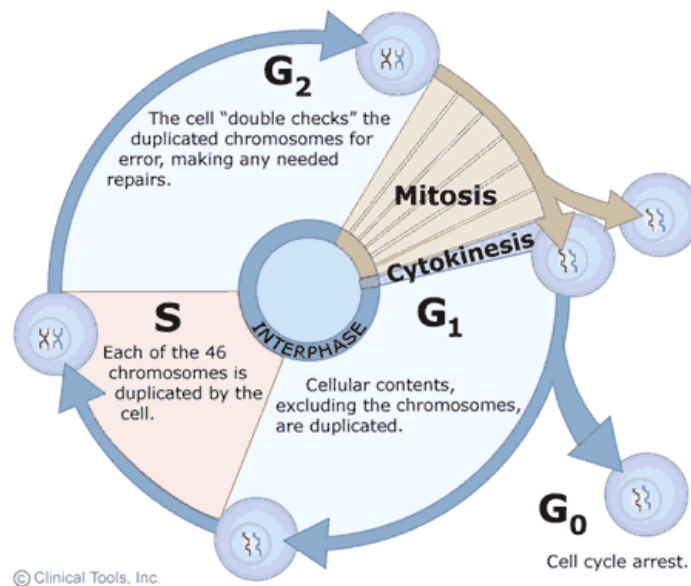
T cells lines such as MT-2, MT-4, H9, CEM, jurkat, ATH8 are most commonly studied for the *in vitro* evaluation of anti-HIV agents.⁷⁰ CEM cells are derived from a malignant human lymphoblastic T cell lymphoma, which produces high levels of IL-2, which acts as an autostimulating cytokine. CEM cells are more commonly used than primary human cells such as peripheral blood mononuclear (PBM) cells and macrophages, since they divide uniformly and produce a lower inter-assay variability. In addition, syncytia formation is easily visible in HIV-infected CEM cells. Furthermore, cancer cells are immortalized and replicate indefinitely, making them very cost efficient to obtain and maintain. However, they may produce results less indicative of cells *in vivo*. Therefore, when possible our laboratory preferred using human PBM cells, which comprise about 50% CD4⁺ T cells and 23% CD8⁺ T cells. About 15% of these cells are activated and produce cytokines.¹⁶⁹ *In vitro*, phytohemagglutinin (PHA) is used to induce T cell mitosis. After 72 hr of PHA-stimulation T cells represent about 98% of the total PBM cells, of which about 40% are dividing.^{170, 171}

In human macrophages the endogenous dNTP synthesis relies almost exclusively on salvage biosynthesis.^{73, 172} Thus, they contain ~200-fold lower dNTP levels than activated CD4⁺ T cells. Despite this limited cellular dNTP substrates environment, HIV-1 can replicate in terminally differentiated macrophages. This ability is likely due to the enzymatic adaptation of HIV-1 RT.¹³⁷ Human dendritic cells and langerhans cells phosphorylated TFV more efficiently and ZDV less efficiently than lymphocytes, CEM and PHA/IL-2 activated PBM cells.¹⁷³ Likewise, human macrophages phosphorylated ZDV less efficiently compared with lymphocytes.¹⁷⁴

1.4.4.2 Cell cycle

The cell cycle is comprised of two stages: M phase and interphase. M phase includes the successive stages of mitosis and cytokinesis. Interphase is divided into G₁, S and G₂ phases, with the S phase being equivalent to the period of DNA synthesis. The G₁ phase, is a regulatory period for continued division or cell cycle exit. The S phase is characterized by chromosome duplication, and DNA synthesis, which requires dNTP (**Figure 20**).

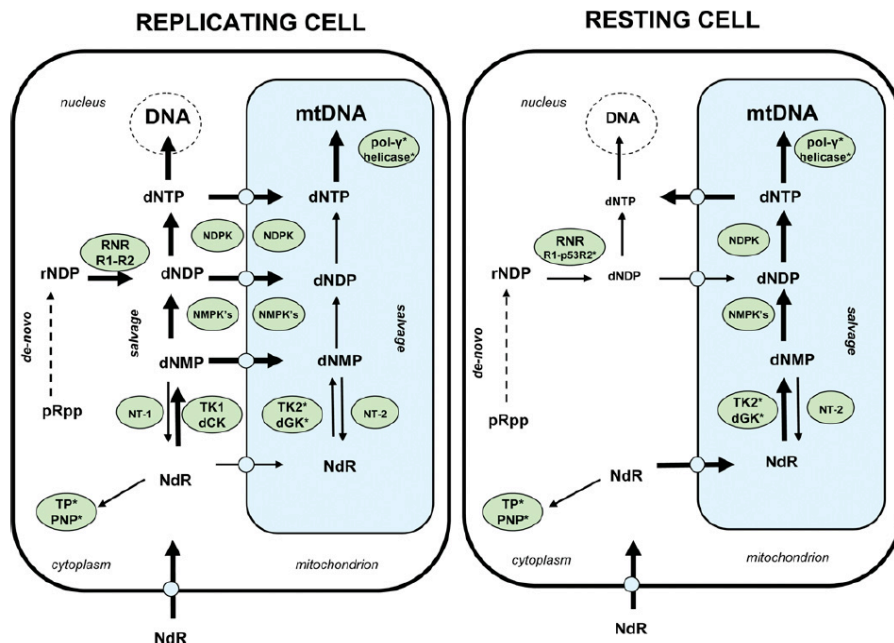
Figure 20: Schematic representation of the cell cycle.



Source: <http://www.le.ac.uk/ge/genie/vgec/images/cellcycle.png>

T lymphocytes meet their dNTP demands *via de novo* and salvage pathways. The salvage biosynthesis is increased in replicating T lymphocytes. Mitochondrial dGK, dCK, TK-2 and 5'-NT are constitutively expressed during cell cycle while cytosolic dGK, dCK, TK-1 and 5'-NT may have a favorable profile in proliferating cells and are considered rate-limiting enzymes.¹⁷⁵ It follows that dNTP levels are lower in resting than in replicating lymphocytes (**Figure 21**).

Figure 21: A schematic illustration of the differences in deoxyribonucleosides in replicating and resting cells.¹⁷⁶



Differential NRTI phosphorylation is related to expression and efficiency of kinases, intracellular dNTP concentrations and incubation times. The rate limiting steps in the phosphorylation of d4T and ZDV are catalyzed by TK 1 and TMPK (**Figure 16**), respectively. Both enzymes are upregulated in the “S” phase of the cell cycle (**Figure 20**).^{79, 88, 89, 177} Therefore, the respective triphosphates are also elevated in dividing cells. Conversely for some purines and cytidine analogues NRTI-TP levels are similar in activated and resting cells. However, the ratio NRTI-TP/dNTP is greater in resting than in activated cells.¹⁴⁹

The assay methodology used for this project has sensitivity to measure NRTI-TP and dNTP in lymphocytes and macrophages. This tool could prove valuable for the mechanistic interpretation of differences in NRTI potency between PBM cells and macrophages, which act as an important reservoir of HIV-1 in the body.

1.5 Detection and quantification of natural and synthetic nucleos(t)ides

Mass spectrometry (MS) is currently the instrument of choice for the identification and quantification of drugs with increased accuracy and sensitivity in pharmaceutical research laboratories, academia and industry. A mass spectrometer analyzes ionized molecules according to their mass to charge (m/z) ratio. The impact of the ions on an electron multiplier generates a current, which is translated into a mass spectrum. Combination of liquid chromatography (LC) with mass spectrometry enhances the sensitivity of detection particularly for applications in complex biological matrix. Nucleosides and nucleotides are small polar molecules present in low quantities in intracellular system and are therefore suitable for LC-ESI(Electrospray ionization)/MS detection.

1.5.1 Chemical properties of nucleosides and nucleotides

Nucleobases are weak bases as demonstrated by the pK_a of their protonated forms. The order for basicity is C (cytosine) > A (adenine) > G (guanine), with T (thymine) and U (uracil) exerting no basic functions in aqueous media. The pK_a of the nucleobases decrease with the addition of a deoxyribose and even more with the addition of a ribose due to the inductive effect of the sugar unit. The pK_a of nucleosides increases with the addition of phosphates, which form nucleotides, due to the electrostatic interactions between the protonated base and the negatively charged phosphate group. The possible protonation site is the nitrogen for A, C, and G. T and U exhibit a significantly lower proton affinity.¹⁷⁸ Most importantly, nucleosides and nucleotides can be solubilized in a mixture of aqueous and organic solvents: properties, which can be exploited for optimizing liquid chromatography and mass spectrometry analysis.

1.5.2 Electrospray ionization tandem mass spectrometry

1.5.2.1 Ion source: How to convert a liquid stream into volatile ions?

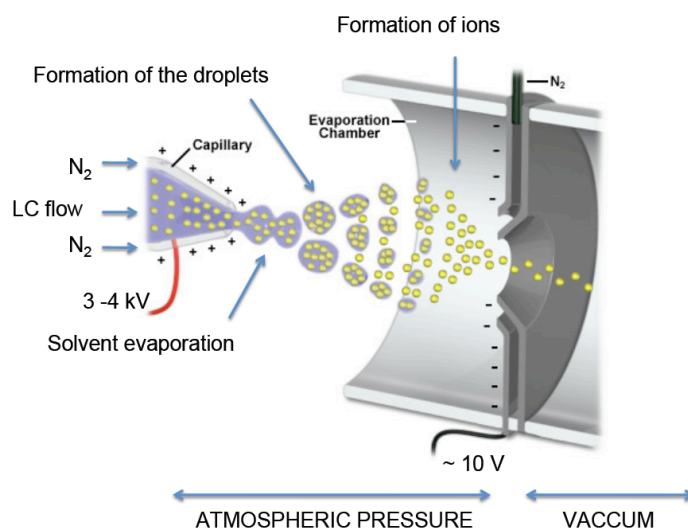
The introduction of the sample to the mass spectrometer and the generation of ions were greatly improved 40 years ago when Dole *et al.* developed the electrospray ionization (ESI) at atmospheric pressure. ESI is a soft ionization process used to generate gaseous ionized species from liquid solutions, *via* the production of a fine liquid spray in the presence of a strong electrical field.¹⁷⁹

The sample solution is sprayed from an electrospray needle to which a high voltage is applied (~2,500 to 4,500 V depending on the nature of the molecules and the solution). Individual droplets containing an excess of charge (positive or negative depending on the direction of the potential gradient) are released from the liquid jet extending from the tip of the Taylor cone.¹⁸⁰ The thermal energy of the ambient gas leads to solvent evaporation, which reduces the size of the droplets and increases the repulsion between the charges at the surface. When the repulsion overcomes the cohesive force of the surface tension, the Rayleigh limit is reached and coulomb fission occurs. This explosion produces a dispersion of smaller droplets, which continue to evaporate. Small charged droplets are capable of producing gas-phase ions (**Figure 22**).

Two theories have been formulated to explain the mechanism by which solute ions are formed from charged droplets namely, a Charge Residue Model (CRM)¹⁷⁹ and the Ion Evaporation Method (IEM).¹⁸¹ In the CRM the process of coulomb explosion continues until the formation of an ion containing a single analyte molecule. The molecule retains some of its droplet's charge to become a free ion as the last fraction of solvent vaporizes.¹⁷⁹ The IEM assumes that before a droplet reaches the ultimate stage, which would be a diameter of less than

10 nM, its surface electric field becomes sufficiently large to directly emit an analyte ion at the surface of the droplet over the energy barrier that prevents its escape.¹⁸¹ The IEM would apply to small inorganic ions while the CRM to macromolecules.¹⁸² The ions formed are electrostatically attracted to the orifice inlet of the mass spectrometer. Positive ions are formed *via* protonation or cation attachment and negative ions by deprotonation, cation dissociation or anion attachment.¹⁸³

Figure 22: Illustration of major processes in the atmospheric pressure region of an ESI ion source run in the positive ion mode.



Adapted from: http://www.magnet.fsu.edu/education/tutorials/tools/images/ionization_esi.jpg

Technically, after entering ion source interface, the ion transfer tube assists in desolvating ions, which are drawn from the atmospheric pressure region and transported to the vacuum manifold by a decreasing pressure gradient.

Understanding the principles of ion generation in the liquid phase and its conversion to the gas phase in the electrospray probe may be used to guide the mass spectrometer user regarding the choice of liquid phase introduced in the source. Since the intended result is the production of a gaseous ion phase, it is usually preferable to select a volatile solvent, and to avoid high concentrations of salts.

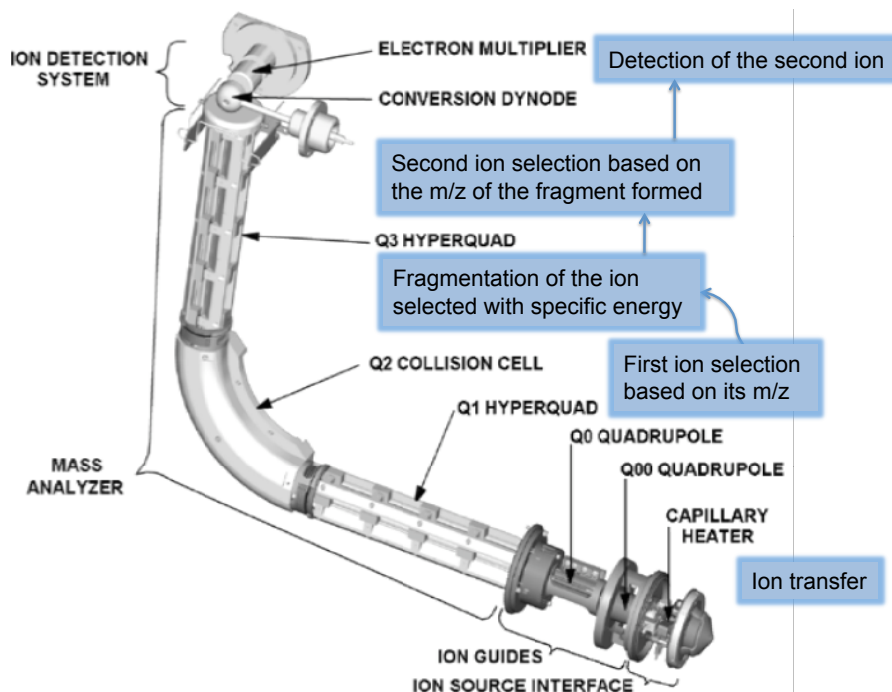
1.5.2.2 Mass analyzers: How to find a “needle in a haystack”?

Prior to the development of mass spectrometers, the most sensitive and specific techniques for studying small molecules in biological matrices relied on radiolabeled molecules and/or the development of radioimmunoassays.¹⁸⁴ However the emergence of mass spectrometry and more precisely tandem mass spectrometry offered a broader range of applications.

The mass analyzer separates ions according to their mass-to-charge ratio (m/z) and then passes them to the ion detection system. Several types of mass analyzers are commercialized, and each of them has a specific application. For instance, time of flight mass spectrometers are useful to calculate the exact mass of the compounds; linear traps are favored for multiple fragmentations and will help identify the structure of the compounds of interest. Hybrid mass spectrometers combining two different kind of mass spectrometer improve the global mass accuracy and resolution useful for the identification of unknown metabolites or macromolecules.¹⁸⁵

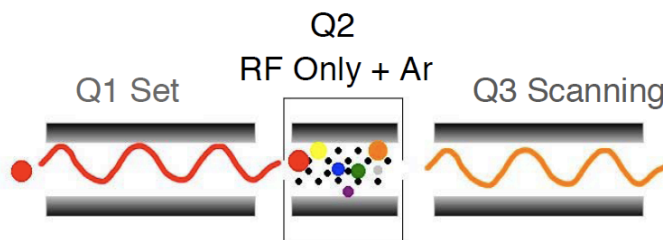
Specificity of analysis is one of the major attributes of a tandem mass spectrometer instrument comprising of three quadrupoles, of which two precede and follow a collision cell, (two mass spectrometers in series, MS/MS). Ions entering the first quadrupole (Q1) will be analyzed according to their m/z and passed on to the collision cell (Q2) where they will be fragmented using ultra pure argon. The fragments are then analyzed by the third quadrupole (Q3) before reaching the detector (**Figure 23**).

Figure 23: Representation of the quadrupoles inside the TSQ quantum ultra. Adapted from the TSQ hardware manual.¹⁸⁶



The analyzer can be used in several ways. In full scan mode, the MS screens all the m/z within the range desired. When activating the “data dependant scan mode”, it is possible to perform selective fragmentation of the most intense ions. The single ion monitoring (SIM) mode consists of selecting only some ions of interest (parent m/z) while the selected reaction monitoring (SRM) mode consists of selecting both parent and product m/z . The SRM mode provides the most specificity (**Figure 24**).

Figure 24: Illustration of the MS/MS scan mode.¹⁸⁶



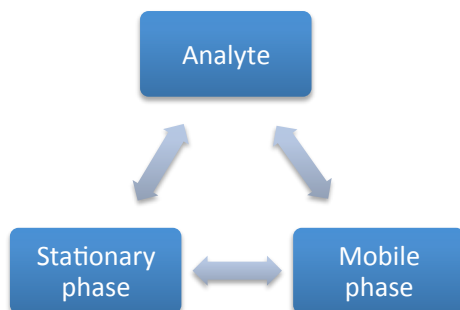
The detection parameters of the analyte of interest, m/z (Q1 and Q3), collision energy (Q2), tube lens voltage (Q0), capillary temperature or spray voltage (ESI source), can be optimized using a direct infusion method.

Tandem mass spectrometry can produce sensitivity in the picogram range with high specificity and nearly instantaneous response, making ESI-MS/MS a state of the art technology for pharmaceutical and clinical applications. Therefore, this methodology was chosen for the detection of nucleosides and nucleotides in cells and plasma.

1.5.3 High Pressure Liquid Chromatography (HPLC)

Chromatography is based on a basic principle of exchange of an analyte between a mobile and a stationary phase (**Figure 25**).

Figure 25: Representation of the interactions governing liquid chromatography.



Mikhail Tvest designed the first liquid adsorption column, using calcium carbonate as adsorbent and petrol ether/ethanol mixtures as eluent to separate chlorophylls and carotenoids. This technique gave its name to the chromatography.¹⁸⁷

The first step in the optimization consists of choosing an optimal HPLC column, which fits the chemical properties of the analyte based on its molecular size, polarity, and electrical charge. The separations based on polarity are classified according to the nature of the mobile and stationary phase. In normal phase chromatography, the stationary phase is polar and the mobile phase non-polar. It is the opposite in reverse phase chromatography. Hydrophilic interaction

chromatography (HILIC) and hydrophobic interaction chromatography (HIC) are also based on the analyte polarity and are the innovative versions of normal and reverse phase chromatography, respectively. The separations based on charge are named ion exchange chromatography (IEC). The separations based on size are divided into two categories, namely size-exclusion chromatography (SEC) or gel permeation chromatography (GPC).¹⁸⁸

The HPLC method optimization also depends on the number of compounds to be analyzed, the amount of sample available and how much do the compounds of interest differ from the biological matrix.

1.5.3.1 Reverse phase chromatography

Reverse phase HPLC is currently the most commonly used separation method for pharmaceutical research. A great variety of columns are available, which are packed with porous silica beads with silanols on their surface and are covalently bonded to alkyl chains. The number of carbons on the alkyl chains varies from 4 to 18 and is selected based on the polarity of the molecules analyzed; increasing the number of carbon atom on the chain reduces the polarity of the stationary phase.

Non-polar compounds will be strongly retained due to their affinity for the stationary phase, while polar compounds will be eluted faster in the aqueous mobile phase. In order to accelerate the elution of non-polar compounds, a gradient can be applied using increasing proportions of organic solvent (typically methanol or acetonitrile) so that the analytes will be washed more rapidly from the stationary phase.

1.5.3.2 Ion-exchange chromatography

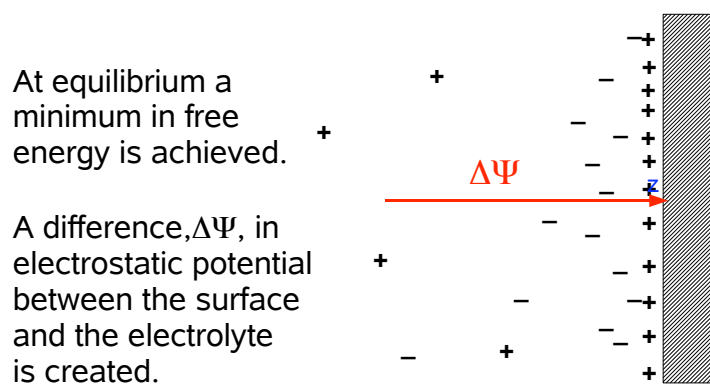
In anion exchange chromatography, the stationary phase is positively charged and retains anions. The opposite principles are applied for cation exchange chromatography. The stationary

phase is characterized by the nature and the strength of the basic or acidic function at their surface. Weak ion exchangers are chemically modified with primary, secondary, or tertiary amines or carboxylic functions which may be neutralized above pH 12 or below pH 3, where they lose their ability to retain ions by charge. However, when used between the appropriate pH range, they retain strong ions. Strong ion exchangers exhibit quaternary amines or sulfonic acids functions, which are always ionized and will retain weak ions.¹⁸⁸

Theoretically, ion-exchange chromatography may be defined as the relative affinity of sample ions for the sites of opposite charge in the stationary phase. This can be achieved either through electrostatic attraction of highly charged ion or through hydrophobic attraction and hydrogen bonding.¹⁸⁹

Another form of ion exchange is known as ion-pair chromatography. Unlike ion-exchange columns, which contain specific charges on their surface, ion-pair chromatography relies on a reverse phase column with the addition of an ion-pair reagent in the mobile phase. A typical ion-pair reagent is tetraalkylammonium salt in combination with an inorganic co-ion.¹⁸⁹ Two theories explain the mechanism of ion-pair chromatography: a stoichiometric and a non-stoichiometric. The stoichiometric theory is based on equilibria between ionic modifier and analytes. The partition mechanism between the mobile phase and the stationary phase can be described by a general equation: $C^+ (mobile) + A^- (mobile) \rightleftharpoons C^+A^- (stationary)$, where C^+ represents a cation and A^- represent an anion. The non-stoichiometric theory models the ionic solute as under the influence of all other ions in the system and presumes the existence of an electrical double layer (**Figure 26**).¹⁹⁰

Figure 26: The model of electrical double layer applied to ion-pair chromatography.¹⁹¹



The stoichiometric theory includes the ion-pair model in which ion-pairs are formed either in the stationary or the mobile phase, which will increase or decrease their retention, respectively. To complete this ion-pair model, the dynamic ion exchange has been described where either the solute and the modifier or the ion-pair formed in the mobile phase are absorbed on the stationary phase. However, Bildingmeyer *et al.* found no evidence for ion-pair formation in the mobile phase.¹⁹² The interaction between the solute and the ion-pair reagent would therefore be restricted at the stationary phase. The last assumption led to a non-stoichiometric explanation, in which the modifier establishes an electrical potential distribution in space and the sample ions respond to that potential (**Figure 26**).¹⁹³

1.5.4 Quantification of nucleosides and nucleotides by LC-MS/MS

Coupling liquid chromatography with tandem mass spectrometry increases the specificity by adding separation in time to separation based on m/z . In addition, the liquid chromatography acts as a concentrating and purifying step. However, the use of ESI/MS as a detection method limits the use of HPLC mobile phase to volatile solvent and not non-volatile or concentrated salts. This is easily manageable in the case of nucleoside analysis, but may be difficult for phosphorylated metabolites, which are negatively charged, and hydrophilic. As mentioned in

section **1.5.1**, nucleotides are polar, basic compounds, which often require the use of ion-pair reagent, to exhibit retention on a lipophilic reverse phase column. Therefore, it was necessary to select a volatile ion-pair reagent and optimize the concentration of ammonium salt, the inorganic co-ion, to levels that do not adversely affect the ionization by electrospray.¹⁹⁴ The method also made use of a microbore column (100 mm x 1 mm) to reduce the flow rate and the amount of ion-pair reagent introduced in the ion source to satisfactory levels.

2 **Objectives**

The focus of this work was to develop a LC-MS/MS method for studying the metabolism of FDA approved and novel NRTI including DXG and its prodrug DAPD in primary human cells in culture and in humans. LC-MS/MS is the preferred instrument for these measurements, due to its sensitivity and its selectivity. Although analytical methods exist for quantifying nucleosides and nucleotides in biological samples, it should be optimized to specific NRTI and NRTI-TP measurement, to achieve the nanomolar limit of quantification needed for clinical studies. Thus, a method was developed and partially validated for quantifying simultaneously the phosphorylated metabolites of FDA approved NRTI as well as DXG and endogenous dNTP in human PBM cells (primary target for HIV-1) and macrophages (one of the potential viral reservoir). These assays could provide additional information to understanding the failure of current therapies to eradicate the virus. This novel assay will be used to evaluate potential compounds that have demonstrated antiviral activity with no cytotoxic effect *in vitro* as part of our drug discovery program to quantify the amount of triphosphate delivered to the various cells and potentially correlate to predicting clinical outcome. One major application was the study of DXG phosphorylation in human PBM cells alone and in combination with other antiviral agents. Finally, a proof-of-concept study for the use of DAPD and reduced dose of ZDV was conducted in HIV-1 infected individuals. Therefore, another method was developed and validated for the simultaneous quantification of DAPD, DXG and ZDV simultaneously in plasma, and scaled up to analyze over 600 patient samples.

3 Material and methods

3.1 Chemicals and Reagents

Reference standards for amdoxovir (DAPD) and 9- β -D-(1,3-dioxolan-4-yl)guanine (DXG) were obtained from RFS Pharma, LLC (Tucker, GA). ZDV was obtained from Samchully Pharmaceuticals Co. Ltd. (Seoul, Korea). 2,6-diaminopurine-2'-deoxyriboside (DPD) and 2'-deoxyadenosine (2'-dA) were purchased from Sigma (St Louis, MO, USA) and 2'-deoxycoformycin (DCF), a potent adenosine deaminase inhibitor, from Waterstone Technology LLC (Carmel, IN). Abacavir (ABC), carbovir (CBV), emtricitabine [(-)-FTC], tenofovir disoproxil fumarate (TDF), tenofovir (TFV, PMPA), lamivudine (3TC) and ribavirin (RBV) were available in the laboratory. The corresponding nucleotides of each of these drugs were synthesized in our laboratory. 2'-deoxyguanosine (dGuo), guanosine (Guo), guanine (Gua), cytidine (Cyd), 2'-deoxycytidine (dCyd), adenosine (Ado) and isotopically labeled nucleotides, [$^{13}\text{C}^{15}\text{N}$]dATP, [$^{13}\text{C}^{15}\text{N}$]dGTP, [$^{13}\text{C}^{15}\text{N}$]dCTP, [$^{13}\text{C}^{15}\text{N}$]TTP, [$^{13}\text{C}^{15}\text{N}$]ATP, [$^{13}\text{C}^{15}\text{N}$]GTP, [$^{13}\text{C}^{15}\text{N}$]CTP, and [$^{13}\text{C}^{15}\text{N}$]UTP were purchased from Sigma Aldrich (St. Louis, MO). Nucleosides and nucleotides were at least 98% pure. Interleukin-2 (IL-2) was purchased from Sigma Aldrich (St. Louis, MO), phytohemagglutinin (PHA) at J-Oils Mills, Inc. (Tokyo, Japan), phosphate-buffered saline (PBS 10X), L-glutamine and penicillin/streptomycin from Cellgro/Mediatech, Inc. (Manassas, VA), fetal bovine serum (FBS) from Atlanta Biologicals (Lawrenceville, GA) and RPMI-1640 from Hyclone (Logan, UT). Solutions of saline (0.9% NaCl) were obtained directly from the VA hospital pharmacy (Decatur, GA).

Ammonium phosphate [$(\text{NH}_4)_3\text{PO}_4$] and *N,N*-dimethylhexylamine (*N,N*-DMHA) were purchased from Sigma Aldrich, (St. Louis, MO). Hexylamine (HA) and ammonium formate (NH_4COOH) were purchased from Acros Organics (Morris Plains, NJ). HPLC-grade methanol,

acetonitrile, ammonium hydroxide (NH₄OH), and ammonium acetate (NH₄CH₃COOH) were obtained from Fisher Scientific International, Inc. (Pittsburgh, PA). Ultrapure water was generated from Elga Ultrapurelab equipped with U.S. filters. Formic acid (HCOOH) and ammonium hydrogen carbonate (NH₄HCO₃) were purchased from Fluka (St. Louis, MO) and high-pressure nitrogen and ultrahigh-purity-high-pressure argon from Nexair, LLC (Suwanee, GA).

3.2 Isolation, differentiation and culture of cells

3.2.1 PBM cells isolation and stimulation

Human PBM cells were isolated from buffy coats derived from healthy HIV-1 negative, HBV/HCV negative donors (Life South Community Blood Center, Gainesville, FL) by Ficoll-Hypaque (Histopaque 1077: Sigma Aldrich, St. Louis, MO) discontinuous gradient centrifugation at 1,000g for 30 min, washed twice with 1X PBS (pH 7.2), and pelleted at 300g for 10 min.¹⁹⁵ Four to eight donors were pooled every time. Unactivated PBM cells were maintained in PHA-free RPMI media supplemented with 20% fetal calf serum, 1% penicillin/streptomycin and 2% L-glutamine for 72 hr prior to cellular pharmacology studies. Activated PBM cells were maintained analogously except supplemented with 6 µg/mL PHA.

3.2.2 Differentiation of PBM cells in macrophages

Monocytes were isolated from buffy coats (see § 3.2.1). Isolated cells were enriched CD14⁺ monocytes using a Rosette Sep antibody cocktail (Stem Cell Technologies, Vancouver, British Columbia). Cells were seeded at a concentration of 10⁶ cells/well for 1 hr at 37°C, 5% CO₂ to confer plastic adherence prior to repeated washes with 1X PBS. For cellular pharmacology studies, the activated macrophages were maintained in 100 U/mL m-CSF containing medium (R&D Systems, Minneapolis, MN) supplemented with 20% fetal calf serum

(Atlanta Biologicals, Lawrenceville, GA), 1% penicillin/streptomycin (Invitrogen, Carlsbad, CA) for 7 days (37°C, 5% CO₂) prior to cellular pharmacology studies. For resting macrophages, cells were maintained in m-CSF-containing medium for 18 hr prior to two washes with 1X PBS to remove m-CSF, and subsequent culture in m-CSF free medium supplemented with 20% fetal calf serum and 1% penicillin/streptomycin for 6 more days prior to cellular pharmacology studies. For all conditions, macrophages were stained with CD11b-APC (Miltenyi Biotec, Auburn, CA) and subjected to fluorescence activated cell sorting to determine purity of > 99%.

3.3 Cellular pharmacology studies

For all cellular pharmacology studies, DXG was used instead of DAPD to bypass the first step deamination. Although adenosine deaminase is a ubiquitous enzyme, DAPD deamination primarily takes place during the first liver pass and in the circulation, but would not occur as efficiently in media.

3.3.1 Studies in PBM cells and in macrophages

After preparation of cells as described above, activated and unactivated macrophages and PBM cells were exposed to 10 µM of ZDV, ABC, (-)-FTC, TDF, 3TC or DXG for 4 hr, 37°C, 5% CO₂.

3.3.2 DXG phosphorylation studies in human PBM cells

Activated human PBM cells were treated with 10 µM DXG (diluted in DMSO) for 4 hr and 24 hr either alone or in combination with 10 or 100 µM of dGuo, Guo, Gua or Gua + Ado. RBV was used as a positive control at 30 µM. Experiments were performed on three different occasions in triplicate or duplicate i.e., 8 and 7 individual data points were analyzed per condition, at 4 hr and 24 hr, respectively.

3.3.3 DXG/ZDV combinations

To understand the kinetics of the combination of DXG and ZDV, activated PBM cells were incubated for up to 72 hr with 10 μ M DXG, 10 μ M ZDV, 10 μ M DXG + 10 μ M ZDV or with DMSO for control. This experiment was conducted in triplicate and the cells were harvested at the following time points: 0, 2, 4, 8, 12, 24, 48 and 72 hr. In addition, the time points from 2 to 24 hr were repeated in four independent experiments. To study the effect of ZDV on DXG phosphorylation in unactivated PBM cells, both activated and unactivated cells were treated with 10 μ M of DXG alone or in the presence of ZDV at 1, 10, 30 and 100 μ M for 4 hr and 24 hr. This experiment was performed in triplicate.

3.3.4 DXG/3TC and DXG/(-)-FTC combinations

Activated human PBM cells were exposed to DXG 10 μ M alone or with increasing concentrations of 3TC or (-)-FTC at 1, 10, 30 and 100 μ M, for 4 hr. Additionally, PBM cells were exposed to 3TC or (-)-FTC at 10 μ M alone or with increasing concentrations of DXG at 1, 10, 30 and 100 μ M for 4 hr. These experiments were performed in triplicate. In order to antagonize DXG, 3TC and (-)-FTC phosphorylation, Guo or dCyd at 10 and 100 μ M were incubated along with DXG, 3TC and (-)-FTC at 10 μ M.

3.3.5 DXG decay

DXG was incubated at 10 μ M in activated PBM cells for 4 hr. The media was removed and the cells were washed twice using a solution of ice cold 1X PBS. The cells were then incubated in a drug-free media for 48 hr and harvested at 30 min, 1, 2, 3, 4, 6, 8, 10, 12, 24 and 48 hr. The dephosphorylation rate of DXG-TP in PBM cells was calculated from the natural logarithm decay of the concentrations found in cells. For all experiments the viability of the cells was greater than 95%.

3.4 Collection of samples for clinical trial

As part of this project, clinical plasma samples were analyzed as described below from a Phase IIa study evaluating the antiviral activity, tolerability and pharmacokinetics of DAPD alone or in combination with two doses of ZDV. The protocol was approved by the following ethics committees in Argentina: Facultad de Medicina- Universidad de Buenos Aires, Comité Independiente de Etica en Investigación (CIEI10 FM-UBA) and the Administración Nacional de Medicamentos, Alimentos y Tecnología Médica (ANMAT), and written informed consent was obtained from all subjects. Subjects were randomized to DAPD 500 mg bid, DAPD 500 mg plus ZDV 200 or 300 mg twice daily from days 1 to 9, and received one dose on day 10. In each arm, subjects were randomized 3:1 to DAPD or placebo. Hispanic HIV-infected volunteers (12 m, 12 f) not receiving antiretroviral therapy, plasma HIV-1 RNA (viral load, VL) $4.5 \log_{10}$ copies/mL (3.6 – 6.0) and $CD4^+$ cell count 417 cells/mm³ (201-1071) at baseline were enrolled. The mean age was 34 years (21 to 52 years) and mean body weight was 68 kg (50.1 to 92.6 kg). All 24 randomized subjects who were dosed completed the study and were included in the PK analysis. Blood samples were drawn after the first dose on day 1 at 0, 0.5, 1, 2, 4, 6, 8, 10 and 12 hr and on day 10 at 0, 0.5, 1, 2, 4, 6, 8, 10, 12, 24 and 48 hr, following the last dose, pre-dose on day 5 and collected in DCF containing EDTA tubes to prevent deamination of DAPD after sample collection. Blood samples were centrifuged and stored at -80°C before being assayed using a LC-MS/MS method. Safety was evaluated by proportion of \geq Grade 3 adverse events per treatment, using AIDS Clinical Trials Group (ACTG) toxicity grading scale and antiviral activity [changes in plasma HIV-1 RNA \log_{10} (viral loads)], were determined daily.^{65, 196}

3.5 Preparation of clinical samples

3.5.1 Intracellular extraction

After incubation, extracellular media was removed and cells were washed with 10 mL ice-cold NaCl 0.9% to remove any residual medium. Cells were resuspended in 70% methanol overnight, and extracts were centrifuged at 20,000g for 10 min. Supernatant was subsequently dried, and resulting samples were reconstituted in the corresponding HPLC mobile phase A for LC-MS/MS analysis. 3TC, 3TC-MP and 3TC-TP were used as internal standards for all experiments and for method development and validation. However, for the measurement of 3TC-TP, ddA-TP was used as internal standard. A total of 10 $\mu\text{L}/10^6$ cells of internal standard (IS) were added to the suspension in order to obtain a final IS concentration of 100 nM upon sample reconstitution.

3.5.2 Plasma extraction

Human blood from healthy subjects was obtained from the American Red Cross (Atlanta, USA) and used as control human plasma. Eppendorf centrifuge model 5417C (Eppendorf North America, NY, USA) was used for plasma preparation. DAPD and DXG were extracted from human plasma using a methanol-based protein precipitation procedure, followed by LC-MS/MS analysis. Prior to analysis, calibration standards, quality controls (QC) and clinical samples (collected at Aclires-Argentina SRL, Buenos Aires, Argentina), were thawed and allowed to equilibrate at room temperature. One hundred μL of plasma (calibration, QC and subject samples) were transferred to a 1.5 mL polypropylene snap-cap tubes and spiked with 400 μL of methanol-based solution containing internal standard (DPD, 250 ng mL^{-1}). The microcentrifuge vials were capped and vortex mixed for 1-2 sec. The samples were allowed to sit for 15 min before being mixed under vortex at high speed for 30 sec to inactivate any HIV present in the

samples. The vials were centrifuged at 14,000g for 5 min followed by the removal of 200 μ L of the supernatant to two microcentrifuge tubes, which was evaporated to dryness under a stream of air. The residue was reconstituted in 125 μ L of 2 mM ammonium formate, pH 4.8 and 0.04 mM 2'-dA and briefly centrifuged at high speed. The supernatant was transferred to a Costar Spin-X microcentrifuge tube filter (Corning Costar, Lowell, MA) and centrifuged at 14,000g for 5 min. Fifty μ L of the filtrate were transferred to 1.5 mL vials containing an insert of 200 μ L, and 5 μ L were injected directly into the chromatographic system.

3.6 LC-MS/MS

3.6.1 Ultimate 3000 and TSQ Quantum Ultra

The HPLC system was a Dionex Packing Ultimate 3000 modular LC system comprising of a ternary pump, vacuum degasser, thermostated autosampler, and thermostated column compartment (Dionex, CA). A TSQ Quantum Ultra triple quadrupole mass spectrometer (Thermo Scientific, Waltham, MA, USA.) was used for detection. Thermo Xcalibur software version 1.3/2.0 was used to operate HPLC, the mass spectrometer and to perform data analyses.

3.6.2 LC-MS/MS for nucleotides

3.6.2.1 Calibration Curve Preparation and LC-MS/MS Analysis

Calibration standards covering the range of 0.5-1,000 nM were prepared by adding appropriate volumes of serially diluted stock solutions to a nontreated cell pellet. Six calibration concentrations (0.5, 1, 5, 10, 50, and 100 nM) and three quality control standards (1, 10, and 100 nM) were used to define the calibration curve and for partial assay validation, respectively for DXG, DXG-MP, DXG-TP, TFV, TFV-DP, (-)-FTC-TP, and CBV-TP. Six calibration concentrations (5, 10, 50, 100, 500, and 1,000 nM) and three quality control standards (10, 100,

and 1,000 nM) were used to define the calibration curve and for partial assay validation, respectively, for ZDV-MP, ZDV-TP, [¹³C¹⁵N]dATP, [¹³C¹⁵N]dGTP, [¹³C¹⁵N]dCTP, and [¹³C¹⁵N]TTP. Calibration curves were calculated using the ratio of the analyte area to the internal standard area by linear regression using a weighting factor of 1/x. The samples were centrifuged for 10 min at 20,000g to remove cellular debris, and the supernatant was evaporated until dry under a stream of air. Prior to analysis, each sample was reconstituted in 100 μL/10⁶ cells of mobile phase A and centrifuged at 20,000g to remove insoluble particulates.

3.6.2.2 Chromatography Columns

Three columns were evaluated: PFP (pentafluorophenyl) propyl, 50 mm x 1 mm, 3 μm particle size, (Restek, Bellefonte, PA); Hypersil GOLD-AQ (aqueous), 100 mm x 1 mm, 3 μm particle size; and Hypersil GOLD-C18, 100 mm x 1 mm, 3 μm particle size (Thermo Scientific, Waltham, MA).

3.6.2.3 Ion-pair method development using Hypersil GOLD-C18 column

Ammonium phosphate buffer (1 and 2 mM) and ammonium hydrogen carbonate (10 and 20 mM) were assayed by preparation of four separate buffers containing 3 mM HA. The pH 7, 8, 9.2 and 10 were tested using four separate buffers containing 10 mM ammonium hydrogen carbonate and 3 mM HA. To obtain pH 7 and 8, and pH 10, the buffer was adjusted with formic acid and ammonium hydroxide, respectively. No adjustments were required to obtain pH 9.2. Finally, the HA concentration at 0, 3, 6, 9 and 12 mM was optimized using a buffer consisting of 1 mM ammonium phosphate. Standard calibration solutions prepared at 50 nM were used. The factors that were considered to discriminate the general quality of the chromatography for all analogues were the tailing factor ($Tf = (A_{5\%} + B_{5\%}) / 2A_{5\%}$, where A and B are the left and the right peak width at 5% of height, respectively), the peak capacity ($k' = (t_r - t_o) / t_o$, where t_r is the retention

time of the compound of interest and t_o is the retention time of an unretained compound), the effective plate number [$Ne = 5.54(t_r - t_o/w_{1/2})$, where $w_{1/2}$ is the peak width at half height] and the peak area.

3.6.2.4 *Optimized ion-pair method used for partial validation.*

A linear gradient separation was performed on a Hypersil GOLD-C18 column (Thermo Scientific, Waltham, MA). The mobile phases A and B consisted of 2 mM ammonium phosphate buffer containing 3 mM HA and acetonitrile, respectively. The flow rate was maintained at 50 $\mu\text{L min}^{-1}$ and a 45 μL injection volume was applied. The autosampler was maintained at 4°C, and the column at 30°C. The gradient used for separation started with 9% acetonitrile and reached 60% in 15 min. The return to initial conditions was achieved without the ramp and the equilibration time was 14 min.

3.6.2.5 *Mass spectrometry conditions.*

The mass spectrometer was operated in positive or negative ionization mode with a spray voltage of 3.0 kV and 4.5 kV, respectively and at a capillary temperature of 390°C; sheath gas was maintained at 60 (arbitrary units), ion sweep gas at 0.3 (arbitrary units), auxiliary gas at 5 (arbitrary units). The collision cell pressure was maintained at 1.5 mTorr with 0.01 sec scan time, 0.1 scan width ($\Delta m/z$) and 0.7 full width half mass (FWHM) resolution (unit resolution) for both quadrupoles (Q1 and Q3) at all transitions. The intensity of selected product ion in the MS/MS spectrum of each compound was optimized using direct infusion of the analytes in the corresponding mobile phase at a concentration of 100 μM , which was loaded separately into the instrument using a syringe pump at 5 $\mu\text{L min}^{-1}$. These selected reaction-monitoring (SRM) transitions were further optimized for each compound at the exact proportion of mobile phase/acetonitrile in source using LC-MS/MS injections. The following scan parameters were

utilized: precursor ion m/z, product ion m/z, collision energy, tube lens offset and ionization mode (**Table 02**).

Table 02. Parent compounds m/z, product compounds m/z, collision energy (V) and tube lens (V) values for all nucleosides, nucleotides, NRTI and NRTI-TP.

	Parent m/z	Product m/z	Collision Energy (V)	Tube Lens (V)	Ionization mode	Retention time (min)
3TC	230	112	15	70	+	3.4
3TC-MP	310	112	27	70	+	4.1
3TC-TP	470	112	27	90	+	8.4
DXG	254	152	15	70	+	3.1
DXG-MP	334	152	26	90	+	4.1
DXG-TP	494	152	30	130	+	8.1
TFV	288	176	20	70	+	4.0
TFV-DP	448	270	27	130	+	9.0
ZDV-MP	348	81	35	90	+	4.5
ZDV-TP	506	380	18	90	-	12.2
(-)-FTC-TP	488	130	30	130	+	9.1
CBV-TP	488	152	35	130	+	10.2
dATP	492	136	20	116	+	9.0
dGTP	508	152	30	110	+	6.8
dCTP	468	112	30	90	+	6.2
TTP	483	81	20	90	+	5.5
[¹³ C ¹⁵ N]dATP	507	146	20	116	+	9.0
[¹³ C ¹⁵ N]dGTP	523	162	30	110	+	6.8
[¹³ C ¹⁵ N]dCTP	480	119	30	90	+	6.2
[¹³ C ¹⁵ N]TTP	495	134	20	90	+	5.5

All nucleosides and nucleotides were analyzed in positive mode from 2 to 11 min, except for ZDV-TP, which was analyzed between 11 and 13 min in negative mode. The chromatography method developed had optimal separation between the last two eluted nucleotides, namely CBV-TP, and ZDV-TP to enable a switch in polarity (from positive to negative) at 11 min. Before 2 min and after 13 min, the effluent from the column was diverted to waste and a cleaning solution was sprayed on the ion source to avoid loss of signal. Multiple cleaning solutions were assessed with different percentages of acetonitrile (20%, 25% and 50%) and with different percentages of formic acid (0%, 0.1% and 0.4%). The combination of

acetonitrile/water: 80/20 (v/v) without formic acid demonstrated the greatest sensitivity over time.

3.6.2.6 *Partial method validation.*

Interday reproducibility was assessed by four injections each at low, medium and high concentrations at 1, 10 and 100 nM of DXG, DXG-MP, DXG-TP, (-)-FTC-TP, TFV, TFV-DP, CBV-TP and 10, 100 and 1,000 nM of ZDV-MP, ZDV-TP, [$^{13}\text{C}^{15}\text{N}$]dATP, [$^{13}\text{C}^{15}\text{N}$]dGTP, [$^{13}\text{C}^{15}\text{N}$]dCTP and [$^{13}\text{C}^{15}\text{N}$]TTP in a matrix containing 10^6 cells/100 μL mobile phase on four consecutive days. Intraday reproducibility was evaluated by five consecutive injections each of the same concentrations noted above. The accuracy was calculated as a percentage of the difference between the theoretical value from experimental value. Precision was expressed as % relative standard deviation (RSD).

3.6.3 LC-MS/MS for nucleosides

3.6.3.1 *Stock standard solutions*

Standard stock solutions were freshly prepared in ultrapure methanol:water (1:1) to achieve the following concentrations: 0.2 mg mL⁻¹ for DAPD, 0.1 mg mL⁻¹ for DXG, 0.5 mg mL⁻¹ for ZDV and 1 mg mL⁻¹ for DCF (for conversion to μM , refer to Tables 2-3). Standards were serially diluted to 100, 10 and 1 $\mu\text{g mL}^{-1}$. Calibration standards covering the range from 2 to 5,000 ng mL⁻¹ were prepared by adding appropriate volumes of serially diluted stock solutions to human plasma containing 10 μL of DCF at 1 mg mL⁻¹ (final volume 5 mL). Eight calibration concentrations (2, 5, 10, 50, 100, 500, 1,000 and 3,000 ng mL⁻¹) were used to define the calibration curve for all three analytes and an additional concentration of 5,000 ng mL⁻¹ was used for ZDV calibration. Five quality control (QC) standards were also used (2, 5, 10, 500 and 3,000 ng mL⁻¹) for assay validation. Aliquots of about 1 mL of calibration standards and QC samples

were transferred to 1.5 mL polypropylene snap-cap tubes and stored frozen at -20°C until analysis. All stock standard solutions were stored at -20°C.

A stock solution of the internal standard, DPD was prepared at 1 mg mL⁻¹ in methanol, and was diluted to a 250 ng mL⁻¹ solution in methanol for use during sample preparation. A stock solution of 100 mM ammonium formate was prepared and adjusted once to pH 4.8 using formic acid followed by filtration under vacuum with nylon discs 0.2 µm (Whatman, New Jersey, USA) and was stored at 4°C. A stock solution of 4 mM 2'-dA was prepared and filtered under vacuum using nylon discs 0.2 µm (Whatman, New Jersey, USA) and was stored at 4°C.

3.6.3.2 Reverse phase chromatography

Chromatographic separation was performed using a Betabasic-C18 column (100 x 1 mm, 3 µm particle size; Thermo Scientific, Waltham, MA, USA). This column was protected from remaining particles by a pre-column filter with 0.2 µm particle size (Thermo Scientific, Waltham, MA, U.S.A.). The mobile phase A consisted of 2 mM ammonium formate buffer, pH 4.8 containing 0.04 mM 2'-dA prepared daily from stock solutions. The mobile phase B consisted of methanol. The initial conditions were 94% A and 6% B at 50 µL min⁻¹. DXG, DAPD and DPD were eluted by this isocratic method during the first 7 min of analysis. From 7.5 min to 8.5 min, the flow rate was increased to 100 µL min⁻¹, from 8.5 min to 13 min, B was increased from 6% to 90% and immediately decreased to 6% at 14.3 min allowing ZDV elution. The flow rate was maintained at 100 µL min⁻¹ until 25 min to accelerate the column re-equilibration and was decreased to 50 µL min⁻¹ in 1 min. The total run time was 29 min, including time for column regeneration, which was optimized in order to maintain an efficient separation of DAPD and DXG on the following run. However, a shorter re-equilibration time led to a co-elution of DAPD and DXG and no benefit was achieved with longer re-equilibration

times. The column temperature was kept constant at 30°C. The column effluent was directed to waste *via* the divert valve of the mass spectrometer at 0 to 3 min, 8 to 13 min and 15 to 29 min. During these intervals, a cleaning solution containing 80% methanol and 0.4% formic acid in water was used at 50 $\mu\text{L min}^{-1}$. This cleaning of the ion source improved the sensitivity of detection. A solution consisting of 80% methanol and 0.1% formic acid in water was used for autosampler loop and syringe cleaning following injection.

3.6.3.3 MS/MS conditions

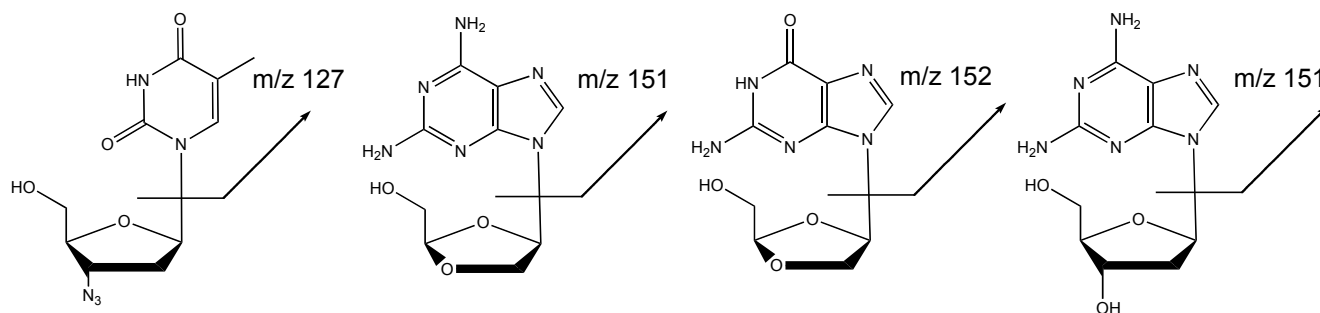
Analytes were protonated by electrospray ionization (ESI) in positive mode. Selected Reaction Monitoring (SRM) mode was used for the acquisition. The intensity of selected product ion in the MS/MS spectrum of each compound was optimized using direct infusion of the analytes in the corresponding mobile phase at 25 $\mu\text{g mL}^{-1}$ and individually into the instrument using a syringe pump at 5 $\mu\text{L min}^{-1}$. The sheath and auxiliary gas (nitrogen) were set at 45 and 0.5 arbitrary units (au), respectively without ion sweep gas. The collision gas (argon) pressure was set at 1.3 mTorr. The spray voltage was 4,000 V. The capillary was heated at 280°C and 0.1 sec scan time was used. The collision-induced dissociation (CID) was at -6 V. Scan parameters were as follows: precursor ion m/z , product ion m/z , collision energy, tube lens offset and the full width half mass (FWHM) resolution (unit resolution) for both quadrupole (Q1 and Q3) and are listed in **Table 03**.

Table 03: Scan parameters of the Thermo TSQ Quantum Ultra triple quadrupole mass spectrometer.

Analyte	Precursor ion (m/z)	Product ion (m/z)	Collision energy (V)	Tube lens offset (V)	FWHM resolution for Q1	FWHM resolution for Q3
DAPD	253	151	27	59	1.00	0.70
DXG	254	152	20	80	0.70	0.50
ZDV	268	127	24	51	0.70	0.50
DPD	267	151	25	68	0.70	0.70

A representation of the hypothesized fragmentation for all nucleosides is shown in **Figure 27**.

Figure 27: Fragmentation hypothesis for ZDV, DAPD, DXG and DPD, respectively from left to right.



3.6.3.4 Method validation

Limit of quantification (LOQ): was defined as the smallest quantity of analyte likely to be quantified accurately with a precision within $\pm 20\%$. For each of the three analytes, QC and calibration standards were prepared at the lower limit of quantification (2 ng mL^{-1}).

Linearity: Ten calibration standards (2, 5, 10, 50, 100, 500, 1000, 3,000 and $5,000 \text{ ng mL}^{-1}$) and four QCs (2, 10, 500 and $3,000 \text{ ng mL}^{-1}$) were prepared in control blank plasma pretreated with DCF, prior to processing the clinical samples. Standards were processed simultaneously with the patient samples and were assayed prior to patient samples. QCs were run along with the clinical samples to ensure confidence in the sample stability during the sequence and in the

accuracy of the quantification. Calibration curves were calculated by linear regression using a weighting factor of $1/x$. Linearity was evaluated by means of back-calculated concentrations of the calibration standards; these values should be within 15% of the nominal concentration and 20% of the nominal concentration at the LLOQ level to be accepted. Based on the criteria, less than 25% of the calibration standards were rejected from the calibration curve.

Specificity and selectivity: Two sets of human blank plasma were prepared and analyzed in the same manner as the calibration standards and QCs, but without the internal standard. The objective was to determine whether any endogenous compounds interfere at the mass transition chosen for DAPD, DXG, DPD and ZDV. Interference can occur when co-eluting endogenous compounds that produce ions with the same m/z values that are used to monitor the analytes and internal standard. The peak area of any endogenous compounds co-eluting with the analyte should not exceed 20% of the analyte peak area at LLOQ or 5% of the internal standard area.

Recovery and Matrix effect: The amount of analyte lost during sample preparation was calculated from the recovery values. Recoveries of DAPD, DXG and ZDV from plasma following sample preparation were assessed in triplicate by comparing the response of each analyte extracted from plasma with the response of the same analyte at the same concentration spiked in post-extracted blank plasma. It was also important to ensure the absence of a significant matrix effect. Significant ion suppression could occur when non-appropriate solvents are used or when endogenous compounds are simultaneously eluted with the analyte of interest resulting in interference with its ionization. The suitable dilution had to be determined to avoid decreasing the MS signal in the presence of increasing amounts of biological sample. The matrix effect was assessed by comparing the response of the post-extracted blank plasma spiked at known concentration and the response of the same analyte at the same concentration prepared in

mobile phase. This value provided information about specific ion suppression in plasma. A low, medium and high-level concentration at 10, 100 and 1,000 ng mL⁻¹, respectively was used to assess recovery and matrix effects.

Accuracy and precision: The intra- and inter-day precision and accuracy were also evaluated at low, medium and high concentrations (10, 100 and 1,000 ng mL⁻¹). For intra-assay precision, one control sample from each of the three concentrations was assayed on six runs in one sequence. For inter-day precision, one control sample from each of the three concentrations was assayed on four separate days (corresponding to four runs). The vial containing the control sample was maintained at -20°C between injections. Inter-day extraction reproducibility was assessed by calculating the precision of five extracted spiked standards in plasma, analyzed on five different days. Intra- and inter-day variations were assessed by comparing means and standard deviations of log-transformed drug concentrations at the three levels. Precision was expressed as % relative standard deviation (RSD) and had acceptance criteria of less than 20%. The accuracy was calculated as a percentage of the difference between the theoretical value from experimental value (% difference or bias) with acceptance criteria of less than 20%.

Stability: The stability of extracted standards from plasma in the autosampler was assayed by quantification of each analyte at 1,000 ng mL⁻¹ after storage for 40 hr and 5 days at 4°C. The stability of the standards during the extraction was assessed by quantification of each analyte at 1,000 ng mL⁻¹ after storage at room temperature for 24 hr. The stability of extracted standards after three freeze/thaw cycles was also evaluated. The analyte was considered stable in biological matrix or extracts when 80-120% of the initial concentration was measured. The re-injection reproducibility was assessed to determine if an analytical run could be re-analyzed in the case of instrument failure.

Carryover: Carryover was evaluated by injecting two matrix blanks immediately following the upper limit of quantification (ULOQ) standard and the lower limit of quantification (LLOQ) standard. Carryover was acceptable as long as the mean carry over in the first blank was less than or equal to 30% of the peak area of the ULOQ and was less than or equal to 20% in the second blank.

3.7 Statistical analysis

A two-way analysis of variance (ANOVA), multiple comparisons and calculation of 95% confidence intervals were performed using Matlab v7.6 software. Planned comparisons were conducted using the Dunnett's test and unplanned comparisons using a Tukey's test using the software SAS (v9.2, Carey, NC). These tests are modifications of the Student t-test, taking into account the effects of multiple comparisons on the type 1 error (falsely rejecting the null hypothesis). These tests are conservative but retain more statistical power than the Bonferroni t-test modification.¹⁹⁷ When two experimental groups were compared, a Student's t-test was performed. The null-hypothesis was rejected when p-values were below 0.05.

4 CHAPTER 1: Quantification of nucleosides and nucleotides in activated and unactivated human primary PBM cells and macrophages

4.1 Simultaneous quantification of intracellular natural and antiretroviral nucleosides and nucleotides by liquid chromatography tandem mass spectrometry¹⁹⁸

The objective of this work was to develop and validate an accurate, rapid and highly sensitive method for the simultaneous quantification of the phosphorylated metabolites of NRTI such as ABC, (-)-FTC, TDF, DAPD and ZDV as well as the natural endogenous 2'-deoxyribonucleosides-5'-triphosphates (dNTP). The discrimination between the successive intracellular metabolites resulting from the conversion of NRTI to NRTI-monophosphate (MP), NRTI-diphosphate (DP) and NRTI-TP was required, since the NRTI-TP are responsible for antiviral efficacy, while the NRTI-MP such as ZDV may be associated with toxicity.^{119, 160} Separation was also essential since NTP generate breakdown products in the electrospray probe, which are mainly the corresponding DP, MP and nucleoside forms,¹⁹⁹ which could lead to errors in the quantification of these metabolites. A high sensitivity of detection was also required, since the levels of natural endogenous dNTP in macrophages and in resting PBM cells are approximately 70 and 315 fmol/10⁶ cells, respectively.¹³⁷ A weak anion-exchange (WAX) method was previously utilized by our group²⁰⁰ and others;^{201, 202} however, the nucleosides were eluted in the void volume of the column and therefore the method had to be modified.

The measurement of intracellular phosphorylated NRTI by LC-MS/MS remained difficult. The first obstacle was the high polarity induced by the phosphate moieties of nucleotides rendering their retention by reverse phase chromatography a challenge. Generally, a volatile solvent is preferred to avoid ion suppression in the mass spectrometer. Thus, two specific

endcapped columns such as PFP propyl and Hypersil GOLD-AQ were selected for their ability to retain polar and basic compounds, including phosphopeptides, without utilizing non-volatiles buffers or extreme pH.^{203, 204} It was interesting to define whether these columns would allow the separation of a wide range of compounds with different polarity and molecular weight similar to what was previously reported by ion-pair chromatography.¹⁰⁸ The second obstacle was the interferences produced by endogenous nucleotide triphosphates and/or other components. For example, ATP, dGTP and ZDV-TP have the same molecular weight (m/z 507) and similar fragmentation pattern in negative ionization mode,²⁰⁵ and therefore, can interfere with respective measurements.²⁰⁶ Similarly, lack of MS/MS specificity occurs between ZDV-MP, AMP and dGMP. Thus, it was necessary to optimize the ionization mode, the column temperature, the composition and the pH of the mobile phase to obtain optimal separation and selectivity to avoid overlapping signals. Our approach applied the specificity offered by the positive ionization mode for most compounds, as suggested by Pruvost *et al.*²⁰⁷ while using the specific fragmentation of ZDV-TP in negative ionization mode as described previously by Compain *et al.*²⁰⁶ This switch in polarity from positive to negative ionization was possible by a highly optimized separation. This optimization was essential, mainly because several antiretroviral combination modalities, such as Combivir include ZDV. The third obstacle was the ability of the phosphate groups of the nucleotides to interact with stainless steel, causing a peak tailing on chromatograms.²⁰⁸ For this reason, all stainless steel devices were generally replaced by PEEK[®] [poly(aryl-ether-ether-ketone)] materials in the instruments. However, we found that this substitution could not be undertaken in the electrospray probe, where the metal needle proved to enhance detection sensitivity. Asakawa *et al.*²⁰⁸ showed that the use of ammonium hydrogen carbonate in the mobile phase prevented peak tailing and was compatible with LC/MS analysis. Furthermore, this

buffer is suitable for the analysis of basic compounds.²⁰⁹ Ammonium phosphate²¹⁰⁻²¹² and ammonium hydroxide²¹³ were successfully used to prevent the interactions between stainless steel and the phosphate groups of nucleotides. Ammonium phosphate buffer is known to be semi-volatile, causes ion-suppression and should be used at low concentration. Moreover, this buffer must be combined with the appropriate ion-pair reagent. Alkylamines, tetra-alkylammonium salt or tetra-butyl ammonium hydroxide have been successfully used for the quantification of nucleosides and nucleotides particularly with an ammonium phosphate buffer, despite their incompatibility with MS detection.^{212, 214} Among the available alkylamines: 1,5-dimethylhexylamine (1,5-DMHA)²⁰⁷ was preferred to *N,N*-dimethylhexylamine (*N,N*-DMHA)²¹⁵ for enhanced ionization in positive mode. Hexylamine (HA) was also successfully used in association with negative ionization mode.^{216, 217} By testing these different conditions, we were able to optimize and validate an LC-MS/MS method for the simultaneous quantification of 13 nucleosides/nucleotides endogenous and analogues.

4.1.1 Column and temperature selection

The methodology using the column Hypersil GOLD-C18 with ion-pair reagent displayed the highest performance. The PFP propyl and the Hypersil-AQ columns designed for the separation of polar compounds along with the use of volatile buffers that are compatible with mass spectrometry detection failed to discriminate the components of interest without the use of an ion-pair reagent. Several buffers were assessed, such as ammonium formate and ammonium acetate with concentrations ranging from 5 to 50 mM adjusted to a pH range from 4 to 8. At pH 4 and 8, no retention was achieved and all nucleoside triphosphates were eluted into the void volume. At pH 5 and 6, retention and separation were observed, but the symmetry of the peaks obtained, the retention capacity and the sensitivity were not sufficient for quantification

purposes. Increasing the organic phase or ammonium salt did not improve these parameters. Thus, the development of an ion-pair methodology using the most efficient Hypersil GOLD-C18 column became the main focus.

The column compartment temperature was evaluated between 20°C and 35°C, and a significant improvement was observed at 30°C, which was chosen as the optimal column temperature.

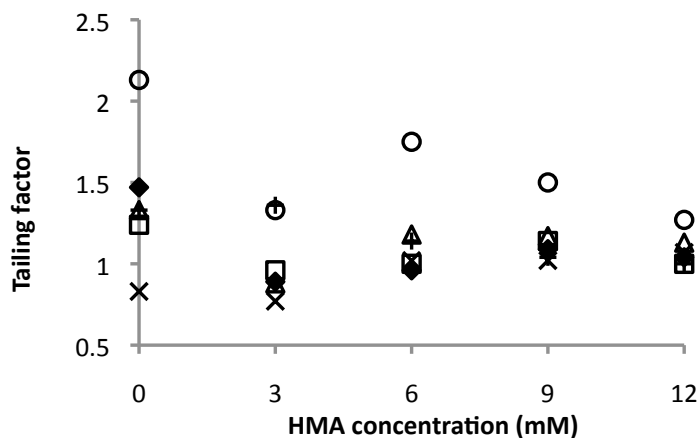
4.1.2 Ion-pair method development

The values of chromatography parameters (N_e , k' , T_f and area) for 3TC, 3TC-MP, 3TC-TP, DXG, DXG-MP, DXG-TP, TFV, TFV-DP, ZDV-TP, (-)-FTC-TP and CBV-TP were used as a guide to select the optimal pH, HA concentration and buffer composition (**Supplement: end of document**).

4.1.2.1 HA concentration effect

HA at 12 mM gave the lowest peak tailing (**Figure 28**), the highest effective plate number and the greatest peak area among all concentrations assessed; however, the ion source was clogged following 10 injections and the sensitivity was decreased without significant improvements even after source cleaning for 15 min between each injection.

Figure 28: Tailing factor (T_f) at five different HA concentrations; 0, 3, 6, 9 and 12 mM. + 3TC-TP, × DXG-TP, ♦ TFV-DP, □ CBV-TP, Δ (-)-FTC-TP and ○ ZDV-TP.

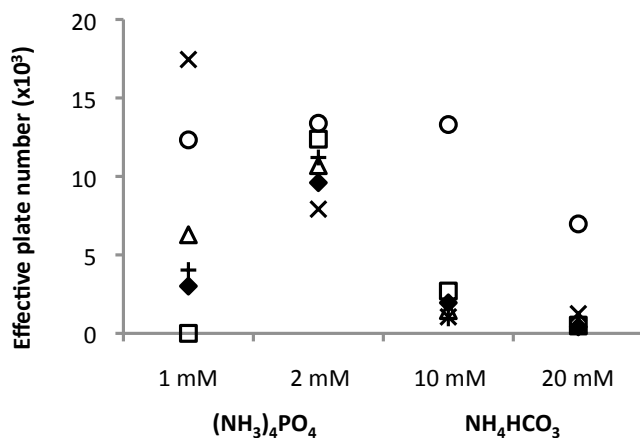


Interestingly, the decrease in peak tailing observed at 9 or 12 mM HA, suggests that HA might possess a silanol-masking activity. Generally, phosphorylated metabolites and pairing ions (HA) undergo a partition mechanism between the mobile phase and the stationary phase.¹⁸⁹ This mechanism can be described by an equation: HA^+ (mobile) + P^- (mobile) \rightleftharpoons HA^+P^- (stationary), where hexylamine (HA^+) is the cation and the phosphorylated nucleotides (P^-) are the anions. Thus, enough HA should be available in the mobile phase for this reaction to occur. Optimized HA concentration at 3 mM was sufficient to obtain a symmetric peak, while avoiding clogging the source and maintaining ionization over time. No increase in retention was observed upon increase in HA concentration.

4.1.2.2 Buffer effect

Ammonium phosphate at 1 and 2 mM and ammonium hydrogen carbonate at 10 and 20 mM were compared. Ammonium hydrogen carbonate caused an increase in peak tailing, a decrease in effective plate numbers for all analytes except for ZDV-TP (**Figure 29**) at both 10 and 20 mM, and worsened the peak symmetry of all analytes at 20 mM. Ammonium phosphate at 2 mM, but not 1 mM, increased the effective plate number of all the analytes tested, except for DXG-TP (**Figure 29**) and appeared to be a superior buffer for running samples over several days, without the peak shift observed with the ammonium hydrogen carbonate buffers.

Figure 29: Effective plate number (Ne) at four different buffer compositions; 1 and 2 mM ammonium phosphate; 10 and 20 mM ammonium hydrogen carbonate. + 3TC-TP, × DXG-TP, ◆ TFV-DP, □ CBV-TP, Δ (-)-FTC-TP and ○ ZDV-TP.

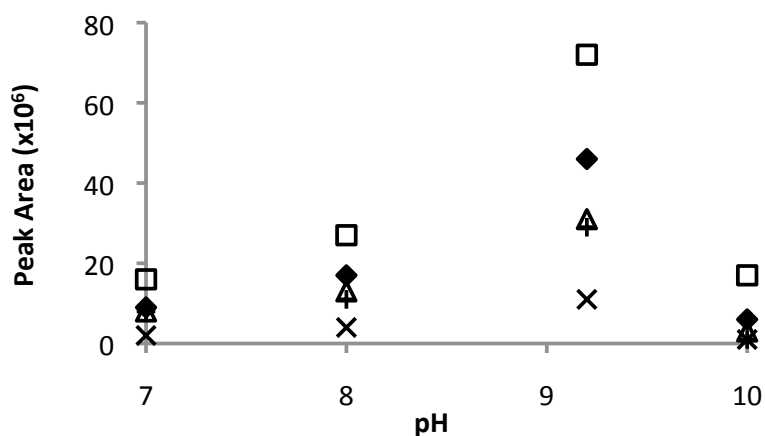


The improved properties obtained by the use of 2 mM ammonium phosphate *versus* ammonium hydrogen carbonate could be explained by its rank in the Hofmeister series, where the carbonate ions are placed lower than phosphate ions.^{218, 219} Carbonate ions would have a lower propensity to retain protonated amines, such as HA, than phosphate ions, explaining the necessity to raise the concentration of ammonium hydrogen carbonate. Carbonate ions would also increase the chaotropic effects, which could destabilize folded proteins, decrease their solubility and give rise to salting-out behavior inside the column.²¹⁹ This was consistent with our observations with 20 mM ammonium hydrogen carbonate wherein a loss in chromatography quality was seen possibly due to clogging of the column (**Figure 29**). In addition, ammonium hydrogen carbonate decomposes, which results in higher variability of the buffer composition and is not suitable for high throughput analysis.²²⁰ Finally, ammonium phosphate buffer is a silanol masking agent and is a potent buffer at high pH especially when high volume of samples are injected and when the pK_a of the compound is ≥ 8 ,²²⁰ which is often the case for nucleotides,¹⁷⁸ producing a better peak shape and making it the optimal buffer for nucleotide analysis.

4.1.2.3 pH effect.

By applying pH 7, 8, 9.2 and 10, there was no noticeable change in the number of effective plates. The peak tailing decreased as the pH increased and the peak capacity was stable from pH 7 to 9.2, but dropped at pH 10. The peak area and the signal intensity were decreased at pH 7, 8 and 10 and were increased at pH 9.2, making pH 9.2 optimal for all nucleotides (**Figure 30**).

Figure 30: Peak area at pH 7.0, 8.0, 9.2 and 10.0. + 3TC-TP, × DXG-TP, ◆ TFV-DP, □ CBV-TP and Δ (-)-FTC-TP.



Also, it was found that increasing HA concentration (pK_a 10.56), raised the pH and produced an improvement of signal intensity. Interestingly, when the pH was adjusted to 10 with ammonium hydroxide, a decrease in the signal intensity occurred (**Figure 30**). Thus, both the pH and the silanol-masking effect of HA might enhance the positive ionization of nucleotides. Furthermore, the addition of ammonium hydroxide or formic acid to the mobile phase could lower the sensitivity as first described by Vela *et al.*²¹² Additionally, the pH influenced the ionization of the nucleotides. At low pH and up to 9.5, ZDV-TP was better ionized in negative mode than in positive mode, due to the inability of the thymine base to accept an extra proton unless conditions are extremely basic (thymidine nucleoside and nucleotide $pK_a > 9.5$).¹⁷⁸ The

selected pH, 9.2, justifies the use of negative mode ionization for ZDV-TP along with a specific transition m/z 506 \rightarrow 380.²⁰⁶

4.1.2.4 *Internal standards selection*

It was critical to choose three internal standards compatible with the chemistries and the retention time of each of the three classes of compounds measured, nucleoside, MP and TP. 3TC, 3TC-MP and 3TC-TP were assessed. However, dCTP was measured by monitoring the ion transitions m/z 468 \rightarrow 112, which slightly differed from the one for 3TC-TP m/z 470 \rightarrow 112. Thus, an additional peak was detectable on 3TC-TP reconstituted ion chromatogram, which represented dCTP isotopic distribution. The separation of the two compounds by over 2 min alleviated the risks of dCTP interference over the peak area of 3TC-TP. 3TC, 3TC-MP and 3TC-TP demonstrated a symmetrical peak shape and a lack of interference with endogenous compounds by injections of cell blanks compared with spiked standards and standards in reconstitution solvent.

4.1.3 **Method sensitivity and partial validation.**

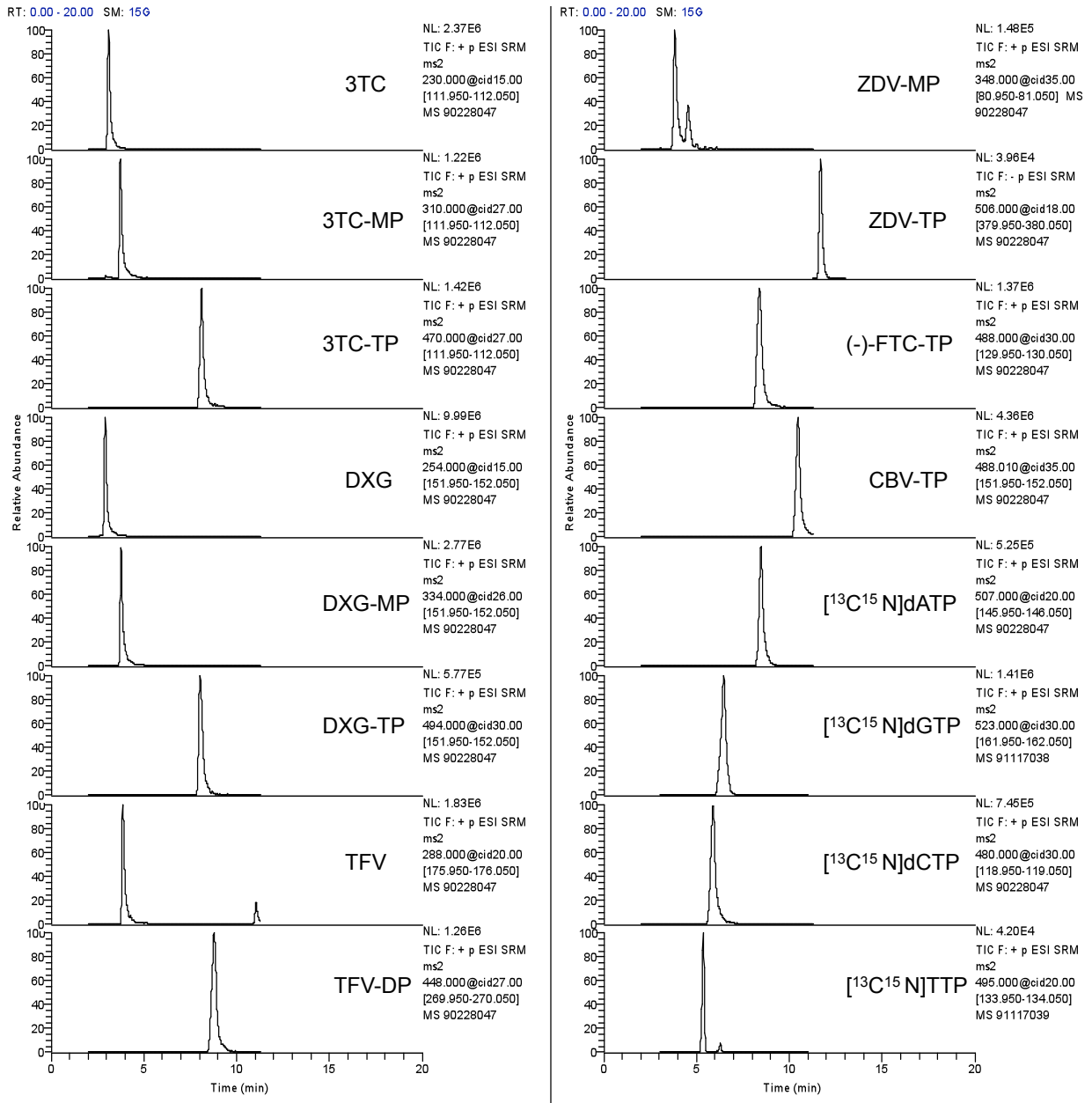
Intraday and interday criteria for all nucleosides and nucleotides studied were within the range of acceptance, precision < 20% and 100 ± 25 % accuracy (**Table 04**).

Table 04. Intraday and interday accuracy and precision for DXG, DXG-MP, DXG-TP, TFV, TFV-DP, ZDV-MP, ZDV-TP, (-)-FTC-TP, CBV-TP, and [¹³C¹⁵N]dNTP

	Concn.(nM)	Interday (n = 4)		Intraday (n = 5)	
		Precision	Accuracy	Precision	Accuracy
DXG	1	3.4	96.1	8.7	94.7
	10	5.3	91.7	3.4	93.7
	100	6.8	108.5	2.4	93.0
DXG-MP	1	10.9	105.4	11.2	102.0
	10	11.9	96.8	4.1	98.7
	100	0.2	102.2	5.4	96.8
DXG-TP	1	3.6	99.6	16.4	113.3
	10	7.5	109.7	3.6	110.4
	100	5.9	109.9	2.0	103.3
TFV	1	6.8	101.8	4.9	96.5
	10	3.6	100.6	2.4	88.7
	100	6.3	106.4	6.0	102.4
TFV-DP	1	14.3	108.8	6.8	96.5
	10	6.9	99.8	6.2	94.7
	100	9.5	93.2	3.3	97.0
ZDV-MP	10	N/A	N/A	N/A	N/A
	100	14.1	105.1	13.1	110.1
	1,000	6.5	98.8	N/A	N/A
ZDV-TP	10	19.8	91.1	13.6	89.2
	100	19.2	86.5	19.4	92.8
	1,000	6.2	104.8	11.4	98.3
(-)-FTC-TP	1	10.7	91.7	7.4	98.7
	10	13.5	99.9	13.0	112.9
	100	12.9	95.7	3.6	110.8
CBV-TP	1	12.3	94.5	6.0	111.2
	10	9.8	115.4	8.1	99.2
	100	20.0	97.7	4.2	95.8
[¹³ C ¹⁵ N]dATP	10	16.9	87.0	19.2	89.4
	100	13.6	106.6	6.6	102.6
	1,000	5.4	97.5	3.9	95.6
[¹³ C ¹⁵ N]dGTP	10	11.9	100.9	11.4	99.1
	100	10.5	108.4	5.1	103.7
	1,000	2.6	97.8	2.9	96.0
[¹³ C ¹⁵ N]dGTP	10	10.1	108.6	10.6	108.3
	100	16.4	101.6	5.3	74.8
	1,000	5.9	103.1	2.9	108.8
[¹³ C ¹⁵ N]TTP	10	N/A	N/A	N/A	N/A
	100	16.4	114.1	5.3	103.8
	1,000	6.0	104.0	3.0	125.0

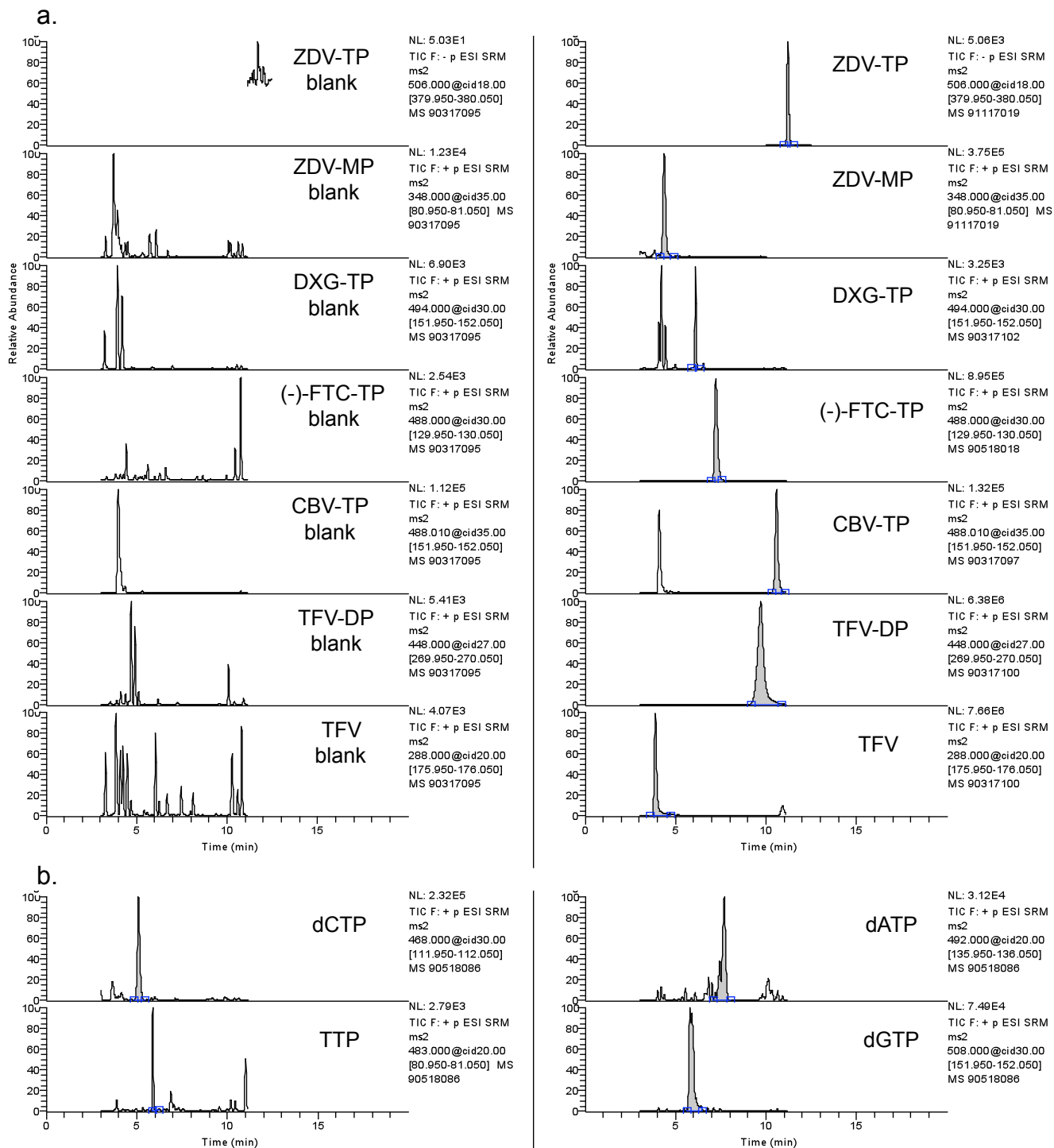
A reconstituted ion chromatogram illustrates the separation obtained for all the calibration standards (Figure 31).

Figure 31: Typical reconstituted ion chromatograms (RIC) displaying all the standards used for the partial validation spiked in a PBM cells matrix containing 10⁶ cells/100 μL mobile phase. The RIC shows the peaks obtained for DXG, DXG-MP, DXG-TP, TFV, TFV-DP, ZDV-MP, ZDV-TP, (-)-FTC-TP, CBV-TP, [¹³C¹⁵N]dATP, [¹³C¹⁵N]dGTP and [¹³C¹⁵N]dCTP at 100 nM, and [¹³C¹⁵N]TTP at 500 nM. Internal standards, 3TC, 3TC-MP and 3TC-TP were at 100 nM.



ZDV-MP was eluted 1 min after an interfering peak, which could be dGMP, AMP or a co-elution of both. Lower limits of quantification were 1 nM for DXG, DXG-MP, DXG-TP, TFV, TFV-DP, (-)-FTC-TP, CBV-TP, 10 nM for [$^{13}\text{C}^{15}\text{N}$]dATP, [$^{13}\text{C}^{15}\text{N}$]dGTP, [$^{13}\text{C}^{15}\text{N}$]dCTP, ZDV-TP and 100 nM for [$^{13}\text{C}^{15}\text{N}$]TTP, ZDV-MP, which was sensitive enough to quantify all NRTI-TP in PBM cells and in macrophages (**Figure 31**) as well as endogenous dNTP. Sensitivity and specificity of the method developed was achieved by the intensity and the specificity of the MS/MS product formed in positive ionization mode.²⁰⁷

Figure 32: a. Typical RIC for NRTI-TP, obtained from macrophages. The left chromatograms represent five background signals obtained from a single injection of untreated macrophage extract; these chromatograms are marked as “blank”. The right chromatograms represent the five signals obtained for ZDV-TP, ZDV-MP, DXG-TP, (-)-FTC-TP, CBV-TP, TFV-DP and TFV respectively from five separate LC-MS/MS injections of treated macrophages extracts, with five drugs ZDV, DXG, (-)-FTC, ABC and TDF at 10 μM , for 4 hr. The sample incubated with TDF was diluted 20 times. b. Typical chromatograms of endogenous dNTP obtained from a single macrophage extract.



4.2 Application: Measurement of NRTI-TP and endogenous nucleotides in PBM cells and in macrophages²²¹

4.2.1 Method cross-validation by comparison to previous published results

In order to have confidence in the validity of the overall methodology, the NRTI-TP levels obtained by our group in activated PBM cells were compared to the one of previous published studies, in which similar assays were used. The values found following NRTI incubations were in the expected range for ZDV-TP, CBV-TP, TFV-DP and DXG-TP. However, the (-)-FTC-TP levels were 4-fold higher than those previously reported, which may be due to variable assay condition (Table 05).^{44, 105}

Table 05. NRTI-TP levels (pmol/10⁶ cells) in 72 hr-PHA stimulated human PBM cells, following a 4 hr incubation of 10 μ M NRTI, in comparison with previously published data using similar assay conditions.

	NRTI-TP	Previous publications
ZDV-TP	1.13 \pm 0.27	\sim 1.1 ²²²
CBV-TP	0.16 \pm 0.002	0.12 \pm 0.07 ¹⁰⁷
TFV-DP	0.05 \pm 0.03	0.038 - 0.11 ¹⁰⁵
(-)-FTC-TP	\sim 16	2.74 - 4.14 ¹⁰⁵
DXG-TP	0.05 \pm 0.03	\sim 0.015 ⁸⁰

4.2.2 The levels of NRTI-TP are lower in macrophages than in PBM cells

4.2.2.1 Rational for experimental design

Previous data have established that NRTI are not effective in chronically infected macrophages. Recent reports have demonstrated that reactivated virus found in the plasma of individuals previously maintaining viral loads below the limit of detection mapped to non-T cell compartments, further implicating and defining macrophages as a causative reservoir for latent HIV-1.⁴⁴

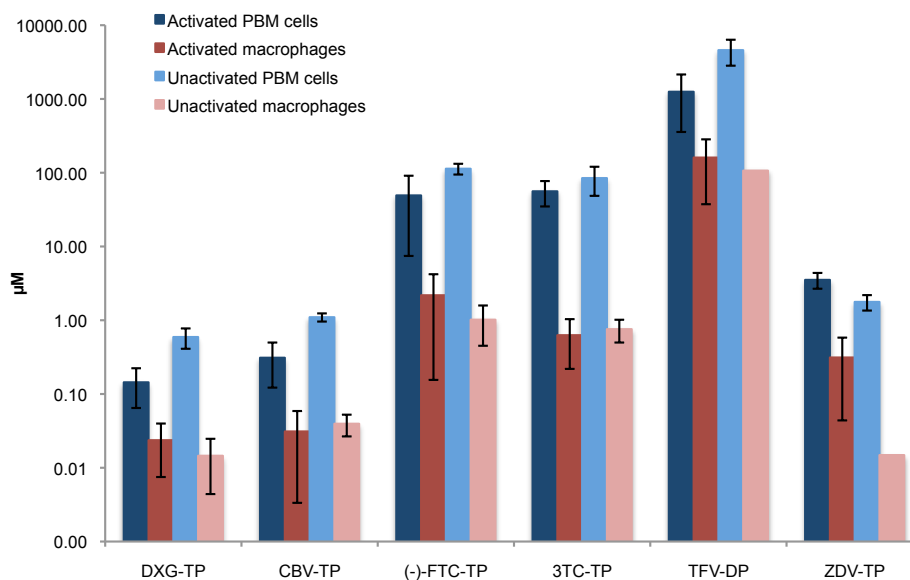
To measure the levels of active NRTI-TP in macrophages, the NRTI of interest were incubated at 10 μ M, which approximates the C_{\max} in plasma for most NRTI after oral administration.^{49, 79} Macrophages are present at various activation states within multiple tissue microenvironments. Lymphocytes, in turn, confer either a “resting” or “activated” phenotype upon exposure to pathogen, and are present in both subsets in the periphery throughout the course of infection. Based on these activation states, and their relevance to HIV-1 infection and ART, both macrophages and lymphocytes were activated or left unactivated to assess their cellular pharmacological profile.²²¹ NRTI-TP levels were expressed in μ mol/L of cytoplasm to take into account the cell volume, assuming cell volumes of 0.320 pL for activated PBM cells, 0.186 pL for resting PBM cells and 2.660 pL for macrophages.¹³⁷

The method described in **4.1** was modified to allow for 3TC-TP quantification, by replacing 3TC-TP with ddATP as an internal standard. The significance of the differences in NRTI-TP levels and NRTI-TP/dNTP ratio were determined by two-way anova followed by multiple comparison analysis with a 95% confidence interval.

4.2.2.2 NRTI-TP levels

The levels of all NRTI-TP were significantly higher in PBM cells than in macrophages ($p < 0.05$). However, in general, activation states (resting or dividing) did not significantly affect NRTI-TP levels macrophages, with the exception of the cell cycle dependent ZDV (**Figure 33**), ZDV-TP levels were higher in activated than in unactivated PBM cells and macrophages.¹⁴⁹ No significant difference was observed between activated and unactivated PBM cells for (-)-FTC-TP and 3TC-TP. Surprisingly, TFV-DP, DXG-TP and CBV-TP were significantly higher in unactivated than in activated PBM cells ($p < 0.001$) (**Figure 33**).

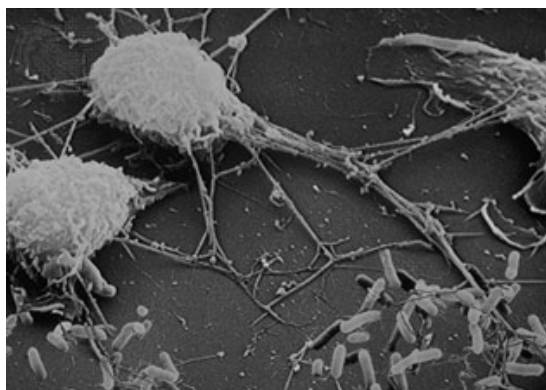
Figure 33: Levels of NRTI-TP after incubation of DXG, ABC, (-)-FTC, 3TC, TDF and ZDV in activated and unactivated human PBM cells and macrophages.



Lower NRTI-TP levels observed in macrophages compared with PBM cells might result from differing cellular uptake or the expression of phosphorylating enzymes. For instance, certain enzymes of the salvage pathway, such as TK1 and dCK, are not expressed in resting cells (Figure 21)^{176, 223} Nucleotide synthesis in macrophages is only performed *via* salvage pathway, since they primarily remain in a resting, G1 state and undergo limited DNA synthesis.^{74, 172} It is also possible that differential expressions of nucleoside transporters influence the accumulation of NRTI in macrophages *versus* PBM cells.^{224, 225} The surface area of macrophages is proportionally larger than PBM cells due to their phagocytic protrusions and convolutions (Figure 34), which could also be involved in drug absorption. We demonstrated that levels of NRTI-TP were greater than the K_i for all drugs tested in lymphocytes, independent of activation state. In macrophages, 3TC-TP and CBV-TP are $< K_i$, DXG-TP and (-)-FTC-TP were approximately equal to the K_i and ZDV-TP and TFV-DP were $> K_i$, implicating ZDV and TDF as optimal drugs to deliver adequate concentrations of drug to macrophages (K_i values

previously summarized in Schinazi, *et al*).⁴⁹ Subsequent comparison to the K_i for the corresponding NRTI-TP links intracellular drug levels and concentration of drug required to inhibit HIV-1 RT.

Figure 34: Shape of a macrophage in phagocytosis (size 25 μm in diameter). Source: www.atm2.fr



4.2.2.3 dNTP levels

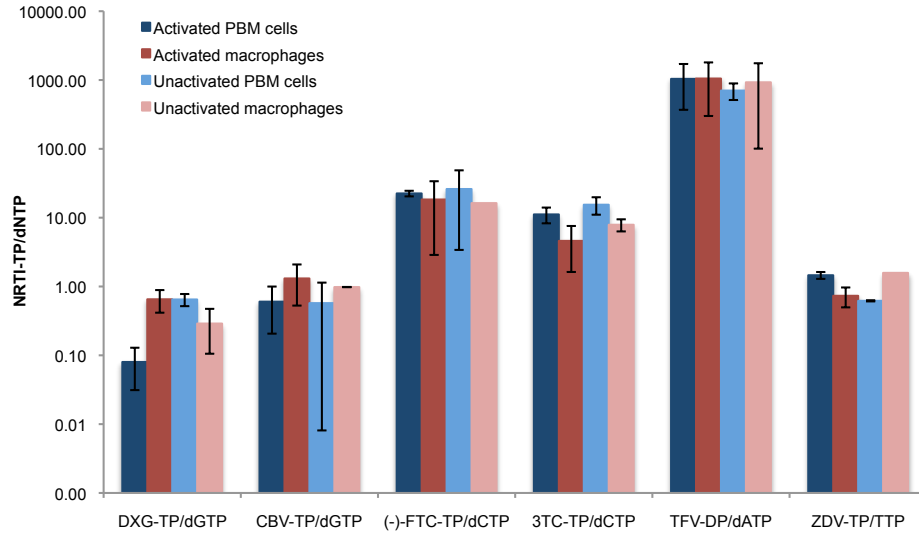
NRTI compete with endogenous dNTP for binding and incorporation by the HIV-1 RT. Therefore, it was important to measure both endogenous dNTP and NRTI-TP levels (**Table 06**). Endogenous dNTP levels were comparable to previous publications,^{137, 149} and were significantly lower in macrophages than in PBM cells (**Table 06**). The ratios NRTI-TP/dNTP are shown in **Figure 35**.

Table 06: Levels of dNTP in activated and unactivated human PBM cells and macrophages.

	dCTP	dGTP	dATP	TTP
	μM			
Activated PBM cells	3.67 ± 2.65	1.52 ± 1.01	9.22 ± 4.5	3.21 ± 1.24
Activated macrophages	0.15 ± 0.10	0.05 ± 0.03	0.10 ± 0.07	0.30 ± 0.15
Unactivated PBM cells	4.46 ± 2.86	0.91 ± 0.35	5.32 ± 2.18	2.87 ± 0.48
Unactivated macrophages	0.07 ± 0.05	0.07 ± 0.05	0.04 ± 0.03	0.24 ± 0.08
	$\text{pmol}/10^6 \text{ cells}$			
Activated PBM cells	1.17 ± 0.85	0.49 ± 0.32	2.95 ± 1.46	1.03 ± 0.40
Activated macrophages	0.39 ± 0.26	0.13 ± 0.08	0.27 ± 0.19	0.80 ± 0.40
Unactivated PBM cells	0.83 ± 0.53	0.17 ± 0.07	0.99 ± 0.41	0.54 ± 0.09
Unactivated macrophages	0.19 ± 0.13	0.18 ± 0.13	0.10 ± 0.07	0.63 ± 0.20

4.2.2.4 NRTI-TP/dNTP ratio

Figure 35: NRTI-TP/dNTP after incubation of DXG, ABC, (-)-FTC, 3TC, TDF and ZDV in activated and unactivated human PBM cells and macrophages.



The DXG-TP/dGTP ratio was significantly higher in activated macrophages and in unactivated PBM cells than in activated PBM cells ($p = 0.009$). The TFV-DP/dATP ratio remained unchanged across groups. Results of the experiments performed with TDF should be interpreted with caution. TDF delivers super physiological concentrations of TFV-TP *in vitro* compared with *in vivo* since the vast majority of the drug is observed as PMPA in the systemic circulation (see § 1.3.1.1). The 3TC-TP/dCTP ratio was significantly higher in unactivated PBM cells than in activated macrophages ($p = 0.01$). 3TC-TP/dCTP ratio was higher in activated *versus* unactivated PBM cells as previously published ($p = 0.04$, two tailed, unpaired Student's T-test).¹⁴⁹ The ZDV-TP/TTP ratio was higher in activated than in unactivated PBM cells or macrophages. Therefore, when looking at the ratio between NRTI-TP/dNTP, DXG may be more potent for inhibiting viral replication in macrophages and in resting lymphocytes than other NRTI.

4.3 Conclusions

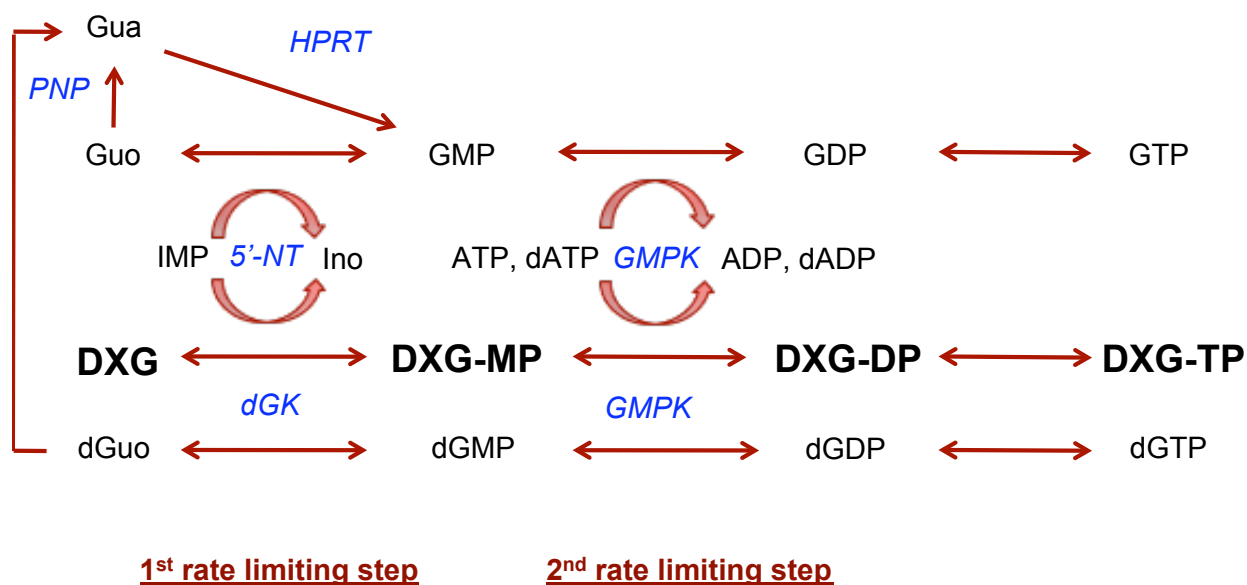
This novel LC-MS/MS method provides an accurate, rapid, simultaneous and selective quantification of most clinically relevant nucleoside and nucleotide analogues. The sensitivity of this method was sufficient to measure NRTI-TP and endogenous dNTP in primary human PBM cells and macrophages. Adequate delivery of ZDV-TP and TFV-TP in macrophages relative to their K_i was demonstrated. However, DXG-TP would offer an enhanced competition *versus* dGTP for binding to the HIV-1 RT in macrophages. Together, these data may explain previous reports that nucleoside analogues are more potent in acutely infected macrophages than lymphocytes.^{174, 226}

On the basis of the previously published studies⁶⁴ and the clinical study evaluating DAPD in combination with ZDV, this combination has the potential to provide benefit as an important nucleoside option, particularly in delaying the emergence of NRTI resistance.⁶⁵ The low cytotoxicity, large therapeutic window, resistance profile and potentially enhanced competition *versus* dGTP in unactivated PBM cells and in macrophages also make DXG an attractive drug (Figure 35). Therefore, DXG metabolism was studied in PBM cells relative to natural purine metabolism.

5 CHAPTER 2: Study of DXG phosphorylation and endogenous nucleotide pool in human peripheral blood mononuclear cells

In this study, the anabolism of DXG was investigated in peripheral blood mononuclear (PBM) cells. Despite a good antiviral activity,⁶⁰ DXG-TP levels are significantly lower than other NRTI-TP such as 3TC-TP and (-)-FTC-TP (**Figure 32**). A high competition with enzymes of the purine phosphorylation pathway might be limiting DXG anabolism. Feng *et al.* suggested that both the first and the second step for DXG phosphorylation may be rate limiting (**Figure 36**).⁸⁰

Figure 36: Representation of the overlap between DXG and Gua, dGuo and Guo phosphorylation pathways.^{80, 227}



DXG demonstrated antiviral synergy with ZDV *in vitro* and in humans, with 3TC *in vitro* and may also be tested together with (-)-FTC for potent combination antiretroviral agent. A previous study demonstrated the lack of interference between ZDV and DXG at the phosphorylation level.²⁰⁰ However, the combinations DXG and 3TC or (-)-FTC have not been assessed yet and their lack of interaction at the phosphorylation level is demonstrated here. To

explain antiviral synergy between DXG and ZDV, we will focus on the ratio between DXG-TP and dGTP since it might play a role in antiviral activity.¹⁴⁴

5.1 DXG phosphorylation is limited by competition with all guanine nucleosides

Several purines, and more particularly guanine nucleosides and nucleobases were used in an attempt to increase competition and thereby inhibit the phosphorylation of DXG. After 4 hr of co-incubation, all exogenous nucleosides/nucleobase evaluated interfered with DXG phosphorylation, most noticeably at the triphosphate level. Cellular contents of DXG-MP were significantly decreased following co-incubation with Guo at 10 and 100 μM and dGuo at 100 μM , but not with Gua. At 24 hr of co-incubation only the highest concentrations (100 μM) of the purine nucleoside and nucleobases Guo, dGuo and Gua were associated with a reduction in DXG-TP levels, and no depletion in DXG-MP was observed (**Table 07**).

Interestingly, the addition of Ado at 100 μM to the treatment with Gua also at 100 μM contributed to a marked restoration in DXG-TP levels at 4 hr and a complete reversal of Gua's effect on DXG-TP levels at 24 hr. Gua did not affect DXG-MP levels at 4 hr or 24 hr (**Table 07**).

The variations in endogenous nucleotide pools were carefully measured to assess their sensitivity to the addition of natural nucleosides/nucleobase. After 4 hr incubation in DXG treated cells, the dGTP, GTP, dATP and ATP levels were 0.46 ± 0.07 , 182 ± 84 , 1.36 ± 0.60 and 791 ± 294 pmol/ 10^6 cells respectively. The addition of 10 μM of natural nucleosides and nucleobase did not affect the endogenous nucleotide pool levels at 4 or 24 hr. On the contrary, the super physiological concentrations selected (100 μM) contributed to imbalances in the purine nucleotide pool levels. The greatest changes were observed with the addition of dGuo, which increased dGTP and GTP pool by 2 to 6-fold and decreased dATP pools by 0.7 to 0.4-fold

(Table 07). Interestingly, in dGuo treated cells, dGTP levels were decreased at 24 hr, while GTP levels increased. The treatment with 100 μ M Gua and Guo increased GTP levels. Guo 100 μ M resulted in a 0.4-fold decrease in dATP levels (Table 07). Treatment with Ado reversed the imbalances in purine nucleotides caused by Gua.

As expected, the positive control RBV treatment produced a 1.8 ± 0.3 and 5.1 ± 1.3 -fold increase in DXG-TP levels, at 4 and 24 hr, respectively, and a 1.3 ± 0.2 and 5.8 ± 0.5 -fold increase in DXG-MP, at 4 and 24 hr, respectively (Table 07).

Table 07: Variations in DXG phosphorylation upon addition of exogenous natural nucleosides/nucleobase and antimetabolite (RBV).

Treatment (DXG 10 μ M + X μ M)	4 hr		24 hr		Significant variation in endogenous purine nucleotide pool level ^c	
	DXG-MP	DXG-TP	DXG-MP	DXG-TP	4 hr	24 hr
	<i>fmol/10⁶ cells</i>		<i>fmol/10⁶ cells</i>		<i>Fold difference</i>	
DXG only	33 \pm 16	295 \pm 157	13 \pm 7	156 \pm 65		
+ dGuo 10 μ M	29 \pm 13	172 \pm 84 ^a	12 \pm 8	148 \pm 96	1.4 (GTP)	
+ dGuo 100 μ M	17 \pm 4 ^a	100 \pm 41 ^{a,b}	9 \pm 3	56 \pm 10 ^a	6 (dGTP)-2(GTP) 0.7 (dATP)	4 (dGTP)-4(GTP) 0.4 (dATP)
+ Guo 10 μ M	13 \pm 4 ^a	137 \pm 53 ^a	15 \pm 7	138 \pm 108		
+ Guo 100 μ M	10 \pm 4 ^a	118 \pm 45 ^a	6 \pm 1	67 \pm 13 ^a	2 (GTP)	4 (GTP) 0.4 (dATP)
+ Gua 10 μ M	34 \pm 8	193 \pm 43 ^a	9 \pm 2	207 \pm 102		
+ Gua 100 μ M	21 \pm 6	101 \pm 44 ^{a,b}	7 \pm 4	58 \pm 6 ^a		2 (GTP)
+ Gua 100 μ M + Ado 100 μ M	27 \pm 16	238 \pm 15 ^a	13 \pm 6	118 \pm 25		
+ RBV 30 μ M	52 \pm 11	701 \pm 174	74 \pm 32	764 \pm 290	0.6 (dGTP)	0.6 (dGTP)

^a Significantly different from the control (DXG only) by two-way anova and multiple comparison analysis

^b Significantly different from DXG 10 μ M + Gua100 μ M + Ado 100 μ M by two-way anova and multiple comparison analysis

^c Fold difference between metabolites in cells treated with DXG + exogenous nucleoside *versus* DXG alone. Data not shown for levels that were not significantly different from the control.

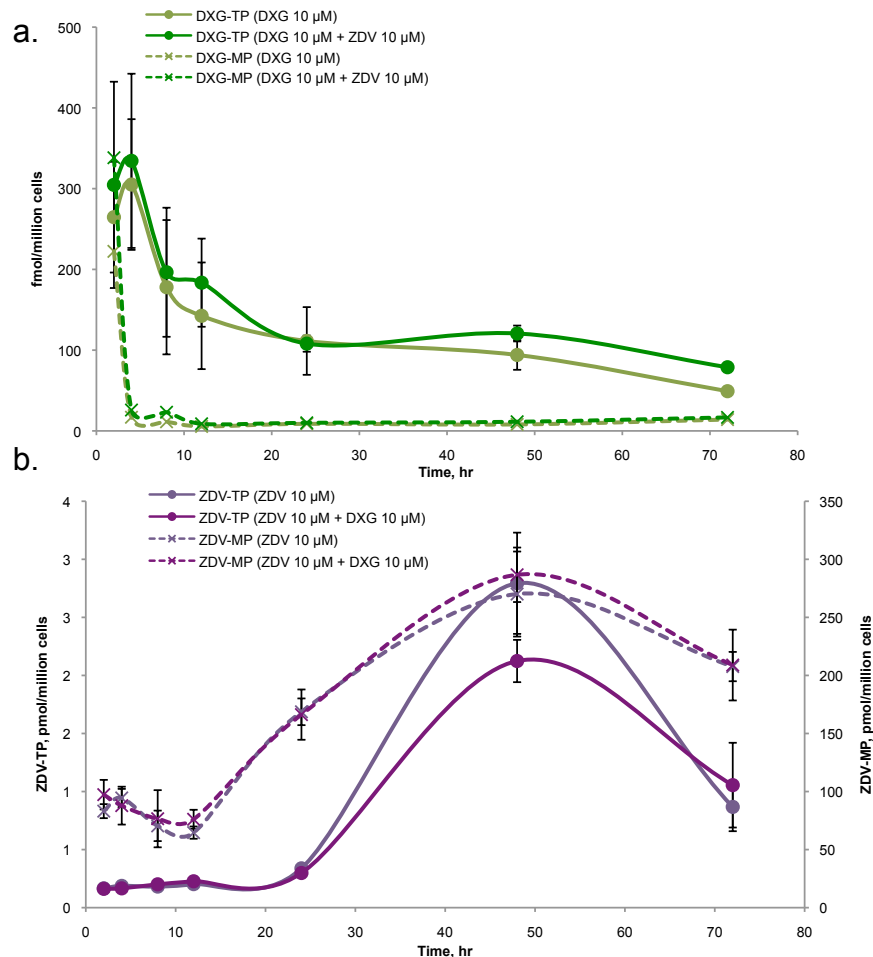
Results are presented in fmol/10⁶ cells in this section for the purpose of comparison with previously published data.

Taken together, these results demonstrate a strong competition between DXG and the endogenous nucleosides for intracellular phosphorylation and also indicate the substrates that may limit DXG phosphorylation, in particular guanosine/guanine.

5.2 Lack of interaction between ZDV and DXG for phosphorylation in PBM cells but decreased endogenous dNTP levels

The activity of NRTI depends on NRTI-TP levels in activated cells. To assess interactions over time, ZDV and DXG phosphorylation in PBM cells were studied for 72 hr incubation (Figure 37).

Figure 37: Levels of (a) DXG and (b) ZDV phosphate derivatives over a 72 hr incubation of both drugs in combination and separately at 10 μ M.

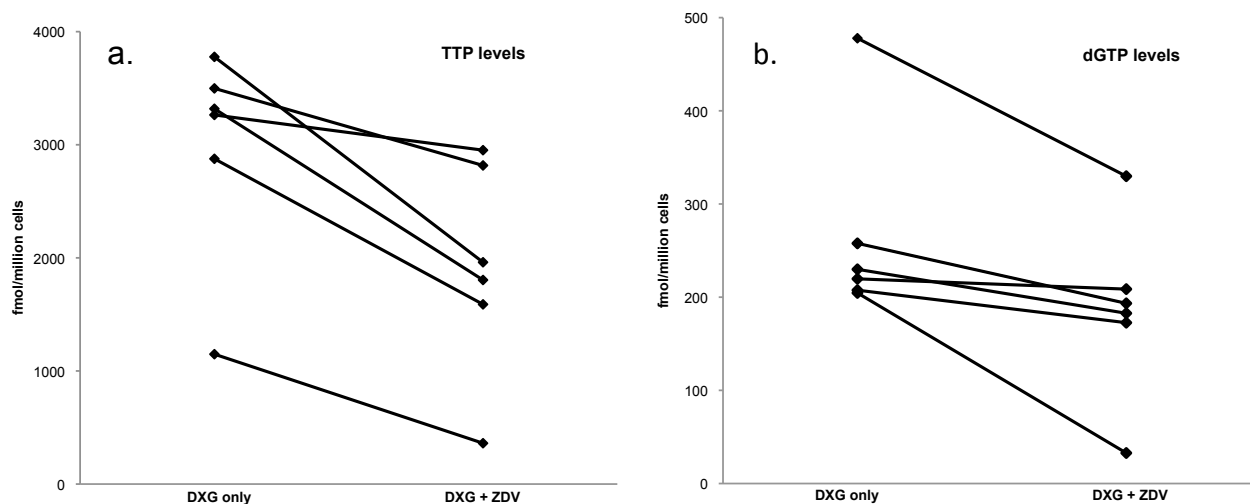


Co-incubation of DXG with ZDV did not affect ZDV-TP or DXG-TP levels respectively, based on two-way ANOVA statistical test ($p = 0.1$ and 0.4 , respectively). DXG-TP levels were higher at 4 hr *versus* any other time points ($p = 0.001$). DXG-MP levels were 24 ± 6 and 4 ± 1 -fold lower than DXG-TP in activated PBM cells at 4 and 72 hr respectively.

A separate decay experiment of DXG-TP in activated PBM cells demonstrated a DXG-TP half-life of 5.0 ± 1.3 hr and undetectable DXG-MP levels within 30 min following drug removal from the media.

Based on these results the synergistic anti-HIV effect between DXG and ZDV is not related to increased DXG-TP or ZDV-TP levels in PBM cells. Therefore, it was considered appropriate to measure the depletion of the corresponding endogenous dNTP pool levels in PBM cells (**Figure 38**).

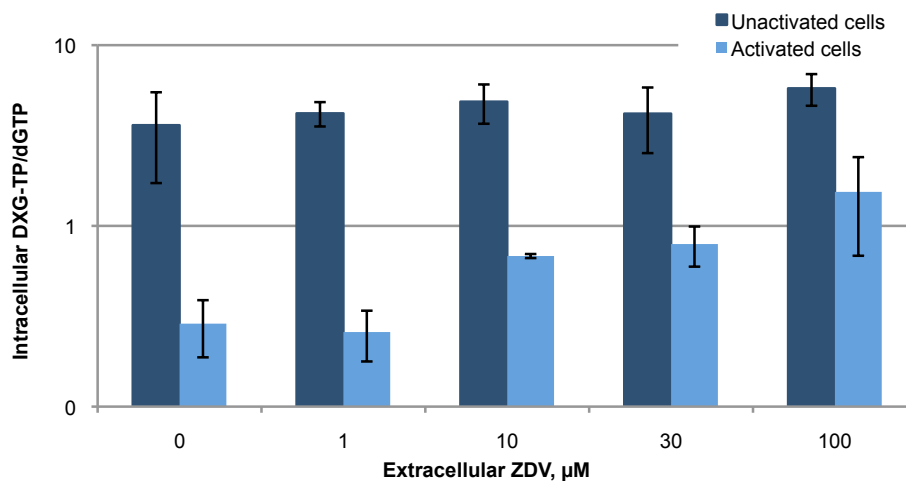
Figure 38: TTP (a) and dGTP (b) levels after 24 hr incubation with DXG alone or with DXG + ZDV.



Co-incubation of cells with ZDV and DXG resulted in a significant decrease in TTP ($p = 0.006$) and dGTP levels ($p = 0.03$), using paired student's T-Test. However, no depletion in dGTP levels was observed in DXG treated cells as compared to untreated control: 287 ± 130 fmol/ 10^6 cells and 363 ± 313 fmol/ 10^6 cells, respectively ($p = 0.5$, $n = 4$, paired, two-tailed

Endogenous dGTP levels were significantly lower in unactivated than in activated cells ($p = 0.01$), as expected (220 ± 44 and 13 ± 2 fmol/ 10^6 cells).

Figure 40: Ratio between DXG-TP and dGTP levels at 24 hr.



The ratio between DXG-TP and dGTP was about 10-fold higher in unactivated than in activated PBM cells in the absence of ZDV. However, this fold difference was reduced to 3, with the addition of ZDV at 100 μM in activated PBM cells.

As expected, ZDV-MP but not ZDV-TP levels increased significantly with concentration (data not shown). In this context, dCTP levels increased 4 and 8-fold at 4 and 24 hr, respectively while, no significant differences in dATP levels were observed.

5.3 Lack of interaction between 3TC or (-)-FTC and DXG for phosphorylation in PBM cells

Prior to the start of the study, appropriate controls were performed to verify that in the presence of exogenous nucleosides, the levels of NRTI-TP would be decreased. DXG-TP, 3TC-TP and (-)-FTC-TP levels were decreased in presence of their main competitor, Guo and dCyd,

respectively. Cyd was also assessed as potent competitor of 3TC and (-)-FTC phosphorylation but in our study, it did not affect the levels of 3TC-TP and (-)-FTC-TP (data not shown).

Table 08: 3TC-TP and (-)-FTC-TP levels in PBM cells treated with 3TC and (-)-FTC at 10 μ M, respectively with increasing concentrations of DXG; and DXG-TP levels in PBM cells treated with DXG 10 μ M and increasing concentrations of 3TC or (-)-FTC for 4 hr.

Dose (X μ M)	DXG-TP	DXG-TP	3TC-TP	(-)-FTC-TP
			pmol/10 ⁶ cells	
Treatment	DXG (10 μ M) + (-)-FTC (X)	DXG (10 μ M) + 3TC (X)	3TC (10 μ M) + DXG (X)	(-)-FTC (10 μ M) + DXG (X)
0	0.18 \pm 0.16	0.32 \pm 0.04	6.1 \pm 0.3	82 \pm 11
1	0.33 \pm 0.07	0.39 \pm 0.14	5.5 \pm 0.6	51 \pm 7
10	0.18 \pm 0.07	0.29 \pm 0.19	5.9 \pm 0.4	71 \pm 10
30	0.42 \pm 0.22	0.30 \pm 0.16	6.0 \pm 0.3	66 \pm 17
100	0.29 \pm 0.20	0.24 \pm 0.07	6.4 \pm 1.2	57 \pm 17
Control	DXG (10 μ M) + Guo (X)		3TC (10 μ M) + dCyd (X)	(-)-FTC (10 μ M) + dCyd (X)
10	0.14		3.6	22.1
100	0.12		1.5	8.4

Exposure of PBM cells to increasing concentrations of DXG did not affect 3TC-TP and (-)-FTC-TP levels ($p = 0.6$ and 0.1 , respectively). Similarly, DXG-TP levels were not affected when co-incubated with increasing concentrations of 3TC and (-)-FTC ($p = 0.7$ and 0.3 respectively) (**Table 08**). In the interest of understanding a possible mechanism of interaction between DXG, 3TC and (-)-FTC on the endogenous nucleotide pool, the levels of dNTP and NTP were also monitored. There was no statistical difference between dNTP and NTP levels at any concentration of DXG, 3TC or (-)-FTC added.

5.4 DXG phosphorylation is strongly inhibited by guanine nucleosides but not by other NRTI

Overall, it was found that DXG phosphorylation does not lead to high levels of DXG-TP (range: 80-250 fmol/10⁶ cells). However, these levels should be sufficient to meet the K_i of

DXG-TP for the reverse transcriptase, which is 0.05 μM and corresponds to ~ 10 fmol/ 10^6 cells (assuming a cell volume of 0.32 pL).⁴⁹ Lower levels of DXG-TP found in this work as compared with previous data from our lab could be due to different analytical methodologies, mass spectrometry *versus* radioactive detection.²⁰⁰ These differences may have resulted from the contamination of [³H]-DXG with $\sim 20\%$ of [³H]-guanine, which once converted to GTP has the same retention times as DXG-TP in the liquid chromatography column.^{60, 80}

Feng *et al.*,⁸⁰ suggested that both the first and the second step of DXG phosphorylation might be rate limiting (**Figure 36**). Therefore, DXG anabolism was studied in the presence of the antimetabolite RBV and several exogenous nucleosides in activated PBM cells.

Co-incubation with RBV successfully increased DXG phosphorylation, probably by increasing IMP, which is the primary source for phosphate (**Figure 36**), overcoming the first rate-limiting step. DXG-MP phosphorylation may be limited by low levels of dATP, the main nucleotide activating the 5'-NT, or low level of IMP.¹⁴² It is also possible that 5'-NT also dephosphorylates DXG-MP, converting it back to DXG (**Figure 36**), which was demonstrated by the rapid decrease in DXG-MP levels after 30 min of DXG removal from extracellular media. As a consequence, DXG-TP decayed in ~ 5 hr in PBM cells.

Co-incubation with guanosine, guanine and 2'-deoxyguanosine decreased DXG-TP levels. DXG-MP levels were not decreased by the addition of guanine, which is directly converted to GMP by hypoxanthine-guanine phosphoribosyl transferase. Subsequently, GMP can interfere with DXG-MP phosphorylation by GMP kinase. These findings support the importance of a second rate-limiting step in DXG phosphorylation.

In this study, DXG + ZDV, DXG + 3TC and DXG + (-)-FTC drug combinations were investigated using PBM cells. Even though these NRTI uses different enzymes of the nucleotide

salvage pathway for their anabolism, indirect effects might occur such as upregulation or downregulation of kinases, which could potentially interfere with phosphorylation and warrants the study of these combinations. As expected and as previously reported²⁰⁰ DXG and ZDV did not interfere with each other at the phosphorylation level in both activated and unactivated PBM cells, and over time. Similarly, DXG + 3TC and DXG + (-)-FTC did not show any changes of their respective triphosphate levels upon co-incubation. Therefore, the synergistic effect between DXG and ZDV and between DXG and 3TC⁶² might be due to another interaction. Molecular modeling approaches have suggested that the synergy between DXG and ZDV or 3TC occurs directly at the level of the HIV-1 RT, in which conformational changes of ZDV and 3TC mutants enhance the binding of DXG-TP to the active site of HIV-RT.¹⁰⁴ Enhanced formation of dead-end complex was also reported in the case of TDF and (-)-FTC,¹⁰² and could also occur in the context of DXG combination with ZDV or 3TC, which have not been assessed yet.

Intracellular variations of the endogenous nucleotide pool were carefully studied for their possible synergy with NRTI antiviral activity (see § 1.3.3.2). Co-incubation of DXG and ZDV resulted in significant decreases in the levels of TTP and dGTP. TTP decrease was attributed to the inhibition of thymidylate kinase by ZDV-MP.⁷⁷ The decline in dGTP is consistent with models of the allosteric regulation of the ribonucleotide reductase, in which low TTP concentrations would decrease the reduction of GDP (**Figure 19**).¹⁴⁸ This decrease in dGTP levels in DXG and ZDV treated cells may facilitate DXG-TP incorporation by the HIV-1 RT. Noteworthy, DXG + 3TC and DXG + (-)-FTC combinations were evaluated only for 4 hr, which might not be sufficient to evaluate variations of the dNTP pools. Similar dGTP levels were observed in DXG treated and untreated cells, excluding the hypothesis of self-synergism.

5.5 Do NRTI affect the endogenous nucleotide pool?

None of the NRTI tested at 4 hr decreased dNTP pool levels in PBM cells except for ZDV. The effect of NRTI on endogenous nucleotide pool was similar to a recent study performed in CEM cells by Vela *et al.* It is interesting to note that similar effects on endogenous dNTP pool were obtained in both cell types at different ZDV concentrations: 1000 μM in CEM cells *versus* 10 μM in PBM cells. Here, the levels of endogenous nucleotide pool were measured in both CEM and PHA activated PBM cells, which were compared to PHA+IL-2 stimulated cells since CEM produce its own IL-2 (**Table 09**).

Table 09: Endogenous dNTP pool in PBM cells and CEM cells.

	dCTP	dGTP	dATP	TTP
	pmol/10 ⁶ cells			
PHA activated PBM cells	1.17 ± 0.85	0.60 ± 0.29	2.95 ± 1.46	1.03 ± 0.40
PHA+IL-2 activated PBM cells	0.79 ± 0.11	1.07 ± 0.22	1.81 ± 0.17	4.67 ± 0.96
CEM cells	7.07 ± 4.45	17.3 ± 2.7	59.4 ± 5.0	97.1 ± 36.4

The levels of endogenous nucleotides were 8 to 100-fold lower in activated PBM cells than in CEM cells. Even though IL-2 stimulation slightly increased TTP and dGTP pools in PBM cells, it remained at least 10-fold lower than in CEM cells. The dNTP levels observed in CEM cells were similar to the range reported by Vela *et al.* (51.5 to 108 pmol/10⁶ cells). ZDV causes imbalances in dNTP pool in CEM cells at extracellular levels, which were 100-fold higher than in activated PBM cells. In summary, a CEM cell model is probably relevant for long-term studies, and might reflect *in vivo* conditions of proliferatively active cells. However, above physiological concentrations may be required in these cells as compared to PBM cells. Studies in primary human cells reflect a response that accounts for physiological levels and increased interindividual metabolic variability.

5.6 Conclusions

In summary, DXG metabolism is limited by the cofactors of its phosphorylation and by direct competition with guanosine ribonucleotides, supporting the existence of two rate limiting phosphorylation steps. As a consequence of the higher levels of ribonucleotide *versus* 2'-deoxyribonucleotides (about 400-fold higher GTP than dGTP levels), DXG-TP levels are low compared with 3TC or (-)-FTC, which compete only with dCyd pools. DXG can be successfully combined with ZDV, 3TC or (-)-FTC without direct intracellular interaction. The decrease of dGTP levels by ZDV-MP might enhance DXG-TP activity in PBM cells. Similarly, greater DXG-TP/dGTP ratio in unactivated compared with activated PBM cells might indicate a beneficial action of this drug in resting memory T lymphocytes, a persistent viral reservoir.

Following *in vitro* studies and preliminary evaluations in animal models,^{67, 228-230} DAPD, prodrug of DXG, was administered to HIV-1 infected subjects.^{63, 147, 231} DAPD monotherapy or as part of a combination was administered safely to over 200 individuals.¹⁹⁶ *In vitro* evaluation of the combination between DAPD/DXG and ZDV has insured of their lack of interaction at the triphosphate level.²⁰⁰ However, it was prudent to conduct a proof-of-concept study in 24 HIV-1 infected individuals to assess the antiviral activity and the pharmacology of this new drug combination in humans. This study was also designed to evaluate ZDV dose reduction, which should decrease toxicity but not antiviral activity.¹¹⁹ To analyze over 600 subject plasma samples from this proof-of-concept study, a new LC-MS/MS methodology had to be developed.

6 CHAPTER 3: Quantification of nucleosides in human plasma by LC-MS/MS as part of a clinical study for DAPD combination with reduced dose of ZDV

6.1 Simultaneous quantification of 9-(β -D-1,3-dioxolan-4-yl)guanine, amdoxovir and zidovudine in human plasma by LC-MS/MS assay²³²

The dosing of antiretroviral agent can be complex due to a significant potential for drug interactions, adverse effects and adherence challenges.^{69, 233} Resistance is still a major concern for NRTI, as is true for all classes of HIV drugs. Therefore, new compounds with improved properties that are safe, effective and with a high genetic barrier to resistance are warranted. Among these new compounds, DAPD has activity *in vitro* against wild type and drug-resistant forms of HIV-1, including viruses that are resistant to ZDV and 3TC (see § 1.3.3.4).^{62, 98, 120, 234}

The current approved oral dose of ZDV is 300 mg twice daily (bid). A recent *in silico* study using population enzyme kinetic and pharmacokinetic data, suggested that decreasing the dose of ZDV from 300 to 200 mg bid would decrease the amount of cellular ZDV-MP associated with hematological toxicity, without significantly reducing the cellular amount of ZDV-TP associated with antiviral efficacy.¹¹⁹ Thus, a clinical proof-of-concept study was conducted evaluating the combination of DAPD at 500 mg bid with standard and reduced doses of ZDV at 200 or 300 mg bid, respectively.¹¹⁹ Both combinations were safe and well tolerated,^{65, 118} and produced a similar 2- \log_{10} decrease in mean plasma HIV-1 RNA from baseline, at day 10, supporting the earlier *in silico* ZDV study.¹¹⁹ Thus, it was essential to develop a robust and validated LC-MS/MS method to measure the drug concentrations of DAPD, DXG and ZDV in plasma.

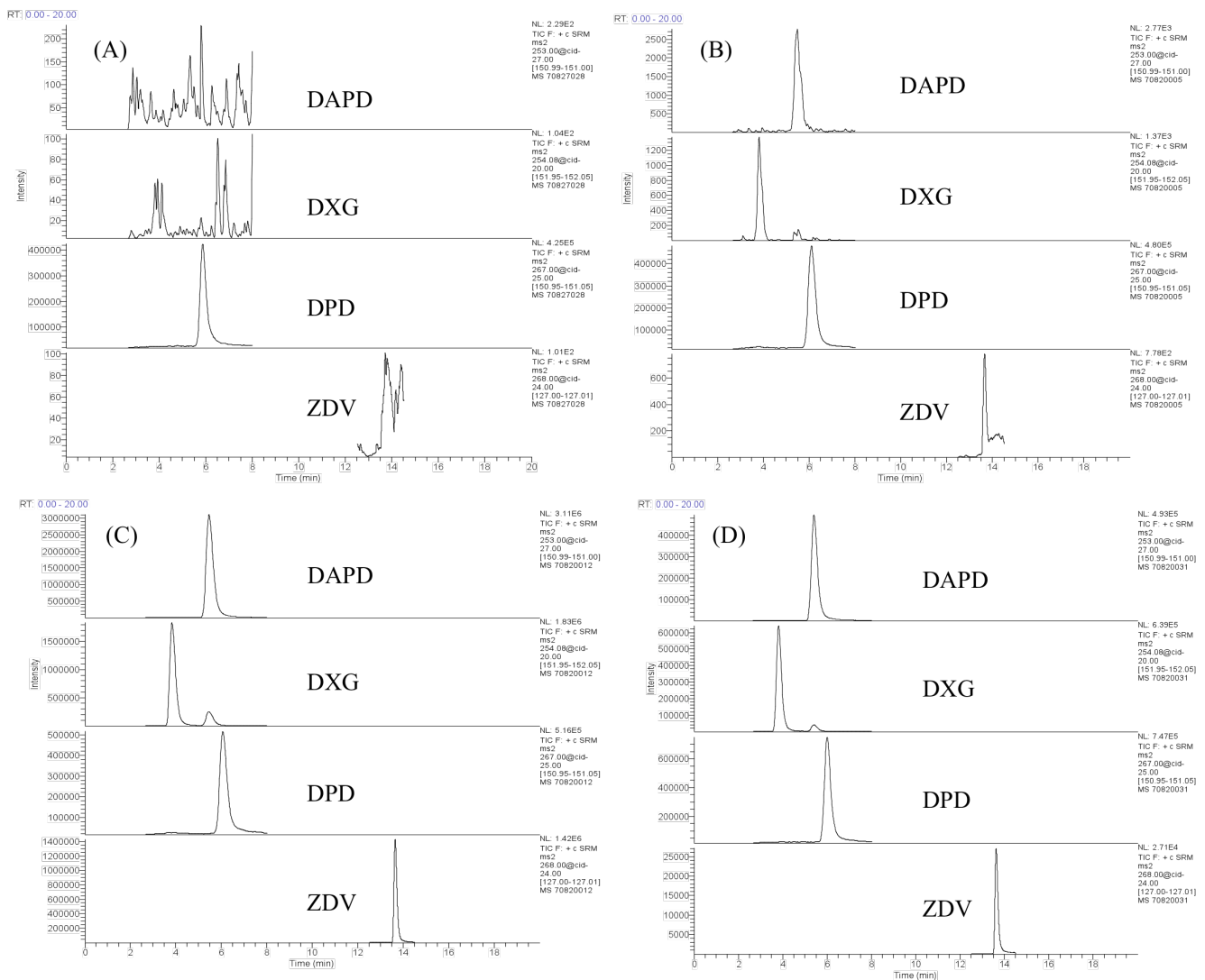
LC-MS/MS methodologies, such as reverse phase chromatography tandem mass spectrometry and electrospray ionization that have been used for the last decade, have demonstrated improved specificity and sensitivity, and are capable of measuring very low concentrations of nucleosides in plasma and other tissues. Recently, levels of quantification as low as 0.5 ng mL⁻¹ of ZDV in plasma were reported.²³⁵ The extraction of the nucleosides from the plasma for these assays typically involves either solid phase extraction,²³⁵⁻²³⁹ or simple sample clean up using a robotic system and disposable Centricon 30 ultra-filtration units.²⁴⁰

Simultaneous measurement of ZDV, DAPD and its major metabolite, DXG was accomplished, despite polarity differences between ZDV and the two guanosine analogues, and the similarity of DAPD and DXG differing by only one functional group (**Figure 26**). A previously unpublished method for DAPD and DXG quantification developed by Triangle Pharmaceuticals Inc. (acquired by Gilead Sciences in 2003) was modified to allow simultaneous quantification of ZDV in plasma. Herein, we present an optimized and improved method for extracting and simultaneously quantifying DAPD, DXG and ZDV in human plasma, as well as evidence of the reproducibility, accuracy and precision of this method.

6.1.1 LC-MS/MS characteristics

Typical LC-MS/MS chromatograms for extracted DAPD, DXG, ZDV and 2,6-diaminopurine-2'-deoxyriboside (DPD, internal standard) compared with standard extracted from plasma blank are shown in **Figure 41**. The retention times of DAPD, DXG, DPD and ZDV were 5.49, 3.86, 6.10 and 13.65 min, respectively.

Figure 41: Reconstituted ion chromatograms (RIC) for (A) patient plasma obtained on first day of treatment before first dose administration, (B) healthy subject plasma at 2 ng mL⁻¹ of each standards, (C) healthy subject plasma at 3,000 ng mL⁻¹ of each standards and (D) patient plasma four hr after the first dose administration; the calculated analyte concentrations were as follow: 328 ng mL⁻¹, 693 ng mL⁻¹ and 43 ng mL⁻¹ for DAPD, DXG and ZDV, respectively (all plasma samples from healthy subjects and patient were treated with methanol containing internal standard, DPD). The top trace is the RIC for DAPD, the second trace is the RIC for DXG, the third trace is the RIC for DPD and the bottom trace is the RIC for ZDV. The retention time appears on top of the peak.



An additional peak was observed at 5.45 min on DXG reconstituted ion chromatogram (RIC) in both patient and standard, but not in blank plasma. This interference was observed at the same retention time as DAPD. This peak was approximately 10% of DAPD signal intensity and resulted from the isotope distribution of DAPD. The chromatographic separation was essential in order to accurately quantify DXG. A plasma sample from a patient was also analyzed without internal standard to confirm that no endogenous substances interfered with any of the analytes, including the internal standard.

The highest intensity for protonated ions was found in positive mode for all analytes and internal standard as they have an ability to accept protons. The introduction of a methanol-water-formic acid (80:20:0.4 v/v/v) solution to the electrospray ionization (ESI) source, while the effluent from the column was diverted to waste, increased the intensity and participated in rinsing the source. The optimization of capillary temperature and nitrogen flow was considered important as they both played an important role in minimizing ion suppression and increasing the sensitivity of the method.

6.1.2 Calibrations curves and limit of quantification

The standard curve was obtained by fitting the ratio of the peak height of DAPD, DXG and ZDV to that of the internal standard against the concentrations (2-3,000 ng mL⁻¹) of DAPD and DXG and (2-5,000 ng mL⁻¹) of ZDV using a $1/x$ weighted linear regression ($y = Ax + B$). The lower limit of quantification (LLOQ) was 2 ng mL⁻¹, which could be quantified accurately with a precision within $\pm 20\%$ for each analyte. This corresponds to an amount of 3.2 pg of analyte injected on column. The upper limit of quantification (ULOQ) was 3,000 ng mL⁻¹ for DAPD and DXG and 5,000 ng mL⁻¹ for ZDV.

6.1.3 Validation results

6.1.3.1 Extraction recovery and matrix effect

Recovery was determined by measuring an extracted sample against a post-extracted spiked sample. Matrix effect was determined by measuring a post-extracted spiked sample and an un-extracted sample. Three concentrations (10, 100 and 1,000 ng mL⁻¹) were used and assayed in duplicates (**Table 10**). Absolute values were determined by comparing areas and relative values determined by comparing ratios (area of the analyte over the area of the internal standard).

Table 10: Recovery and matrix effect (10, 100 and 1,000 ng mL⁻¹) in duplicate.

Analyte	Conc. (ng mL ⁻¹) ^a	Absolute recovery (%)	Relative recovery (%)	Absolute matrix effect (%)	Relative matrix effect (%)
DXG	10	81.8	91.8	33.1	23.0
DAPD		95.3	92.3	9.5	-3.0
ZDV		101.3	97.3	12.6	0.8
DXG	100	97.2	104.9	34.2	16.6
DAPD		89.3	94.5	21.0	-0.6
ZDV		91.4	95.6	22.5	2.5
DXG	1,000	92.3	106.5	19.7	15.0
DAPD		86.9	93.2	3.3	-2.6
ZDV		67.4	80.4	5.1	-0.3

^aTo convert ng mL⁻¹ to nM, the concentration should be divided by 253, 252, 267 for DXG, DAPD and ZDV, respectively.

The relative recovery and matrix effect values reflect general analyte loss on both the analyte and the internal standard. The absolute values represent specific loss occurring during the extraction or specific ion suppression. For all analytes, the recovery values provided confidence in the extraction process. Greater matrix effect was observed for DXG compared with DAPD and ZDV, but the ion suppression did not significantly vary with increasing concentrations of DXG, allowing the linearity of the response.

6.1.3.2 Accuracy and precision

The results of intra-assay and inter-assay precision for three concentrations (low, medium and high) are summarized in **Table 11**. Instrument intra-assay precision was < 5% and accuracy was > 95% at all concentrations. Instrument inter-assay precision was < 10% at all concentrations, accuracy was > 80% at low concentration and > 99% at high and medium concentrations. Extraction reproducibility was in the range of 94.1-103.6 % accuracy and 7.1-13.5% precision.

Table 11: Intra- and inter-assay precision and inter-assay reproducibility for all three analytes.

Analyte	Conc. ^a (ng mL ⁻¹)	Intra-assay precision (n = 6 runs)		Inter-assay precision (n = 4 runs)		Inter-assay extraction reproducibility (n = 5 replicates)	
		Accuracy (%)	CV (%)	Accuracy (%)	CV (%)	Accuracy (%)	CV (%)
DXG	10	104.6	3.4	90.8	2.7	99.1	9.2
DAPD		104.5	4.1	82.7	7.0	97.2	8.1
ZDV		97.2	1.4	85.0	5.1	101.7	10.9
DXG	100	108.2	3.2	107.4	8.5	103.6	10.5
DAPD		106.1	0.4	104.5	9.3	97.9	7.7
ZDV		103.7	3.1	102.4	3.5	103.1	13.5
DXG	1,000	106.8	2.5	105.4	4.6	101.3	7.1
DAPD		106.1	1.4	102.9	4.8	94.1	10.3
ZDV		105.7	1.5	99.3	1.9	96.8	9.11

^aTo convert ng mL⁻¹ to nM, the concentration should be divided by 253, 252, 267 for DXG, DAPD and ZDV, respectively.

6.1.3.3 Stability

The analytes were found to be stable under all conditions tested and the variation in concentration was minimal with 84% to 110% recovery (**Table 12**).

Table 12: Stability of the analytes extracted from plasma spiked at 1,000 ng mL⁻¹ under temperature variation conditions.

Analyte	24 hr at room temperature (% Recovery)	40 hr at 4°C (% Recovery)	5 days at 4°C (% Recovery)	4 freeze/thaw cycles at - 20°C (% Recovery)
DXG	101	104	91	110
DAPD	92	100	95	99
ZDV	96	91	84	104

6.1.3.4 Carryover

At LLOQ, for ZDV and DXG, the peaks in the blank following the injection at 2 ng mL⁻¹ were in the range of the background noise of the reconstituted ion chromatogram and consequently were not integrated. For DAPD, at LLOQ, the carryover was 8% in the first blank and 4% in the second blank, which were acceptable. For all analytes, at ULOQ, the carryover was below 0.08% in the first blank and below 0.03% in the second.

6.1.4 Discussion of the analytical advances by the present method

An improved method was developed and validated for high throughput simultaneous measurement of DAPD, DXG and ZDV levels in plasma, generating data necessary for clinical and pharmacokinetic analysis. LC-MS/MS methods have been used successfully for the last decade for quantification of antiretroviral agents, including NRTI in biological matrix. Limited work was available for DAPD and DXG. However, ZDV quantification by LC-MS/MS, using reverse phase chromatography, has been described previously.^{235-237, 240, 241} Short runs were used for ZDV detection with mobile phase containing 0.1% of acetic acid²⁴¹ or at neutral pH.^{235, 240} However, at pH 4.8, which improved DAPD and DXG separation, ZDV retention was increased, which could be explained by the work of Bezy et al, who demonstrated that at a pH between 5 and 7, ZDV was neutral and its retention was increased, whereas at pH 9, ZDV became negatively charged with a low retention.²³⁶ ZDV was detected either in positive^{242, 243} or

negative mode,^{235-237, 240, 241} depending on the mobile phase used. In our case, the positive mode was found to have greater sensitivity for all analytes. The challenge was to obtain a discriminating and rapid separation of DAPD and DXG, which have similar molecular weights and fragmentation patterns, while still achieving simultaneous detection of ZDV, which is less polar than DAPD and DXG.

A binary method was developed, consisting of an isocratic elution of DAPD, DXG and DPD in the first 8 min of the run followed by a fast gradient for ZDV elution, because of its strong affinity for the stationary phase. Following the gradient, it became essential to optimize the equilibration time of the column with 6% methanol in order to maintain consistent retention times for DAPD and DXG for the subsequent injection, since these retention times were very sensitive to slight variations in methanol concentration. The peak shape of all analytes was improved by the addition of 0.04 mM of 2'-dA, creating a shift in baseline signal of the reconstituted ion chromatogram, and decreasing background noise. 2'-dA may act as a silanol-masking agent, which could prevent the non-specific binding of the analytes to the column. It may also produce an ion-pairing effect with other nucleosides, enhancing the shape of the peaks. The peak shape was also greatly improved by using a microbore column with 3 µm particle size, which allowed the use of lower flow rates than wider columns with bigger particle size, while increasing the backpressure. Increasing the particle size to 5 µm and using a different column such as Hypersil GOLD-C18 (100 x 1 mm, 5 µm particle size; Thermo Scientific, Waltham, MA, USA) caused a peak broadening. However, the use of shorter column to reduce the run time decreased the resolution between DXG and DAPD introducing quantification error due to signal overlap. Several gradients were tested, but the steepest slope was necessary to shorten the re-equilibration time. The use of this column improved the assay sensitivity by decreasing the need

for sample dilution. Furthermore, a reduction in mobile phase volume introduced to the ion source provided the added benefit of decreasing the ion suppression over time, rendering high throughput analysis of the clinical trial samples possible. In addition, reducing the amount of mobile phase, and therefore the amount of organic solvent, was advantageous, since it reduced the cost of the analysis, and was also more ecological. For the clinical study, 43 clinical samples were successfully assayed in sequences of 26 hr, including standards and QCs.

In this method, the extraction was performed manually, which was time consuming, but could be further adapted and applied in high throughput applications. Kenney et al. used a robotic system, which decrease bias and imprecision, as well as increase the throughput.²⁴⁰ The extraction imprecision and inaccuracy did not exceed 15% for five days, achieving the limits required for validation of the method.

6.2 Application: Pharmacokinetics of DAPD plus ZDV¹⁹⁶

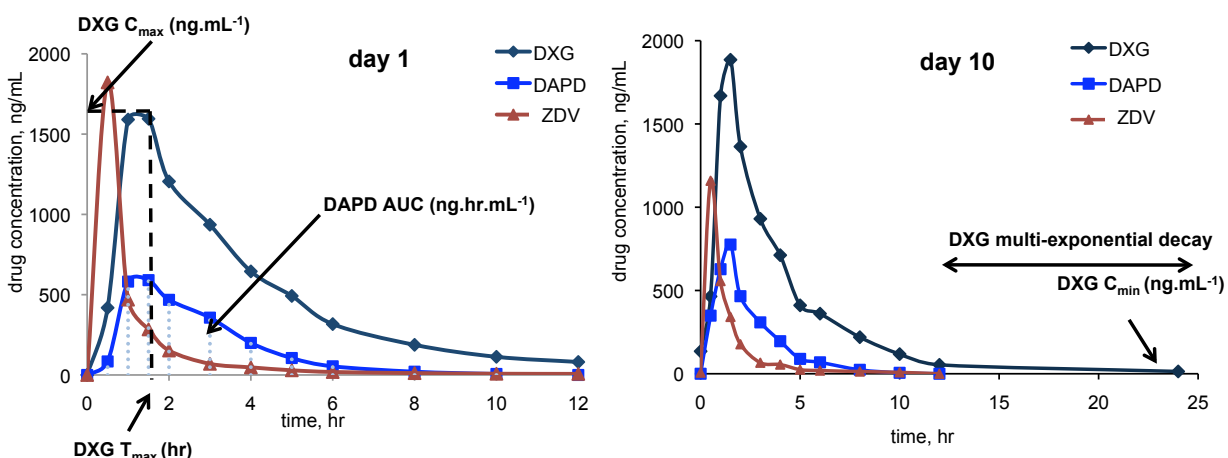
This new method allowed simultaneous measurement of DAPD, DXG and ZDV in clinical samples for assessment of potential two-way drug-drug interactions. It also contributed to the assessment of pharmacokinetics (PK), particularly for DAPD and DXG, and in combination with reduced and standard doses of ZDV. PK of ZDV (as monotherapy and in combinatorial regimens) has been extensively studied over the past 20 years. These results have extended the information on the rate and amount of DXG formation from DAPD.¹¹⁹

6.2.1 Non-compartmental PK analysis

Non-compartmental pharmacokinetic analysis was performed on the plasma data using Kinetica software (v5.0, Thermo Scientific, Waltham, MA) to determine areas under the plasma concentration *versus* time curves between doses: 12 hours, AUC_{12 hr} (**Figure 42**). The ratios

$AUC_{12\text{ hr day10}}/AUC_{\text{day1}}$ were used to determine drug accumulation, assuming steady state at day 10. Half-lives were estimated from the slowest apparent first-order decline period of the curve for that dose.¹⁹⁶

Figure 42: A typical plasma concentration *versus* time curve for a random patient administered all DAPD/ZDV at day 1 and day 10. Physical representation for the maximal and minimal concentration (C_{max} , C_{min} , respectively), time at C_{max} (T_{max}) and the AUC are displayed.



6.2.2 Evidence for the lack of interaction between DAPD and ZDV

DAPD C_{max} ranged between 446 and 748 ng mL^{-1} . DXG C_{max} ranged between 1,275 and 1,922 ng mL^{-1} . There were no significant differences between DAPD or DXG PK parameters in plasma whether it was administered alone or with ZDV 200 or 300 mg, by Tukey's paired comparisons ($p > 0.5$).¹⁹⁶ DAPD declined more rapidly than DXG with $t_{1/2}$ of 1.3 to 1.6 hr compared with 2.5 to 2.9, respectively. At day 10 DXG plasma levels were still above the limit of detection at 24 hr, and in some patients were even higher at 48 hr than at 12 hr. When including the 24 hr and 48 hr points, DXG $t_{1/2}$ was 14.7 to 17.6 hr, which is indicative of a multi-exponential decay in plasma (**Figure 42**). This dose accumulation of DXG could result in a higher potency. On the contrary, no dose accumulation was observed for DAPD. The mean steady-state (day 10) plasma concentrations of DXG were between 75 and 121 ng mL^{-1} for all

cohorts (n = 18), which exceeded the anti-HIV-1 (wild type) EC₅₀ (50% effective concentration) *in vitro* of 0.25 ± 0.17 μM (equivalent to 63 ± 43 ng mL⁻¹) measured using PHA stimulated PBM cells,⁶⁰ and 0.05 ± 0.02 μM (12 ± 4 ng mL⁻¹) using human cord blood mononuclear cells.¹⁰³

There was no significant difference between ZDV PK parameters whether it was administered alone or with DAPD, by Tukey's paired comparisons (p > 0.5). The AUC_{12hr day 10}/AUC_{day 1} ranged from 0.86 to 1.21, suggesting limited dose accumulation, as expected due to the relatively short t_{1/2} of ZDV.¹⁹⁶

6.3 Conclusions

A sensitive and robust LC-MS/MS method was developed and validated for simultaneous measurement of DAPD, DXG and ZDV in plasma. The ability to simultaneously measure these NRTI was essential for effectively scaling-up the measurement of a large numbers of samples with low limits of quantifications in the clinical trial. The results obtained¹⁹⁶ using this optimized method were in agreement with previous studies of the pharmacokinetics of DAPD/DXG^{63, 244} as monotherapy and ZDV^{229, 245, 246} given alone or in combination with existing HAART. It was prudent to perform a proof-of-concept study to assess whether any clinically significant two-way PK interactions occur between ZDV and DAPD or its metabolite, DXG as a prelude of to larger phase IIb study. Another objective of that study was to determine whether ZDV could be administered at a reduced dosage of 200 mg bid *versus* the accepted 300 mg bid, without compromising efficacy. This approach was considered to reduce the dose limiting toxicities of ZDV as suggested by Barry, et al.²⁴⁷

7 **Conclusions and perspectives**

The research presented in this dissertation demonstrates the efficiency and utility of the LC-MS/MS technique for measuring nucleosides and nucleotides in biological matrices. Our laboratory is focused on HIV and hepatitis drug discovery. The LC-MS/MS assay enabled mechanistic and clinical study of NRTI in various cell types and in humans. Comparing the metabolism of NRTI in primary human lymphocytes, the main HIV-1 target and macrophages, a major viral reservoir, may contribute to the design of more efficient drugs leading potentially to viral eradication.⁴⁴ Factors limiting drug efficacy must be identified such as drug-drug interactions, as well as pharmacokinetic limitations in adsorption, distribution, metabolism, and excretion.

Technically, both cellular and plasma samples demonstrate a high interference with the mass spectrometer signal. These constraints required optimization of sample preparation, and efficient chromatography separation, which added to the ESI-MS/MS sensitivity and specificity. The choice of a microbore column for both plasma and cellular methodologies reduced the need for sample dilution and overcame ion suppression, thereby increasing the detection sensitivity to acceptable levels. The final method was robust and allowed for the quantification of over 15 nucleosides and nucleotides (natural and antiviral agents).

The first chapter describes the development of an ion-pair chromatography methodology for the simultaneous measurement of NRTI-TP and endogenous dNTP in primary human lymphocytes and macrophages. Both NRTI-TP and endogenous dNTP levels were significantly lower in macrophages than in lymphocytes, which may be due to the lower expression of phosphorylating enzymes or nucleoside transporters in non-replicating cells. Individual differences may be seen when comparing NRTI-TP levels with their corresponding endogenous

deoxyribonucleotides. In this study, DXG-TP/dGTP ratio was greater in macrophages than in lymphocytes, suggesting a higher probability for DXG-TP to be incorporated by the HIV-1 RT.

This methodology was applied in the second chapter, to evaluate the limitations of DXG metabolism, which results in low levels of DXG-TP in PBM cells likely due to the competition with a large pool of ribonucleosides for phosphorylation. This might apply to other purine analogues, such as ddi, ABC (**Figure 32**) or TFV,¹⁴⁵ which are less efficiently phosphorylated than cytidine analogues. The study of DXG in combination with ZDV, 3TC and (-)-FTC confirmed the lack of interaction between these nucleoside analogues at the phosphorylation levels.²⁰⁰ It also confirmed previous findings regarding the depletion of TTP and dGTP upon ZDV exposure.⁷⁷ Therefore, the synergistic effect between DXG and ZDV might be due to the increased probability of DXG-TP incorporation by the HIV-1 RT in the presence of ZDV. To verify this hypothesis, it would be interesting to measure the synergism of these two drugs in the presence of an optimized amount of uridine. If the uridine is added at such a concentration that DXG-TP and ZDV-TP levels remains unchanged, but endogenous dGTP and TTP return to normal, the synergistic effect should disappear. If it does not, our hypothesis would be wrong.

The last chapter presents the development and validation of a LC-MS/MS methodology for plasma analysis. This method contributed to the elucidation of the pharmacokinetics of DAPD/DXG in combination with standard and reduced dose of ZDV, establishing the lack of interaction between DAPD/DXG and ZDV in HIV-1 infected persons.

In vitro results must be interpreted with caution, rendering human studies necessary. For instance, the combination of DAPD with an IMPDH inhibitor in humans, failed to increase its potency despite promising *in vitro* results.¹⁴⁷ Although levels of DXG-TP are low in PBM cells and display an attenuated half-life, the half-life of DXG in plasma is significantly longer, ranging

from 3-18 hr. Continuous exposure of human PBM cells in the periphery to DXG may serve as a compensatory mechanism to continually supply these cells with drug, resulting in an extended intracellular half-life of DXG-TP in humans.¹⁹⁶ *In vivo*, both DAPD and DXG deliver DXG-TP to the cells, which might result in increased levels *versus in vitro* incubation of DXG only. Despite the promising results of the recent proof-of-concept study in humans,^{65, 196} new prodrugs of DXG should be designed to increase its solubility.⁶⁶ Since the antiviral activity of NRTI correlates with the cellular accumulation of NRTI-TP, rather than NRTI plasma concentrations,¹⁰⁸ it will be important to measure the accumulation of NRTI-TP in the PBM cells of these 24 HIV-infected individuals to explore whether they are indeed correlated with the decreased viral loads observed in individuals enrolled in the study.

Another future project is to measure the ribonucleotides (rNTP) in lymphocytes *versus* macrophages. The ratio of rNTP/dNTP is substantially higher in macrophages than in lymphocytes. Since rNTP can also be incorporated in the DNA template synthesized by HIV-1 RT, higher rNTP availability in macrophages might explain the greater error-prone DNA synthesis in these cells *versus* lymphocytes.²⁴⁸

Technically, the ion-pair methodology may be improved with the use of a porous graphitic column.^{199, 210}

In conclusion, this work has provided specific, sensitive and accurate LC-MS/MS methodologies to better understand the metabolism of NRTI in PBM cells, in macrophages and in humans. It provides a foundation for extensive *in vitro* screening for the metabolism of new antiviral agents and for future analysis of the interplay between antiretroviral NRTI and natural nucleosides in clinical studies.

8 References

1. Pneumocystis pneumonia--Los Angeles. MMWR Morb Mortal Wkly Rep 1981;30:250-2.
2. Kaposi's sarcoma and Pneumocystis pneumonia among homosexual men--New York City and California. MMWR Morb Mortal Wkly Rep 1981;30:305-8.
3. Francis DP, Curran JW, Essex M. Epidemic acquired immune deficiency syndrome: epidemiologic evidence for a transmissible agent. J Natl Cancer Inst 1983;71:1-4.
4. Gallo RC, Sarin PS, Gelmann EP, et al. Isolation of human T-cell leukemia virus in acquired immune deficiency syndrome (AIDS). Science 1983;220:865-7.
5. Barre-Sinoussi F, Chermann JC, Rey F, et al. Isolation of a T-lymphotropic retrovirus from a patient at risk for acquired immune deficiency syndrome (AIDS). Science 1983;220:868-71.
6. Basavapathruni A, Anderson KS. Reverse transcription of the HIV-1 pandemic. FASEB J 2007;21:3795-808.
7. Fauci AS. HIV and AIDS: 20 years of science. Nat Med 2003;9:839-43.
8. Sharp PM, Hahn BH. AIDS: prehistory of HIV-1. Nature 2008;455:605-6.
9. Worobey M, Gemmel M, Teuwen DE, et al. Direct evidence of extensive diversity of HIV-1 in Kinshasa by 1960. Nature 2008;455:661-4.
10. UNAIDS/WHO. 2009 AIDS epidemic update. In: Joint United Nations Programme on HIV/AIDS (UNAIDS) and world health organization (WHO); 2009.
11. Flint SJ, Enquist L.W., Racaniell, V.R., Skalka, A.M. Human Immunodeficiency Virus Pathogenesis. In: press A, ed. Principles of Virology, ed2. Washington, D.C; 2001:653-23.
12. Sierra S, Kupfer B, Kaiser R. Basics of the virology of HIV-1 and its replication. J Clin Virol 2005;34:233-44.
13. Lasky LA, Nakamura G, Smith DH, et al. Delineation of a region of the human immunodeficiency virus type 1 gp120 glycoprotein critical for interaction with the CD4 receptor. Cell 1987;50:975-85.
14. Stevenson M. Basic science summary. Top HIV Med 2009;17:30-4.
15. Goff SP. Retroviral reverse transcriptase: synthesis, structure, and function. J Acquir Immune Defic Syndr 1990;3:817-31.
16. Jacobo-Molina A, Arnold E. HIV reverse transcriptase structure-function relationships. Biochemistry 1991;30:6351-6.
17. di Marzo Veronese F, Copeland TD, DeVico AL, et al. Characterization of highly immunogenic p66/p51 as the reverse transcriptase of HTLV-III/LAV. Science 1986;231:1289-91.
18. Kohlstaedt LA, Wang J, Friedman JM, Rice PA, Steitz TA. Crystal structure at 3.5 Å resolution of HIV-1 reverse transcriptase complexed with an inhibitor. Science 1992;256:1783-90.
19. Jacobo-Molina A, Ding J, Nanni RG, et al. Crystal structure of human immunodeficiency virus type 1 reverse transcriptase complexed with double-stranded DNA at 3.0 Å resolution shows bent DNA. Proc Natl Acad Sci U S A 1993;90:6320-4.
20. Rodgers DW, Gamblin SJ, Harris BA, et al. The structure of unliganded reverse transcriptase from the human immunodeficiency virus type 1. Proc Natl Acad Sci U S A 1995;92:1222-6.
21. Preston BD, Poiesz BJ, Loeb LA. Fidelity of HIV-1 reverse transcriptase. Science 1988;242:1168-71.
22. Menendez-Arias L. Targeting HIV: antiretroviral therapy and development of drug resistance. Trends Pharmacol Sci 2002;23:381-8.
23. Mansky LM, Temin HM. Lower in vivo mutation rate of human immunodeficiency virus type 1 than that predicted from the fidelity of purified reverse transcriptase. J Virol 1995;69:5087-94.
24. Coffin JM. HIV population dynamics in vivo: implications for genetic variation, pathogenesis, and therapy. Science 1995;267:483-9.

25. Gao F, Chen Y, Levy DN, Conway JA, Kepler TB, Hui H. Unselected mutations in the human immunodeficiency virus type 1 genome are mostly nonsynonymous and often deleterious. *J Virol* 2004;78:2426-33.
26. Roberts JD, Bebenek K, Kunkel TA. The accuracy of reverse transcriptase from HIV-1. *Science* 1988;242:1171-3.
27. Smith RA, Loeb LA, Preston BD. Lethal mutagenesis of HIV. *Virus Res* 2005;107:215-28.
28. Julias JG, Pathak VK. Deoxyribonucleoside triphosphate pool imbalances in vivo are associated with an increased retroviral mutation rate. *J Virol* 1998;72:7941-9.
29. Chen R, Wang H, Mansky LM. Roles of uracil-DNA glycosylase and dUTPase in virus replication. *J Gen Virol* 2002;83:2339-45.
30. Goff SP. Death by deamination: a novel host restriction system for HIV-1. *Cell* 2003;114:281-3.
31. Stevenson M. HIV-1 pathogenesis. *Nat Med* 2003;9:853-60.
32. Margolis L, Shattock R. Selective transmission of CCR5-utilizing HIV-1: the 'gatekeeper' problem resolved? *Nat Rev Microbiol* 2006;4:312-7.
33. Douek DC, Picker LJ, Koup RA. T cell dynamics in HIV-1 infection. *Annu Rev Immunol* 2003;21:265-304.
34. Douek D. HIV disease progression: immune activation, microbes, and a leaky gut. *Top HIV Med* 2007;15:114-7.
35. Coffin JM, Hughes SH, Varmus HE, eds. *Retroviruses*. CSHL Press ed: Library of Congress Cataloging-in-Publication Data; 1997.
36. Chun TW, Engel D, Berrey MM, Shea T, Corey L, Fauci AS. Early establishment of a pool of latently infected, resting CD4(+) T cells during primary HIV-1 infection. *Proc Natl Acad Sci U S A* 1998;95:8869-73.
37. Igarashi T, Brown CR, Endo Y, et al. Macrophage are the principal reservoir and sustain high virus loads in rhesus macaques after the depletion of CD4+ T cells by a highly pathogenic simian immunodeficiency virus/HIV type 1 chimera (SHIV): Implications for HIV-1 infections of humans. *Proc Natl Acad Sci U S A* 2001;98:658-63.
38. Aquaro S, Calio R, Balzarini J, Bellocchi MC, Garaci E, Perno CF. Macrophages and HIV infection: therapeutical approaches toward this strategic virus reservoir. *Antiviral Res* 2002;55:209-25.
39. Richman DD, Margolis DM, Delaney M, Greene WC, Hazuda D, Pomerantz RJ. The challenge of finding a cure for HIV infection. *Science* 2009;323:1304-7.
40. Gartner S, Markovits P, Markovitz DM, Kaplan MH, Gallo RC, Popovic M. The role of mononuclear phagocytes in HTLV-III/LAV infection. *Science* 1986;233:215-9.
41. Koenig S, Gendelman HE, Orenstein JM, et al. Detection of AIDS virus in macrophages in brain tissue from AIDS patients with encephalopathy. *Science* 1986;233:1089-93.
42. Weinberg JB, Matthews TJ, Cullen BR, Malim MH. Productive human immunodeficiency virus type 1 (HIV-1) infection of nonproliferating human monocytes. *J Exp Med* 1991;174:1477-82.
43. Chun TW, Carruth L, Finzi D, et al. Quantification of latent tissue reservoirs and total body viral load in HIV-1 infection. *Nature* 1997;387:183-8.
44. Gavegnano C, Schinazi RF. Antiretroviral therapy in macrophages: implication for HIV eradication. *Antivir Chem Chemother* 2009;20:63-78.
45. Wiley CA, Schrier RD, Nelson JA, Lampert PW, Oldstone MB. Cellular localization of human immunodeficiency virus infection within the brains of acquired immune deficiency syndrome patients. *Proc Natl Acad Sci U S A* 1986;83:7089-93.
46. Pomerantz RJ, Horn DL. Twenty years of therapy for HIV-1 infection. *Nat Med* 2003;9:867-73.
47. Rothenberg R, Woelfel M, Stoneburner R, Milberg J, Parker R, Truman B. Survival with the acquired immunodeficiency syndrome. Experience with 5833 cases in New York City. *N Engl J Med* 1987;317:1297-302.
48. The food and drug administration. Antiretroviral drugs used in the treatment of HIV infection; 2010 January 12th, 2010.
<http://www.fda.gov/ForConsumers/byAudience/ForPatientAdvocates/HIVandAIDSActivities/ucm118915.htm>

49. Schinazi RF, Hernandez-Santiago BI, Hurwitz SJ. Pharmacology of current and promising nucleosides for the treatment of human immunodeficiency viruses. *Antiviral Res* 2006;71:322-34.
50. Mitsuya H, Weinhold KJ, Furman PA, et al. 3'-Azido-3'-deoxythymidine (BW A509U): an antiviral agent that inhibits the infectivity and cytopathic effect of human T-lymphotropic virus type III/lymphadenopathy-associated virus in vitro. *Proc Natl Acad Sci U S A* 1985;82:7096-100.
51. Mitsuya H, Broder S. Inhibition of the in vitro infectivity and cytopathic effect of human T-lymphotropic virus type III/lymphadenopathy-associated virus (HTLV-III/LAV) by 2',3'-dideoxynucleosides. *Proc Natl Acad Sci U S A* 1986;83:1911-5.
52. Yarchoan R, Mitsuya H, Thomas RV, et al. In vivo activity against HIV and favorable toxicity profile of 2',3'-dideoxyinosine. *Science* 1989;245:412-5.
53. Yarchoan R, Perno CF, Thomas RV, et al. Phase I studies of 2',3'-dideoxycytidine in severe human immunodeficiency virus infection as a single agent and alternating with zidovudine (AZT). *Lancet* 1988;1:76-81.
54. Baba M, Pauwels R, Herdewijn P, De Clercq E, Desmyter J, Vandeputte M. Both 2',3'-dideoxythymidine and its 2',3'-unsaturated derivative (2',3'-dideoxythymidinene) are potent and selective inhibitors of human immunodeficiency virus replication in vitro. *Biochem Biophys Res Commun* 1987;142:128-34.
55. Schinazi RF, Chu CK, Peck A, et al. Activities of the four optical isomers of 2',3'-dideoxy-3'-thiacytidine (BCH-189) against human immunodeficiency virus type 1 in human lymphocytes. *Antimicrob Agents Chemother* 1992;36:672-6.
56. Ray AS, Schinazi RF, Murakami E, et al. Probing the mechanistic consequences of 5-fluorine substitution on cytidine nucleotide analogue incorporation by HIV-1 reverse transcriptase. *Antivir Chem Chemother* 2003;14:115-25.
57. Daluge SM, Good SS, Faletto MB, et al. 1592U89, a novel carbocyclic nucleoside analog with potent, selective anti-human immunodeficiency virus activity. *Antimicrob Agents Chemother* 1997;41:1082-93.
58. Robbins BL, Srinivas RV, Kim C, Bischofberger N, Fridland A. Anti-human immunodeficiency virus activity and cellular metabolism of a potential prodrug of the acyclic nucleoside phosphonate 9-R-(2-phosphonomethoxypropyl)adenine (PMPA), Bis(isopropylloxymethylcarbonyl)PMPA. *Antimicrob Agents Chemother* 1998;42:612-7.
59. Tsai CC, Follis KE, Sabo A, et al. Prevention of SIV infection in macaques by (R)-9-(2-phosphonylmethoxypropyl)adenine. *Science* 1995;270:1197-9.
60. Furman PA, Jeffrey J, Kiefer LL, et al. Mechanism of action of 1-beta-D-2,6-diaminopurine dioxolane, a prodrug of the human immunodeficiency virus type 1 inhibitor 1-beta-D-dioxolane guanosine. *Antimicrob Agents Chemother* 2001;45:158-65.
61. Corbett AH, Rublein JC. DAPD (Emory University/Triangle Pharmaceuticals/Abbott Laboratories). *Curr Opin Investig Drugs* 2001;2:348-53.
62. Gu Z, Wainberg MA, Nguyen-Ba N, et al. Mechanism of action and in vitro activity of 1',3'-dioxolanyl-purine nucleoside analogues against sensitive and drug-resistant human immunodeficiency virus type 1 variants. *Antimicrob Agents Chemother* 1999;43:2376-82.
63. Thompson MA, Kessler HA, Eron JJ, Jr., et al. Short-term safety and pharmacodynamics of amdoxovir in HIV-infected patients. *AIDS* 2005;19:1607-15.
64. Won SY, Kessler HA. *Amdoxovir. The use of antibiotics: a clinical review of antibacterial, antifungal and antiviral drugs.* Avon: The Bath Press; 2009.
65. Murphy RL, Kivel NM, Zala C, et al. Antiviral activity and tolerability of amdoxovir in combination with zidovudine in a randomized double-blind placebo controlled study in HIV-1 infected persons. *Antiviral therapy* 2010;15(2):185-92.
66. Narayanasamy J, Pullagurla MR, Sharon A, Wang J, Schinazi RF, Chu CK. Synthesis and anti-HIV activity of (-)-beta-D-(2R,4R)-1,3-dioxolane-2,6-diamino purine (DAPD) (amdoxovir) and (-)-beta-D-(2R,4R)-1,3-dioxolane guanosine (DXG) prodrugs. *Antiviral Res* 2007;75:198-209.

67. Menne S, Asif G, Narayanasamy J, et al. Antiviral effect of orally administered (-)-beta-D-2-aminopurine dioxolane in woodchucks with chronic woodchuck hepatitis virus infection. *Antimicrob Agents Chemother* 2007;51:3177-84.
68. Mehellou Y, De Clercq E. Twenty-six years of anti-HIV drug discovery: where do we stand and where do we go? *J Med Chem*;53:521-38.
69. van de Waterbeemd H, Gifford E. ADMET in silico modelling: towards prediction paradise? *Nat Rev Drug Discov* 2003;2:192-204.
70. Tan X, Chu CK, Boudinot FD. Development and optimization of anti-HIV nucleoside analogs and prodrugs: A review of their cellular pharmacology, structure-activity relationships and pharmacokinetics. *Adv Drug Deliv Rev* 1999;39:117-51.
71. Sharma PL, Nurpeisov V, Hernandez-Santiago B, Beltran T, Schinazi RF. Nucleoside inhibitors of human immunodeficiency virus type 1 reverse transcriptase. *Curr Top Med Chem* 2004;4:895-919.
72. Plagemann PG, Wohlhueter RM, Woffendin C. Nucleoside and nucleobase transport in animal cells. *Biochim Biophys Acta* 1988;947:405-43.
73. Pastor-Anglada M, Cano-Soldado P, Molina-Arcas M, et al. Cell entry and export of nucleoside analogues. *Virus Res* 2005;107:151-64.
74. Schuetz JD, Connelly MC, Sun D, et al. MRP4: A previously unidentified factor in resistance to nucleoside-based antiviral drugs. *Nat Med* 1999;5:1048-51.
75. Bousquet L, Pruvost A, Didier N, Farinotti R, Mabondzo A. Emtricitabine: Inhibitor and substrate of multidrug resistance associated protein. *Eur J Pharm Sci* 2008;35:247-56.
76. Bousquet L, Pruvost A, Guyot AC, Farinotti R, Mabondzo A. Combination of tenofovir and emtricitabine plus efavirenz: in vitro modulation of ABC transporter and intracellular drug accumulation. *Antimicrob Agents Chemother* 2009;53:896-902.
77. Furman PA, Fyfe JA, St Clair MH, et al. Phosphorylation of 3'-azido-3'-deoxythymidine and selective interaction of the 5'-triphosphate with human immunodeficiency virus reverse transcriptase. *Proc Natl Acad Sci U S A* 1986;83:8333-7.
78. Furman PA, Barry DW. Spectrum of antiviral activity and mechanism of action of zidovudine. An overview. *Am J Med* 1988;85:176-81.
79. Stein DS, Moore KH. Phosphorylation of nucleoside analog antiretrovirals: a review for clinicians. *Pharmacotherapy* 2001;21:11-34.
80. Feng JY, Parker WB, Krajewski ML, et al. Anabolism of amdoxovir: phosphorylation of dioxolane guanosine and its 5'-phosphates by mammalian phosphotransferases. *Biochem Pharmacol* 2004;68:1879-88.
81. Moore KH, Barrett JE, Shaw S, et al. The pharmacokinetics of lamivudine phosphorylation in peripheral blood mononuclear cells from patients infected with HIV-1. *AIDS* 1999;13:2239-50.
82. Kreimeyer A, Schneider B, Sarfati R, et al. NDP kinase reactivity towards 3TC nucleotides. *Antiviral Res* 2001;50:147-56.
83. Bourdais J, Biondi R, Sarfati S, et al. Cellular phosphorylation of anti-HIV nucleosides. Role of nucleoside diphosphate kinase. *J Biol Chem* 1996;271:7887-90.
84. Cammack N, Rouse P, Marr CL, et al. Cellular metabolism of (-) enantiomeric 2'-deoxy-3'-thiacytidine. *Biochem Pharmacol* 1992;43:2059-64.
85. Krishnan P, Fu Q, Lam W, Liou JY, Dutschman G, Cheng YC. Phosphorylation of pyrimidine deoxynucleoside analog diphosphates: selective phosphorylation of L-nucleoside analog diphosphates by 3-phosphoglycerate kinase. *J Biol Chem* 2002;277:5453-9.
86. Schneider B, Sarfati R, Deville-Bonne D, Veron M. Role of nucleoside diphosphate kinase in the activation of anti-HIV nucleoside analogs. *J Bioenerg Biomembr* 2000;32:317-24.
87. Schneider B, Biondi R, Sarfati R, et al. The mechanism of phosphorylation of anti-HIV D4T by nucleoside diphosphate kinase. *Mol Pharmacol* 2000;57:948-53.
88. Eriksson S, Kierdaszuk B, Munch-Petersen B, Oberg B, Johansson NG. Comparison of the substrate specificities of human thymidine kinase 1 and 2 and deoxycytidine kinase toward antiviral and cytostatic nucleoside analogs. *Biochem Biophys Res Commun* 1991;176:586-92.

89. Eriksson BF, Schinazi RF. Combinations of 3'-azido-3'-deoxythymidine (zidovudine) and phosphonoformate (foscarnet) against human immunodeficiency virus type 1 and cytomegalovirus replication in vitro. *Antimicrob Agents Chemother* 1989;33:663-9.
90. Lavie A, Schlichting I, Vetter IR, Konrad M, Reinstein J, Goody RS. The bottleneck in AZT activation. *Nat Med* 1997;3:922-4.
91. Lavie A, Vetter IR, Konrad M, Goody RS, Reinstein J, Schlichting I. Structure of thymidylate kinase reveals the cause behind the limiting step in AZT activation. *Nat Struct Biol* 1997;4:601-4.
92. Tornevik Y, Jacobsson B, Britton S, Eriksson S. Intracellular metabolism of 3'-azidothymidine in isolated human peripheral blood mononuclear cells. *AIDS Res Hum Retroviruses* 1991;7:751-9.
93. Kewn S, Wang LH, Hoggard PG, et al. Enzymatic assay for measurement of intracellular DXG triphosphate concentrations in peripheral blood mononuclear cells from human immunodeficiency virus type 1-infected patients. *Antimicrob Agents Chemother* 2003;47:255-61.
94. Meyer PR, Matsuura SE, Mian AM, So AG, Scott WA. A mechanism of AZT resistance: an increase in nucleotide-dependent primer unblocking by mutant HIV-1 reverse transcriptase. *Mol Cell* 1999;4:35-43.
95. De Clercq E. Strategies in the design of antiviral drugs. *Nat Rev Drug Discov* 2002;1:13-25.
96. Gotte M, Rausch JW, Marchand B, Sarafianos S, Le Grice SF. Reverse transcriptase in motion: Conformational dynamics of enzyme-substrate interactions. *Biochim Biophys Acta* 2010;1804(5):1202-12.
97. Smith AJ, Scott WA. The influence of natural substrates and inhibitors on the nucleotide-dependent excision activity of HIV-1 reverse transcriptase in the infected cell. *Curr Pharm Des* 2006;12:1827-41.
98. Jeffrey JL, Feng JY, Qi CC, Anderson KS, Furman PA. Dioxolane guanosine 5'-triphosphate, an alternative substrate inhibitor of wild-type and mutant HIV-1 reverse transcriptase. Steady state and pre-steady state kinetic analyses. *J Biol Chem* 2003;278:18971-9.
99. Staszewski S, Loveday C, Picazo JJ, et al. Safety and efficacy of lamivudine-zidovudine combination therapy in zidovudine-experienced patients. A randomized controlled comparison with zidovudine monotherapy. Lamivudine European HIV Working Group. *JAMA* 1996;276:111-7.
100. Ruiz L, Romeu J, Martinez-Picado J, et al. Efficacy of triple combination therapy with zidovudine (ZDV) plus zalcitabine (ddC) plus lamivudine (3TC) versus double (ZDV+3TC) combination therapy in patients previously treated with ZDV+ddC. *AIDS* 1996;10:F61-6.
101. Kuritzkes DR, Quinn JB, Benoit SL, et al. Drug resistance and virologic response in NUCA 3001, a randomized trial of lamivudine (3TC) versus zidovudine (ZDV) versus ZDV plus 3TC in previously untreated patients. *AIDS* 1996;10:975-81.
102. Feng JY, Ly JK, Myrick F, et al. The triple combination of tenofovir, emtricitabine and efavirenz shows synergistic anti-HIV-1 activity in vitro: a mechanism of action study. *Retrovirology* 2009;6:44.
103. Gu Z, Wainberg MA, Nguyen-Ba P, L'Heureux L, de Muys JM, Rando RF. Anti-HIV-1 activities of 1,3-dioxolane guanine and 2,6-diaminopurine dioxolane. *Nucleosides Nucleotides* 1999;18:891-2.
104. Chong Y, Borroto-Esoda K, Furman PA, Schinazi RF, Chu CK. Molecular mechanism of DAPd/DXG against zidovudine- and lamivudine- drug resistant mutants: a molecular modelling approach. *Antivir Chem Chemother* 2002;13:115-28.
105. Borroto-Esoda K, Vela JE, Myrick F, Ray AS, Miller MD. In vitro evaluation of the anti-HIV activity and metabolic interactions of tenofovir and emtricitabine. *Antivir Ther* 2006;11:377-84.
106. Ray AS, Olson L, Fridland A. Role of purine nucleoside phosphorylase in interactions between 2',3'-dideoxyinosine and allopurinol, ganciclovir, or tenofovir. *Antimicrob Agents Chemother* 2004;48:1089-95.
107. Ray AS, Myrick F, Vela JE, et al. Lack of a metabolic and antiviral drug interaction between tenofovir, abacavir and lamivudine. *Antivir Ther* 2005;10:451-7.
108. Ray AS. Intracellular interactions between nucleos(t)ide inhibitors of HIV reverse transcriptase. *AIDS Rev* 2005;7:113-25.

109. Balzarini J. Effect of antimetabolite drugs of nucleotide metabolism on the anti-human immunodeficiency virus activity of nucleoside reverse transcriptase inhibitors. *Pharmacol Ther* 2000;87:175-87.
110. Hoggard PG, Sales SD, Kewn S, et al. Correlation between intracellular pharmacological activation of nucleoside analogues and HIV suppression in vitro. *Antivir Chem Chemother* 2000;11:353-8.
111. Tong W, Lu CD, Sharma SK, Matsuura S, So AG, Scott WA. Nucleotide-induced stable complex formation by HIV-1 reverse transcriptase. *Biochemistry* 1997;36:5749-57.
112. Tchesnokov EP, Obikhod A, Massud I, et al. Mechanisms associated with HIV-1 resistance to acyclovir by the V75I mutation in reverse transcriptase. *J Biol Chem* 2009;284:21496-504.
113. Shafer RW, Schapiro JM. HIV-1 drug resistance mutations: an updated framework for the second decade of HAART. *AIDS Rev* 2008;10:67-84.
114. Johnson VA, Brun-Vezinet F, Clotet B, et al. Update of the drug resistance mutations in HIV-1: December 2009. *Top HIV Med* 2009;17:138-45.
115. Cihlar T, Ray AS. Nucleoside and nucleotide HIV reverse transcriptase inhibitors: 25 years after zidovudine. *Antiviral Res*;85:39-58.
116. Parikh UM, Koontz DL, Chu CK, Schinazi RF, Mellors JW. In vitro activity of structurally diverse nucleoside analogs against human immunodeficiency virus type 1 with the K65R mutation in reverse transcriptase. *Antimicrob Agents Chemother* 2005;49:1139-44.
117. White KL, Margot NA, Wrin T, Petropoulos CJ, Miller MD, Naeger LK. Molecular mechanisms of resistance to human immunodeficiency virus type 1 with reverse transcriptase mutations K65R and K65R+M184V and their effects on enzyme function and viral replication capacity. *Antimicrob Agents Chemother* 2002;46:3437-46.
118. Rapp KL, M. Ruckstuhl M, and Schinazi RF. The combination of zidovudine and amdoxovir prevents the selection of thymidine analogue mutations in primary human lymphocytes. In: *Antiviral therapy*. Barbados, West Indies: IHL; 2007:130.
119. Hurwitz SJ, Asif G, Kivel NM, Schinazi RF. Development of an optimized dose for coformulation of zidovudine with drugs that select for the K65R mutation using a population pharmacokinetic and enzyme kinetic simulation model. *Antimicrob Agents Chemother* 2008;52:4241-50.
120. Mewshaw JP, Myrick FT, Wakefield DA, et al. Dioxolane guanosine, the active form of the prodrug diaminopurine dioxolane, is a potent inhibitor of drug-resistant HIV-1 isolates from patients for whom standard nucleoside therapy fails. *J Acquir Immune Defic Syndr* 2002;29:11-20.
121. Klaassen CD. *Casarett and Doull's Toxicology: The Basic Science of Poisons*: Ovid; 2009.
122. Johnson AA, Ray AS, Hanes J, et al. Toxicity of antiviral nucleoside analogs and the human mitochondrial DNA polymerase. *J Biol Chem* 2001;276:40847-57.
123. Anderson PL, Kakuda TN, Lichtenstein KA. The cellular pharmacology of nucleoside- and nucleotide-analogue reverse-transcriptase inhibitors and its relationship to clinical toxicities. *Clin Infect Dis* 2004;38:743-53.
124. Spiga MG, Weidner DA, Trentesaux C, LeBoeuf RD, Sommadossi JP. Inhibition of beta-globin gene expression by 3'-azido-3'-deoxythymidine in human erythroid progenitor cells. *Antiviral Res* 1999;44:167-77.
125. Richman DD, Fischl MA, Grieco MH, et al. The toxicity of azidothymidine (AZT) in the treatment of patients with AIDS and AIDS-related complex. A double-blind, placebo-controlled trial. *N Engl J Med* 1987;317:192-7.
126. Collier AC, Bozzette S, Coombs RW, et al. A pilot study of low-dose zidovudine in human immunodeficiency virus infection. *N Engl J Med* 1990;323:1015-21.
127. Stretcher BN, Pesce AJ, Frame PT, Greenberg KA, Stein DS. Correlates of zidovudine phosphorylation with markers of HIV disease progression and drug toxicity. *AIDS* 1994;8:763-9.
128. Hetherington S, McGuirk S, Powell G, et al. Hypersensitivity reactions during therapy with the nucleoside reverse transcriptase inhibitor abacavir. *Clin Ther* 2001;23:1603-14.

129. Walsh JS, Reese MJ, Thurmond LM. The metabolic activation of abacavir by human liver cytosol and expressed human alcohol dehydrogenase isozymes. *Chem Biol Interact* 2002;142:135-54.
130. Uetrecht JP. New concepts in immunology relevant to idiosyncratic drug reactions: the "danger hypothesis" and innate immune system. *Chem Res Toxicol* 1999;12:387-95.
131. Chen CH, Vazquez-Padua M, Cheng YC. Effect of anti-human immunodeficiency virus nucleoside analogs on mitochondrial DNA and its implication for delayed toxicity. *Mol Pharmacol* 1991;39:625-8.
132. Kohler JJ, Lewis W. A brief overview of mechanisms of mitochondrial toxicity from NRTIs. *Environ Mol Mutagen* 2007;48:166-72.
133. Venhoff N, Setzer B, Melkaoui K, Walker UA. Mitochondrial toxicity of tenofovir, emtricitabine and abacavir alone and in combination with additional nucleoside reverse transcriptase inhibitors. *Antivir Ther* 2007;12:1075-85.
134. Reichard P. Interactions between deoxyribonucleotide and DNA synthesis. *Annu Rev Biochem* 1988;57:349-74.
135. Meuth M. The molecular basis of mutations induced by deoxyribonucleoside triphosphate pool imbalances in mammalian cells. *Exp Cell Res* 1989;181:305-16.
136. Murray RK BD, Botham KM, Kennelly PJ, Rodwell VW, Weil PA. Metabolism of Purine & Pyrimidine Nucleotides. In: *Harper's Illustrated Biochemistry*, 28e: Mc Graw Hill Medical; 2009.
137. Diamond TL, Roshal M, Jamburuthugoda VK, et al. Macrophage tropism of HIV-1 depends on efficient cellular dNTP utilization by reverse transcriptase. *J Biol Chem* 2004;279:51545-53.
138. Sandrini MP, Piskur J. Deoxyribonucleoside kinases: two enzyme families catalyze the same reaction. *Trends Biochem Sci* 2005;30:225-8.
139. KEGG PATHWAY database. In: *Kyoto Encyclopedia of Genes and Genomes*; 2010. <http://www.genome.jp/kegg/pathway.html>
140. Balzarini J, Lee CK, Herdewijn P, De Clercq E. Mechanism of the potentiating effect of ribavirin on the activity of 2',3'-dideoxyinosine against human immunodeficiency virus. *J Biol Chem* 1991;266:21509-14.
141. Pesi R, Turriani M, Allegrini S, et al. The bifunctional cytosolic 5'-nucleotidase: regulation of the phosphotransferase and nucleotidase activities. *Arch Biochem Biophys* 1994;312:75-80.
142. Spsychala J, Madrid-Marina V, Fox IH. High Km soluble 5'-nucleotidase from human placenta. Properties and allosteric regulation by IMP and ATP. *J Biol Chem* 1988;263:18759-65.
143. Hartman NR, Ahluwalia GS, Cooney DA, et al. Inhibitors of IMP dehydrogenase stimulate the phosphorylation of the anti-human immunodeficiency virus nucleosides 2',3'-dideoxyadenosine and 2',3'-dideoxyinosine. *Mol Pharmacol* 1991;40:118-24.
144. Borroto-Esoda K, Myrick F, Feng J, Jeffrey J, Furman P. In vitro combination of amdoxovir and the inosine monophosphate dehydrogenase inhibitors mycophenolic acid and ribavirin demonstrates potent activity against wild-type and drug-resistant variants of human immunodeficiency virus type 1. *Antimicrob Agents Chemother* 2004;48:4387-94.
145. Margot NA, Miller MD. In vitro combination studies of tenofovir and other nucleoside analogues with ribavirin against HIV-1. *Antivir Ther* 2005;10:343-8.
146. Vispo E, Barreiro P, Pineda JA, et al. Low response to pegylated interferon plus ribavirin in HIV-infected patients with chronic hepatitis C treated with abacavir. *Antivir Ther* 2008;13:429-37.
147. Margolis DM, Mukherjee AL, Fletcher CV, et al. The use of beta-D-2,6-diaminopurine dioxolane with or without mycophenolate mofetil in drug-resistant HIV infection. *AIDS* 2007;21:2025-32.
148. Frick LW, Nelson DJ, St Clair MH, Furman PA, Krenitsky TA. Effects of 3'-azido-3'-deoxythymidine on the deoxynucleotide triphosphate pools of cultured human cells. *Biochem Biophys Res Commun* 1988;154:124-9.
149. Gao WY, Agbaria R, Driscoll JS, Mitsuya H. Divergent anti-human immunodeficiency virus activity and anabolic phosphorylation of 2',3'-dideoxynucleoside analogs in resting and activated human cells. *J Biol Chem* 1994;269:12633-8.

150. Morris GW, Iams TA, Slepchenko KG, McKee EE. Origin of pyrimidine deoxyribonucleotide pools in perfused rat heart: implications for 3'-azido-3'-deoxythymidine-dependent cardiotoxicity. *Biochem J* 2009;422:513-20.
151. Lynx MD, Kang BK, McKee EE. Effect of AZT on thymidine phosphorylation in cultured H9c2, U-937, and Raji cell lines. *Biochem Pharmacol* 2008;75:1610-5.
152. Vela JE, Miller MD, Rhodes GR, Ray AS. Effect of nucleoside and nucleotide reverse transcriptase inhibitors of HIV on endogenous nucleotide pools. *Antivir Ther* 2008;13:789-97.
153. Parker WB, Shaddix SC, Bowdon BJ, et al. Metabolism of carbovir, a potent inhibitor of human immunodeficiency virus type 1, and its effects on cellular metabolism. *Antimicrob Agents Chemother* 1993;37:1004-9.
154. Meng Q, Walker DM, Olivero OA, et al. Zidovudine-didanosine coexposure potentiates DNA incorporation of zidovudine and mutagenesis in human cells. *Proc Natl Acad Sci U S A* 2000;97:12667-71.
155. Kewn S, Hoggard PG, Henry-Mowatt JS, et al. Intracellular activation of 2',3'-dideoxyinosine and drug interactions in vitro. *AIDS Res Hum Retroviruses* 1999;15:793-802.
156. Cote HC. Possible ways nucleoside analogues can affect mitochondrial DNA content and gene expression during HIV therapy. *Antivir Ther* 2005;10 Suppl 2:M3-11.
157. Saada A. Mitochondrial deoxyribonucleotide pools in deoxyguanosine kinase deficiency. *Mol Genet Metab* 2008;95:169-73.
158. Gattermann N, Dadak M, Hofhaus G, et al. Severe impairment of nucleotide synthesis through inhibition of mitochondrial respiration. *Nucleosides Nucleotides Nucleic Acids* 2004;23:1275-9.
159. Tornevik Y, Ullman B, Balzarini J, Wahren B, Eriksson S. Cytotoxicity of 3'-azido-3'-deoxythymidine correlates with 3'-azidothymidine-5'-monophosphate (AZTMP) levels, whereas anti-human immunodeficiency virus (HIV) activity correlates with 3'-azidothymidine-5'-triphosphate (AZTTP) levels in cultured CEM T-lymphoblastoid cells. *Biochem Pharmacol* 1995;49:829-37.
160. Sales SD, Hoggard PG, Sunderland D, Khoo S, Hart CA, Back DJ. Zidovudine phosphorylation and mitochondrial toxicity in vitro. *Toxicol Appl Pharmacol* 2001;177:54-8.
161. Dolce V, Fiermonte G, Runswick MJ, Palmieri F, Walker JE. The human mitochondrial deoxynucleotide carrier and its role in the toxicity of nucleoside antivirals. *Proc Natl Acad Sci U S A* 2001;98:2284-8.
162. Walker UA, Venhoff N, Koch EC, Olschewski M, Schneider J, Setzer B. Uridine abrogates mitochondrial toxicity related to nucleoside analogue reverse transcriptase inhibitors in HepG2 cells. *Antivir Ther* 2003;8:463-70.
163. Setzer B, Lebrecht D, Walker UA. Pyrimidine nucleoside depletion sensitizes to the mitochondrial hepatotoxicity of the reverse transcriptase inhibitor stavudine. *Am J Pathol* 2008;172:681-90.
164. Venhoff N, Lebrecht D, Deveaud C, et al. Oral uridine supplementation antagonizes the peripheral neuropathy and encephalopathy induced by antiretroviral nucleoside analogues. *AIDS*;24:345-52.
165. Lynx MD, LaClair DD, McKee EE. Effects of zidovudine and stavudine on mitochondrial DNA of differentiating 3T3-F442a cells are not associated with imbalanced deoxynucleotide pools. *Antimicrob Agents Chemother* 2009;53:1252-5.
166. Bebenek K, Roberts JD, Kunkel TA. The effects of dNTP pool imbalances on frameshift fidelity during DNA replication. *J Biol Chem* 1992;267:3589-96.
167. Sidi Y, Mitchell BS. 2'-deoxyguanosine toxicity for B and mature T lymphoid cell lines is mediated by guanine ribonucleotide accumulation. *J Clin Invest* 1984;74:1640-8.
168. Batiuk TD, Schnizlein-Bick C, Plotkin Z, Dagher PC. Guanine nucleosides and Jurkat cell death: roles of ATP depletion and accumulation of deoxyribonucleotides. *Am J Physiol Cell Physiol* 2001;281:C1776-84.

169. Bisset LR, Lung TL, Kaelin M, Ludwig E, Dubs RW. Reference values for peripheral blood lymphocyte phenotypes applicable to the healthy adult population in Switzerland. *Eur J Haematol* 2004;72:203-12.
170. Fairbanks LD, Bofill M, Ruckemann K, Simmonds HA. Importance of ribonucleotide availability to proliferating T-lymphocytes from healthy humans. Disproportionate expansion of pyrimidine pools and contrasting effects of de novo synthesis inhibitors. *J Biol Chem* 1995;270:29682-9.
171. Jacobsson B, Britton S, Tornevik Y, Eriksson S. Decrease in thymidylate kinase activity in peripheral blood mononuclear cells from HIV-infected individuals. *Biochem Pharmacol* 1998;56:389-95.
172. Barankiewicz J, Cohen A. Purine nucleotide metabolism in resident and activated rat macrophages in vitro. *Eur J Immunol* 1985;15:627-31.
173. Balzarini J, Van Herrewege Y, Vanham G. Metabolic activation of nucleoside and nucleotide reverse transcriptase inhibitors in dendritic and Langerhans cells. *AIDS* 2002;16:2159-63.
174. Aquaro S, Perno CF, Balestra E, et al. Inhibition of replication of HIV in primary monocyte/macrophages by different antiviral drugs and comparative efficacy in lymphocytes. *J Leukoc Biol* 1997;62:138-43.
175. Fyrberg A, Albertioni F, Lotfi K. Cell cycle effect on the activity of deoxynucleoside analogue metabolising enzymes. *Biochem Biophys Res Commun* 2007;357:847-53.
176. Saada A. Fishing in the (deoxyribonucleotide) pool. *Biochem J* 2009;422:e3-6.
177. Bello LJ. Regulation of thymidine kinase synthesis in human cells. *Exp Cell Res* 1974;89:263-74.
178. Nordhoff EK, F; Roepstorff, P. . *Mass Spectrometry of Nucleic Acids*. *Mass Spectrometry Reviews* 1996;15:67-138.
179. Dole MM, L.L.; Hines, R.L. Molecular beams of macroions. *The Journal of Chemical Physics* 1968;49.
180. Mora JF, Van Berkel GJ, Enke CG, Cole RB, Martinez-Sanchez M, Fenn JB. Electrochemical processes in electrospray ionization mass spectrometry. *J Mass Spectrom* 2000;35:939-52.
181. Kebarle P. A brief overview of the present status of the mechanisms involved in electrospray mass spectrometry. *J Mass Spectrom* 2000;35:804-17.
182. Kebarle P, Verkerk UH. Electrospray: from ions in solution to ions in the gas phase, what we know now. *Mass Spectrom Rev* 2009;28:898-917.
183. Roboz J. *Mass Spectrometry in cancer research*: CRC PRESS; 2002.
184. McLafferty FW. Tandem mass spectrometry. *Science* 1981;214:280-7.
185. Dresen S, Ferreiros N, Gnann H, Zimmermann R, Weinmann W. Detection and identification of 700 drugs by multi-target screening with a 3200 Q TRAP((R)) LC-MS/MS system and library searching. *Analytical and bioanalytical chemistry*;396(7):2425-34.
186. Thermo. Finnigan™ TSQ® Quantum Hardware Manual 70111-97043 Revision A ed: TECHNICAL PUBLICATIONS; 2003.
187. Debenedetti E. [Michele Tsvet, the discoverer of chromatography.]. *Minerva Med* 1956;47:536-8.
188. HPLC Separation Modes. In: Waters Education and Events; 2010.
<http://www.waters.com/waters/nav.htm?cid=10048919>
189. Fritz JS. Factors affecting selectivity in ion chromatography. *J Chromatogr A* 2005;1085:8-17.
190. Stahlberg J. Retention models for ions in chromatography. *J Chromatogr A* 1999;855:3-55.
191. Ståhlberg J. How Theory and Practice Meet in Ion Pair Chromatography. In: *Chromatography AoC*, ed. EAS meeting. Sweden. www.academyofchromatography.com/.../EAS_meeting_AoC_link_pdf.
192. Bidlingmeyer BA, Deming SN, Price WP, B.Sachok, Petrusek M. Retention mechanism for reversed-phase ion-pair liquid chromatography. *Journal of Chromatography* 1979;186:419-34.
193. Chen JG, Weber SG, Glavina LL, Cantwell FF. Electrical double-layer models of ion-modified (ion-pair) reversed-phase liquid chromatography. *J Chromatogr* 1993;656:549-76.
194. Kostianinen R, Kauppila TJ. Effect of eluent on the ionization process in liquid chromatography-mass spectrometry. *J Chromatogr A* 2009;1216:685-99.

195. Schinazi RF, Cannon DL, Arnold BH, Martino-Saltzman D. Combinations of isoprinosine and 3'-azido-3'-deoxythymidine in lymphocytes infected with human immunodeficiency virus type 1. *Antimicrob Agents Chemother* 1988;32:1784-7.
196. Hurwitz SJ, Asif G, Fromentin E, Tharnish PM, Schinazi RF. Lack of Pharmacokinetic Interaction Between Amdoxovir and Reduced and Standard Dose Zidovudine in HIV-1 Infected Individuals. *Antimicrob Agents Chemother* 2010;54(3):1248-55.
197. Hayter AJ. A Proof of the Conjecture that the Tukey-Kramer Multiple Comparisons Procedure is Conservative. *The Annals of Statistics* 1984;12:61-75.
198. Fromentin E, Gavegnano C, Obikhod A, Schinazi RF. Simultaneous Quantification of Intracellular Natural and Antiretroviral Nucleosides and Nucleotides by Liquid Chromatography-Tandem Mass Spectrometry. *Anal Chem* 2010; 82, 1982–1989.
199. Jansen RS, Rosing H, Schellens JH, Beijnen JH. Retention studies of 2'-2'-difluorodeoxycytidine and 2'-2'-difluorodeoxyuridine nucleosides and nucleotides on porous graphitic carbon: development of a liquid chromatography-tandem mass spectrometry method. *J Chromatogr A* 2009;1216:3168-74.
200. Hernandez-Santiago BI, Obikhod A, Fromentin E, Hurwitz SJ, Schinazi RF. Short communication cellular pharmacology of 9-(beta-D-1,3-dioxolan-4-yl) guanine and its lack of drug interactions with zidovudine in primary human lymphocytes. *Antivir Chem Chemother* 2007;18:343-6.
201. Jansen RS, Rosing H, de Wolf CJ, Beijnen JH. Development and validation of an assay for the quantitative determination of cladribine nucleotides in MDCKII cells and culture medium using weak anion-exchange liquid chromatography coupled with tandem mass spectrometry. *Rapid Commun Mass Spectrom* 2007;21:4049-59.
202. Shi G, Wu JT, Li Y, et al. Novel direct detection method for quantitative determination of intracellular nucleoside triphosphates using weak anion exchange liquid chromatography/tandem mass spectrometry. *Rapid Commun Mass Spectrom* 2002;16:1092-9.
203. Bell DS, Jones AD. Solute attributes and molecular interactions contributing to "U-shape" retention on a fluorinated high-performance liquid chromatography stationary phase. *J Chromatogr A* 2005;1073:99-109.
204. Gilar M, Yu YQ, Ahn J, Fournier J, Gebler JC. Mixed-mode chromatography for fractionation of peptides, phosphopeptides, and sialylated glycopeptides. *J Chromatogr A* 2008;1191:162-70.
205. Hennere G, Becher F, Pruvost A, Goujard C, Grassi J, Benech H. Liquid chromatography-tandem mass spectrometry assays for intracellular deoxyribonucleotide triphosphate competitors of nucleoside antiretrovirals. *J Chromatogr B Analyt Technol Biomed Life Sci* 2003;789:273-81.
206. Compain S, Durand-Gasselien L, Grassi J, Benech H. Improved method to quantify intracellular zidovudine mono- and triphosphate in peripheral blood mononuclear cells by liquid chromatography-tandem mass spectrometry. *J Mass Spectrom* 2007;42:389-404.
207. Pruvost A, Theodoro F, Agrofoglio L, Negredo E, Benech H. Specificity enhancement with LC-positive ESI-MS/MS for the measurement of nucleotides: application to the quantitative determination of carbovir triphosphate, lamivudine triphosphate and tenofovir diphosphate in human peripheral blood mononuclear cells. *J Mass Spectrom* 2008;43:224-33.
208. Asakawa Y, Tokida N, Ozawa C, Ishiba M, Tagaya O, Asakawa N. Suppression effects of carbonate on the interaction between stainless steel and phosphate groups of phosphate compounds in high-performance liquid chromatography and electrospray ionization mass spectrometry. *J Chromatogr A* 2008;1198-1199:80-6.
209. Espada A, Rivera-Sagredo A. Ammonium hydrogencarbonate, an excellent buffer for the analysis of basic drugs by liquid chromatography-mass spectrometry at high pH. *J Chromatogr A* 2003;987:211-20.
210. Seifar RM, Ras C, van Dam JC, van Gulik WM, Heijnen JJ, van Winden WA. Simultaneous quantification of free nucleotides in complex biological samples using ion pair reversed phase liquid chromatography isotope dilution tandem mass spectrometry. *Anal Biochem* 2009;388:213-9.

211. Claire RL, 3rd. Positive ion electrospray ionization tandem mass spectrometry coupled to ion-pairing high-performance liquid chromatography with a phosphate buffer for the quantitative analysis of intracellular nucleotides. *Rapid Commun Mass Spectrom* 2000;14:1625-34.
212. Vela JE, Olson LY, Huang A, Fridland A, Ray AS. Simultaneous quantitation of the nucleotide analog adefovir, its phosphorylated anabolites and 2'-deoxyadenosine triphosphate by ion-pairing LC/MS/MS. *J Chromatogr B Analyt Technol Biomed Life Sci* 2007;848:335-43.
213. Tuytten R, Lemiere F, Witters E, et al. Stainless steel electrospray probe: a dead end for phosphorylated organic compounds? *J Chromatogr A* 2006;1104:209-21.
214. Hawkins T, Veikley W, St Claire RL, 3rd, Guyer B, Clark N, Kearney BP. Intracellular pharmacokinetics of tenofovir diphosphate, carbovir triphosphate, and lamivudine triphosphate in patients receiving triple-nucleoside regimens. *J Acquir Immune Defic Syndr* 2005;39:406-11.
215. Cordell RL, Hill SJ, Ortori CA, Barrett DA. Quantitative profiling of nucleotides and related phosphate-containing metabolites in cultured mammalian cells by liquid chromatography tandem electrospray mass spectrometry. *J Chromatogr B Analyt Technol Biomed Life Sci* 2008;871:115-24.
216. Coulier L, Bas R, Jespersen S, Verheij E, van der Werf MJ, Hankemeier T. Simultaneous quantitative analysis of metabolites using ion-pair liquid chromatography-electrospray ionization mass spectrometry. *Anal Chem* 2006;78:6573-82.
217. Crauste C, Lefebvre I, Hovaneissian M, et al. Development of a sensitive and selective LC/MS/MS method for the simultaneous determination of intracellular 1-beta-D-arabinofuranosylcytosine triphosphate (araCTP), cytidine triphosphate (CTP) and deoxycytidine triphosphate (dCTP) in a human follicular lymphoma cell line. *J Chromatogr B Analyt Technol Biomed Life Sci* 2009;877:1417-25.
218. Roberts JM, Diaz AR, Fortin DT, Friedle JM, Piper SD. Influence of the hofmeister series on the retention of amines in reversed-phase liquid chromatography. *Anal Chem* 2002;74:4927-32.
219. Zhang Y, Cremer PS. Interactions between macromolecules and ions: The Hofmeister series. *Curr Opin Chem Biol* 2006;10:658-63.
220. McCalley DV. Rationalization of retention and overloading behavior of basic compounds in reversed-phase HPLC using low ionic strength buffers suitable for mass spectrometric detection. *Anal Chem* 2003;75:3404-10.
221. Gavegnano C, Fromentin E, Schinazi RF. Anti-HIV-1 Nucleoside Analogue Triphosphate Levels are Significantly Lower in Primary Human Macrophages Than in Lymphocytes. In: Press I, ed. 4th International Workshop on HIV-1 Persistence St. Martin, West Indies: IHL Press; 2009:43.
222. Qian M, Chandrasena G, Ho RJ, Unadkat JD. Comparison of rates of intracellular metabolism of zidovudine in human and primate peripheral blood mononuclear cells. *Antimicrob Agents Chemother* 1994;38:2398-403.
223. Perno CF, Svicher V, Schols D, Pollicita M, Balzarini J, Aquaro S. Therapeutic strategies towards HIV-1 infection in macrophages. *Antiviral Res* 2006;71:293-300.
224. Plagemann PG. Na(+)-dependent, concentrative nucleoside transport in rat macrophages. Specificity for natural nucleosides and nucleoside analogs, including dideoxynucleosides, and comparison of nucleoside transport in rat, mouse and human macrophages. *Biochem Pharmacol* 1991;42:247-52.
225. Soler C, Garcia-Manteiga J, Valdes R, et al. Macrophages require different nucleoside transport systems for proliferation and activation. *FASEB J* 2001;15:1979-88.
226. Aquaro S, Svicher V, Schols D, et al. Mechanisms underlying activity of antiretroviral drugs in HIV-1-infected macrophages: new therapeutic strategies. *J Leukoc Biol* 2006;80:1103-10.
227. Hunsucker SA, Mitchell BS, Sychala J. The 5'-nucleotidases as regulators of nucleotide and drug metabolism. *Pharmacol Ther* 2005;107:1-30.
228. Chen H, Boudinot FD, Chu CK, McClure HM, Schinazi RF. Pharmacokinetics of (-)-beta-D-2-aminopurine dioxolane and (-)-beta-D-2-amino-6-chloropurine dioxolane and their antiviral metabolite (-)-beta-D-dioxolane guanine in rhesus monkeys. *Antimicrob Agents Chemother* 1996;40:2332-6.

229. Chen H, Schinazi RF, Rajagopalan P, et al. Pharmacokinetics of (-)-beta-D-dioxolane guanine and prodrug (-)-beta-D-2,6-diaminopurine dioxolane in rats and monkeys. *AIDS Res Hum Retroviruses* 1999;15:1625-30.
230. Manouilov KK, Manouilova LS, Boudinot FD, Schinazi RF, Chu CK. Biotransformation and pharmacokinetics of prodrug 9-(beta-D-1,3-dioxolan-4-yl)-2-aminopurine and its antiviral metabolite 9-(beta-D-1,3-dioxolan-4-yl)guanine in mice. *Antiviral Res* 1997;35:187-93.
231. Gripshover BM, Ribaud H, Santana J, et al. Amdoxovir versus placebo with enfuvirtide plus optimized background therapy for HIV-1-infected subjects failing current therapy (AACTG A5118). *Antivir Ther* 2006;11:619-23.
232. Fromentin E, Asif G, Obikhod A, Hurwitz SJ, Schinazi RF. Simultaneous quantification of 9-(beta-D-1,3-dioxolan-4-yl)guanine, Amdoxovir and Zidovudine in human plasma by liquid chromatography-tandem mass spectrometric assay. *J Chromatogr B Analyt Technol Biomed Life Sci* 2009;877:3482-8.
233. Plipat N, Ruan PK, Fenton T, Yogev R. Rapid human immunodeficiency virus decay in highly active antiretroviral therapy (HAART)-experienced children after starting mega-HAART. *J Virol* 2004;78:11272-5.
234. Seignerès B, Pichoud C, Martin P, Furman P, Trepo C, Zoulim F. Inhibitory activity of dioxolane purine analogs on wild-type and lamivudine-resistant mutants of hepadnaviruses. *Hepatology* 2002;36:710-22.
235. Compain S, Schlemmer D, Levi M, et al. Development and validation of a liquid chromatographic/tandem mass spectrometric assay for the quantitation of nucleoside HIV reverse transcriptase inhibitors in biological matrices. *J Mass Spectrom* 2005;40:9-18.
236. Bezy V, Morin P, Couerbe P, Leleu G, Agrofoglio L. Simultaneous analysis of several antiretroviral nucleosides in rat-plasma by high-performance liquid chromatography with UV using acetic acid/hydroxylamine buffer Test of this new volatile medium-pH for HPLC-ESI-MS/MS. *J Chromatogr B Analyt Technol Biomed Life Sci* 2005;821:132-43.
237. Loregian A, Scarpa MC, Pagni S, Parisi SG, Palu G. Measurement of ribavirin and evaluation of its stability in human plasma by high-performance liquid chromatography with UV detection. *J Chromatogr B Analyt Technol Biomed Life Sci* 2007;856:358-64.
238. Volosov A, Alexander C, Ting L, Soldin SJ. Simple rapid method for quantification of antiretrovirals by liquid chromatography-tandem mass-spectrometry. *Clin Biochem* 2002;35:99-103.
239. Wiesner JL, Sutherland FC, Smit MJ, et al. Sensitive and rapid liquid chromatography-tandem mass spectrometry method for the determination of stavudine in human plasma. *J Chromatogr B Analyt Technol Biomed Life Sci* 2002;773:129-34.
240. Kenney KB, Wring SA, Carr RM, Wells GN, Dunn JA. Simultaneous determination of zidovudine and lamivudine in human serum using HPLC with tandem mass spectrometry. *J Pharm Biomed Anal* 2000;22:967-83.
241. Gehrig AK, Mikus G, Haefeli WE, Burhenne J. Electrospray tandem mass spectroscopic characterisation of 18 antiretroviral drugs and simultaneous quantification of 12 antiretrovirals in plasma. *Rapid Commun Mass Spectrom* 2007;21:2704-16.
242. Estrela Rde C, Salvadori MC, Suarez-Kurtz G. A rapid and sensitive method for simultaneous determination of lamivudine and zidovudine in human serum by on-line solid-phase extraction coupled to liquid chromatography/tandem mass spectrometry detection. *Rapid Commun Mass Spectrom* 2004;18:1147-55.
243. Robbins BL, Poston PA, Neal EF, Slaughter C, Rodman JH. Simultaneous measurement of intracellular triphosphate metabolites of zidovudine, lamivudine and abacavir (carbovir) in human peripheral blood mononuclear cells by combined anion exchange solid phase extraction and LC-MS/MS. *J Chromatogr B Analyt Technol Biomed Life Sci* 2007;850:310-7.
244. Wang LHB, J.W.; Brosnan-Cook, M.; Sista, N.D.; Rousseau, F. and the DAPD-101 Clinical Trial Group. . The Disposition of DAPD and Its Active Metabolite DXG in Therapy Naïve and Experienced

HIV-Infected Subjects. In: Conference of Retroviruses and Opportunistic Infections, Chicago, IL; Feb 2001.

245. Cremieux AC, Katlama C, Gillotin C, Demarles D, Yuen GJ, Raffi F. A comparison of the steady-state pharmacokinetics and safety of abacavir, lamivudine, and zidovudine taken as a triple combination tablet and as abacavir plus a lamivudine-zidovudine double combination tablet by HIV-1-infected adults. *Pharmacotherapy* 2001;21:424-30.

246. Marier JF, Dimarco M, Guilbaud R, et al. Pharmacokinetics of lamivudine, zidovudine, and nevirapine administered as a fixed-dose combination formulation versus coadministration of the individual products. *J Clin Pharmacol* 2007;47:1381-9.

247. Barry MG, Khoo SH, Veal GJ, et al. The effect of zidovudine dose on the formation of intracellular phosphorylated metabolites. *AIDS* 1996;10:1361-7.

248. Kennedy E, Schinazi RF, Gavegnano C, Fromentin E, Kim B. Elevated rNTP incorporation by HIV-1 RT with dNTP/rNTP pools found in human macrophages. In. Palm Springs Symposium on HIV/AIDS, CA. March 11-13, 2010.

Supplemental Materials:

- Supplement table: Values of chromatography parameters (Ne, k', Tf and area) for 3TC, 3TC-MP, 3TC-TP, DXG, DXG-MP, DXG-TP, TFV, TFV-DP, ZDV-TP, (-)-FTC-TP and CBV-TP.

- Papers published as a first author entitled:

- Simultaneous Quantification of Intracellular Natural and Antiretroviral Nucleosides and Nucleotides by Liquid Chromatography-Tandem Mass Spectrometry

- Simultaneous quantification of 9-(β -D-1,3-dioxolan-4-yl)guanine, Amdoxovir and Zidovudine in human plasma by liquid chromatography–tandem mass spectrometric assay

Supplement: Values of chromatography parameters (Ne, k', Tf and area) for 3TC, 3TC-MP, 3TC-TP, DXG, DXG-MP, DXG-TP, TFV, TFV-DP, ZDV,TP, (-)-FTC-TP and CBV-TP.

pH		9.2					9.2					7.0	8.0	9.2	10.0	
Buffer composition		1 mM (NH ₄) ₃ PO ₄					1 mM (NH ₄) ₃ PO ₄	2 mM (NH ₄) ₃ PO ₄	10 mM NH ₄ HCO ₃	20 mM NH ₄ HCO ₃	1 mM (NH ₄) ₃ PO ₄					
HMA concentration (mM)		0	3	6	9	12	3					3				
3TC	Ne	110	73	54	52	73	73	92	62	92	251	287	169	188		
	k'	1.13	1.13	1.11	1.11	1.11	1.16	1.16	1.16	1.17	1.34	1.35	1.33	1.34		
	Tf	0.88	1.75	1.19	1.28	1.35	1.02	1.17	1.26	1.02	0.96	1.1	1.15	0.8		
	Area	65	15	25	29	30	75	54.5	126.5	175	348	421	449	209		
3TC-MP	Ne	8	143	627	500	483	678	556	385	225	751	626	778	1030		
	k'	1.13	1.27	1.26	1.25	1.25	1.31	1.29	1.25	1.17	1.57	1.56	1.47	1.03		
	Tf	3	1.5	1.33	1.08	1.04	1.07	1.04	1.25	1.02	1.16	0.9	1	1.13		
	Area	split	12	22	22	22	21	20	23	15	8	9	22	3		
3TC-TP	Ne	368	722	712	813	1086	4035	11206	956	453	23382	24153	25573	33229		
	k'	1.23	1.43	1.45	1.48	1.5	2.39	2.49	2.08	1.47	2.93	2.95	3.01	1.61		
	Tf	1.33	1.36	1.14	1.04	1	0.98	0.84	1	0.77	1.05	1	1	1		
	Area	5	24	16	16	16	17	15.5	18	5.5	8	11	29	1		
DXG	Ne	21	38	22	15	21	109	135	94	116	55	79	98	76		
	k'	1.06	1.06	1.06	1.05	1.06	1.1	1.1	1.09	1.09	1.16	1.17	1.19	1.09		
	Tf	1.83	1.3	1.13	1.21	0.89	0.78	1	1.44	0.72	1.13	1.57	1	1.07		
	Area	125	48	50	45	49	51	83	96	141	60	88	68	38		
DXG-MP	Ne	9	693	681	616	595	735	547	335	219	682	984	713	1162		
	k'	1.13	1.27	1.27	1.25	1.25	1.32	1.31	1.27	1.18	1.64	1.65	1.6	1.06		
	Tf	1.54	1.57	1.56	1.14	1.96	1.05	1	1.37	1.38	1.1	0.92	0.91	1.09		
	Area	split	19	26	28	27	31	30	28.5	17	4	6	14	1		
DXG-TP	Ne	646	518	620	918	1458	17449	7915	1050	1252	27058	23998	25787	19012		
	k'	1.23	1.51	1.6	1.65	1.65	2.44	2.47	1.97	1.39	2.93	2.95	3.01	1.7		
	Tf	0.83	0.77	1.02	1.02	1.07	0.85	0.94	1.04	1.06	1.1	1	1	0.93		
	Area	0.4	1.6	2.3	2.9	3	5	3.5	4	1	2	4	11	1		
TFV	Ne	277	640	527	536	637	349	728	502	196	3758	3129	4761	1773		
	k'	1.21	1.28	1.26	1.26	1.26	1.34	1.37	1.37	1.26	2.27	2.26	2.11	1.14		
	Tf	1.47	1.79	1.15	1.54	1.02	1.67	1.09	1	0.96	1.05	1.09	1.13	1.03		
	Area	25	38	26	27	22	28	N/A	16	11.5	4	6	10	3		
TFV-DP	Ne	457	254	670	1072	1141	3010	9601	1947	415	23998	24674	26325	21769		
	k'	1.24	1.59	1.65	1.67	1.64	2.5	2.53	2.18	1.64	2.96	2.97	3.04	2.04		
	Tf	1.47	0.89	0.96	1.09	1.04	1	0.92	2.5	1.44	1.13	1.13	1.05	0.95		
	Area	2	7	8	9	10	38	26.5	22	9.5	9	17	46	6		
ZDV-TP	Ne	1267	10054	16355	7202	6464	12329	13388	13306	6974						
	k'	1.26	2.4	2.42	2.42	2.44	2.62	2.7	2.63	1.66						
	Tf	2.13	1.33	1.75	1.5	1.27	1.07	1	1	1						
	Area	0.08	0.8	0.32	0.36	0.32	2	2	0.5	0.4						
(-)-FTC-TP	Ne	646	658	584	1018	1151	6282	10686	1448	473	20591	24361	22603	24727		
	k'	1.23	1.48	1.49	1.54	1.54	2.44	2.52	2.11	1.53	2.94	2.96	3.02	1.75		
	Tf	1.33	0.88	1.18	1.17	1.13	0.98	1.02	1.06	0.97	1.75	1.93	1.23	1.07		
	Area	1	4	6	7	9.6	28	21.5	19	7.5	8	13	31	3		
CBV-TP	Ne	374	417	1002	2224	2182		12374	2697	527	18851	17163	20950	25947		
	k'	1.25	2.01	2.17	2.19	2.15	N/A	2.58	2.38	2.21	2.98	3	3.08	2.61		
	Tf	1.24	0.96	1	1.14	1	N/A	1.02	1.13	1.25	1.75	1.45	1.07	1		
	Area	5	23	30	38	37	N/A	46	33	12	16	27	72	17		

Simultaneous Quantification of Intracellular Natural and Antiretroviral Nucleosides and Nucleotides by Liquid Chromatography–Tandem Mass Spectrometry

Emilie Fromentin, Christina Gavegnano, Aleksandr Obikhod, and Raymond F. Schinazi*

Center for AIDS Research, Laboratory of Biochemical Pharmacology, Department of Pediatrics, Emory University School of Medicine, Atlanta, Georgia 30332, and Veterans Affairs Medical Center, Decatur, Georgia 30033

Nucleoside reverse transcriptase inhibitors (NRTI) require intracellular phosphorylation, which involves multiple enzymatic steps to inhibit the human immunodeficiency virus type 1 (HIV-1). NRTI-triphosphates (NRTI-TP) compete with endogenous 2'-deoxyribonucleosides-5'-triphosphates (dNTP) for incorporation by the HIV-1 reverse transcriptase (RT). Thus, a highly sensitive analytical methodology capable of quantifying at the low femtomoles/10⁶ cells level was necessary to understand the intracellular metabolism and antiviral activity of NRTIs in human peripheral blood mononuclear (PBM) cells and in macrophages. A novel, rapid, and a reproducible ion-pair chromatography–tandem mass spectrometry (MS/MS) method was developed to simultaneously quantify the intracellular phosphorylated metabolites of abacavir, emtricitabine, tenofovir disoproxil fumarate, amdoxovir, and zidovudine, as well as four natural endogenous dNTP. Positive or negative electrospray ionization was chosen with specific MS/MS transitions for improved selectivity on all the compounds studied. The sample preparation, the ion-pair reagent concentration, and buffer composition were optimized, resulting in the simultaneous quantification of 13 different nucleotides in a total run time of 30 min. This novel method demonstrated optimal sensitivity (limit of detection 1–10 nM for various analytes), specificity, and reproducibility to successfully measure NRTI-TP and dNTP in human PBM cells and macrophages.

Nucleoside reverse transcriptase inhibitors (NRTI) remain key components of highly active antiretroviral therapy (HAART) for first line therapy for the treatment of human immunodeficiency virus type 1 (HIV-1). Understanding their uptake and metabolism in human peripheral blood mononuclear (PBM) cells and macrophages can provide insights on their potency as antiviral agents.^{1–4} Although plasma levels of nucleosides are important in terms of maximum concentration (C_{max}), which represents the

loading dose, it is well established that the triphosphate (TP) of the NRTI, which interacts with the viral polymerase, is the active metabolite and more relevant for this class of drugs. Thus, accurate measurement of the intracellular concentration of nucleoside triphosphates is essential.^{5–8}

The objective of this work was to develop and validate an accurate, rapid, and a highly sensitive method for the simultaneous quantification of the phosphorylated metabolites of NRTIs such as abacavir (ABC), emtricitabine [(-)-FTC], tenofovir disoproxil fumarate (TDF), amdoxovir (DAPD), and zidovudine (ZDV) as well as the natural endogenous 2'-deoxyribonucleosides-5'-triphosphates (dNTP). TDF, DAPD, and ABC-MP are bioconverted to tenofovir (TFV), 9- β -D-(1,3-dioxolan-4-yl)guanine (DXG), and (-)-carbovir-monophosphate (CBV-MP), respectively, prior to being converted to their NRTI-TP forms.^{9–11} The discrimination between the successive intracellular metabolites resulting from the conversion of NRTI to NRTI-monophosphate (MP), NRTI-diphosphate (DP), and NRTI-TP was required, since the NRTI-TP are responsible for antiviral efficacy, while the NRTI-MP such as ZDV may be associated with toxicity.^{12,13} Separation was also essential since NTPs generate breakdown products in the electrospray probe, which are mainly the corresponding DP, MP, and nucleoside forms,¹⁴ which could lead to errors in the quantification of these metabolites. A high sensitivity of detection was also

* Corresponding author. Mailing address: Dr. R. F. Schinazi, Veterans Affairs Medical Center, Medical Research 151H, 1670 Clairmont Road, Decatur, GA 30033. Phone: +1-404-728-7711. Fax: +1-404-728-7726. E-mail: rschina@emory.edu.

(1) Bowman, M. C.; Archin, N. M.; Margolis, D. M. *Expert Rev. Mol. Med.* 2009, 11, e6.

(2) Aquaro, S.; Calio, R.; Balzarini, J.; Bellocchi, M. C.; Garaci, E.; Perno, C. F. *Antiviral Res.* 2002, 55, 209–225.

(3) Aquaro, S.; Svicher, V.; Schols, D.; Pollicita, M.; Antinori, A.; Balzarini, J.; Perno, C. F. *J. Leukocyte Biol.* 2006, 80, 1103–1110.

(4) Alexaki, A.; Liu, Y.; Wigdahl, B. *Curr. HIV Res.* 2008, 6, 388–400.

(5) Schinazi, R. F.; Hernandez-Santiago, B. I.; Hurwitz, S. *J. Antiviral Res.* 2006, 71, 322–334.

(6) Balzarini, J. *Pharm. World Sci.* 1994, 16, 113–126.

(7) Balzarini, J. *Pharmacol. Ther.* 2000, 87, 175–187.

(8) Furman, P. A.; Fyfe, J. A.; St. Clair, M. H.; Weinhold, K.; Rideout, J. L.; Freeman, G. A.; Lehrman, S. N.; Bolognesi, D. P.; Broder, S.; Mitsuya, H.; et al. *Proc. Natl. Acad. Sci. U.S.A.* 1986, 83, 8333–8337.

(9) Durand-Gasselin, L.; Van Rompay, K. K.; Vela, J. E.; Henne, I. N.; Lee, W. A.; Rhodes, G. R.; Ray, A. S. *Mol. Pharm.* 2009, 6, 1145–1151.

(10) Yuen, G. J.; Weller, S.; Pakes, G. E. *Clin. Pharmacokinet.* 2008, 47, 351–371.

(11) Gu, Z.; Wainberg, M. A.; Nguyen-Ba, N.; L'Heureux, L.; de Muys, J. M.; Bowlin, T. L.; Rando, R. F. *Antimicrob. Agents Chemother.* 1999, 43, 2376–2382.

(12) Hurwitz, S. J.; Asif, G.; Kivel, N. M.; Schinazi, R. F. *Antimicrob. Agents Chemother.* 2008, 52, 4241–4250.

(13) Sales, S. D.; Hoggard, P. G.; Sunderland, D.; Khoo, S.; Hart, C. A.; Back, D. J. *Toxicol. Appl. Pharmacol.* 2001, 177, 54–58.

required, since the levels of natural endogenous dNTP in macrophages and in resting PBM cells are approximately 70 and 315 fmol/10⁶ cells, respectively.¹⁵ A weak anion-exchange (WAX) method was previously utilized by our group¹⁶ and others;^{17,18} however, the nucleosides were eluted in the void volume of the column and therefore the method had to be modified.

The measurement of intracellular phosphorylated NRTI by liquid chromatography–tandem mass spectrometry (LC–MS/MS) remains difficult. The first obstacle is the high polarity induced by the phosphate moieties of nucleotides rendering their retention by reverse-phase chromatography a challenge. Generally, a volatile solvent is preferred to avoid ion suppression in the mass spectrometer. Thus, two specific end-capped columns such as PFP propyl and Hypersil GOLD-AQ were selected for their ability to retain polar and basic compounds, including phosphopeptides, without utilizing nonvolatiles buffers or extreme pH.^{19,20} It is interesting to define whether these columns would allow the separation of a wide range of compounds with different polarity and molecular weight similar to previously reports by ion-pair chromatography.²¹ The second obstacle is the interferences produced by endogenous nucleotide triphosphates and/or other components. For example, ATP, dGTP, and ZDV-TP have the same molecular weight (507 g/mol) and similar fragmentation pattern in negative ionization mode,²² and therefore, can interfere with respective measurements.²³ Similarly, lack of MS/MS specificity occurs between ZDV-MP, AMP, and dGMP. Thus, it was necessary to optimize the ionization mode, the column temperature, the composition and the pH of the mobile phase to obtain optimal separation and selectivity to avoid overlapping signals. Our approach applied the specificity offered by the positive ionization mode for most compounds, as suggested by Pruvost et al.²⁴ while using the specific fragmentation of ZDV-TP in the negative ionization mode as described previously by Compain et al.²³ This switch in polarity from positive to negative ionization was made possible by a highly optimized separation. This optimization was essential, mainly because several antiretroviral combination modalities, such as Combivir include ZDV. The third obstacle resides in the ability of the phosphate groups of the nucleotides to interact with stainless steel, causing a peak tailing on chromatograms.²⁵ For this reason, all stainless steel devices were generally replaced by PEEK [poly(aryl-ether-ether-ketone)]

materials in the instruments. However, we found that this substitution could not be undertaken in the electrospray probe, where the metal needle has proved to enhance detection sensitivity. Asakawa et al.²⁵ showed that the use of ammonium hydrogen carbonate in the mobile phase prevented peak tailing and was compatible with LC–MS analysis. Furthermore, this buffer is suitable for the analysis of basic compounds.²⁶ Ammonium phosphate^{27–29} and ammonium hydroxide³⁰ were successfully used to prevent the interactions between stainless steel and the phosphate groups of nucleotides. Ammonium phosphate buffer is known to be semivolatile, causes ion-suppression, and should be used at low concentration. Moreover, this buffer must be combined with the appropriate ion-pair reagent. Alkylamines, tetraalkylammonium salt or tetrabutyl ammonium hydroxide have been successfully used for the quantification of nucleosides and nucleotides particularly with an ammonium phosphate buffer, despite their incompatibility with MS detection.^{27,31} Among the available alkylamines: 1,5-dimethylhexylamine (1,5-DMHA)²⁴ was preferred to *N,N*-dimethylhexylamine (*N,N*-DMHA)³² for enhanced ionization in the positive mode.²⁴ Hexylamine (HMA) was also successfully used in association with the negative ionization mode.^{33,34} By testing these different conditions, we were able to optimize and validate an LC–MS/MS method for the simultaneous quantification of 13 endogenous nucleoside/nucleotides and analogues.

EXPERIMENTAL SECTION

Chemicals and Reagents. Ammonium phosphate [(NH₄)₃PO₄] and *N,N*-DMHA were purchased from Sigma Aldrich, (St. Louis, MO). Hexylamine (HMA) and ammonium formate (NH₄COOH) were purchased from Acros Organics (Morris Plains, NJ). HPLC-grade methanol, acetonitrile, ammonium hydroxide (NH₄OH), and ammonium acetate (NH₄CH₃COOH) were obtained from Fisher Scientific International, Inc. (Pittsburgh, PA). Ultrapure water was generated from Elga Ultrapurelab equipped with U.S. filters. Formic acid (HCOOH) and ammonium hydrogen carbonate (NH₄HCO₃) were purchased from Fluka (St. Louis, MO). High-pressure nitrogen and ultrahigh-purity-high-pressure argon were purchased from Nexair, LLC (Suwanee, GA). Nucleotides were obtained commercially from Sigma Aldrich (St. Louis, MO) or were synthesized in our laboratory. Isotopically labeled nucleotides, [¹³C¹⁵N]dATP, [¹³C¹⁵N]dGTP, [¹³C¹⁵N]dCTP, and

(14) Jansen, R. S.; Rosing, H.; Schellens, J. H.; Beijnen, J. H. *J. Chromatogr., A* **2009**, *1216*, 3168–3174.
 (15) Diamond, T. L.; Roshal, M.; Jamburuthugoda, V. K.; Reynolds, H. M.; Merriam, A. R.; Lee, K. Y.; Balakrishnan, M.; Bambara, R. A.; Planelles, V.; Dewhurst, S.; Kim, B. *J. Biol. Chem.* **2004**, *279*, 51545–51553.
 (16) Hernandez-Santiago, B. I.; Obikhod, A.; Fromentin, E.; Hurwitz, S. J.; Schinazi, R. F. *Antiviral Chem. Chemother.* **2007**, *18*, 343–346.
 (17) Jansen, R. S.; Rosing, H.; de Wolf, C. J.; Beijnen, J. H. *Rapid Commun. Mass Spectrom.* **2007**, *21*, 4049–4059.
 (18) Shi, G.; Wu, J. T.; Li, Y.; Geleziunas, R.; Gallagher, K.; Emm, T.; Olah, T.; Unger, S. *Rapid Commun. Mass Spectrom.* **2002**, *16*, 1092–1099.
 (19) Bell, D. S.; Cramer, H. M.; Jones, A. D. *J. Chromatogr., A* **2005**, *1095*, 113–118.
 (20) Gilar, M.; Yu, Y. Q.; Ahn, J.; Fournier, J.; Gebler, J. C. *J. Chromatogr., A* **2008**, *1191*, 162–170.
 (21) Ray, A. S. *AIDS Rev.* **2005**, *7*, 113–125.
 (22) Hennere, G.; Becher, F.; Pruvost, A.; Goujard, C.; Grassi, J.; Benech, H. *J. Chromatogr., B: Anal. Technol. Biomed. Life Sci.* **2003**, *789*, 273–281.
 (23) Compain, S.; Durand-Gassel, L.; Grassi, J.; Benech, H. *J. Mass Spectrom.* **2007**, *42*, 389–404.
 (24) Pruvost, A.; Theodoro, F.; Agrofoglio, L.; Negro, E.; Benech, H. *J. Mass Spectrom.* **2008**, *43*, 224–233.

(25) Asakawa, Y.; Tokida, N.; Ozawa, C.; Ishiba, M.; Tagaya, O.; Asakawa, N. *J. Chromatogr., A* **2008**, *1198–1199*, 80–86.
 (26) Espada, A.; Rivera-Sagredo, A. *J. Chromatogr., A* **2003**, *987*, 211–220.
 (27) Vela, J. E.; Olson, L. Y.; Huang, A.; Fridland, A.; Ray, A. S. *J. Chromatogr., B: Anal. Technol. Biomed. Life Sci.* **2007**, *848*, 335–343.
 (28) Seifar, R. M.; Ras, C.; van Dam, J. C.; van Gulik, W. M.; Heijnen, J. J.; van Winden, W. A. *Anal. Biochem.* **2009**, *388*, 213–219.
 (29) Claire, R. L. *Rapid Commun. Mass Spectrom.* **2000**, *14*, 1625–1634.
 (30) Tuytten, R.; Lemiere, F.; Witters, E.; Van Dongen, W.; Slegers, H.; Newton, R. P.; Van Onckelen, H.; Esmans, E. L. *J. Chromatogr., A* **2006**, *1104*, 209–221.
 (31) Hawkins, T.; Veikley, W.; St. Claire, R. L., 3rd; Guyer, B.; Clark, N.; Kearney, B. P. *JAIDS, J. Acquired Immune Defic. Syndr.* **2005**, *39*, 406–411.
 (32) Cordell, R. L.; Hill, S. J.; Ortori, C. A.; Barrett, D. A. *J. Chromatogr., B: Anal. Technol. Biomed. Life Sci.* **2008**, *871*, 115–124.
 (33) Coulier, L.; Bas, R.; Jespersen, S.; Verheij, E.; van der Werf, M. J.; Hankemeier, T. *Anal. Chem.* **2006**, *78*, 6573–6582.
 (34) Crauste, C.; Lefebvre, I.; Hovaneissian, M.; Puy, J. Y.; Roy, B.; Peyrottes, S.; Cohen, S.; Guillon, J.; Dumontet, C.; Perigaud, C. *J. Chromatogr., B: Anal. Technol. Biomed. Life Sci.* **2009**, *877*, 1417–1425.

[¹³C¹⁵N]TTP used for endogenous dNTP quantification were purchased from Sigma Aldrich (St. Louis, MO). Nucleosides and nucleotides were at least 98% pure.

Cell Isolation and Cell Treatment Procedure. Human PBM cells were isolated from buffy coats derived from healthy donors using a Histopaque technique. Cells were cultured in flasks for 18 h, 37 °C, 5% CO₂. Suspension cells (PBM cells) were removed and phytohemagglutinin (PHA) stimulated (6 μg/mL) for 72 h prior to treatment with NRTI. Adherent cells (monocytes) were exposed to 1 000 U/mL monocyte colony stimulating factor (m-CSF) for 18 h to confer differentiation. Macrophages were maintained for 7 days before treatment with NRTI. Cells were exposed to media containing 10 μM of DXG, TDF, ZDV, (–)-FTC, or ABC for 4 h at 37 °C. Cells were washed with 1× PBS and centrifuged at 350g for 10 min at 4 °C and counted using a Vi-cell XR counter (Beckman Coulter, Fullerton, CA; viability >98%). Cell pellets were resuspended in 1 mL of ice cold 70% methanol and subjected to vortexing for 30 s. The tubes were then kept at –20 °C for at least 1 h to allow for nucleotide extraction. A total of 10 μL/10⁶ cells of lamivudine (3TC), 3TC-MP, and 3TC-TP (internal standard, IS) were added to the suspension in order to obtain a final concentration of 100 nM for all three IS upon sample reconstitution.

Calibration Curve Preparation and LC–MS/MS Analysis. Calibration standards covering the range of 0.5–1 000 nM were prepared by adding appropriate volumes of serially diluted stock solutions to a nontreated cell pellet. Six calibration concentrations (0.5, 1, 5, 10, 50, and 100 nM) and three quality control standards (1, 10, and 100 nM) were used to define the calibration curve and for partial assay validation, respectively for DXG, DXG-MP, DXG-TP, TFV, TFV-DP, (–)-FTC-TP, and CBV-TP. Six calibration concentrations (5, 10, 50, 100, 500, and 1 000 nM) and three quality control standards (10, 100, and 1 000 nM) were used to define the calibration curve and for partial assay validation, respectively, for ZDV-MP, ZDV-TP, [¹³C¹⁵N]dATP, [¹³C¹⁵N]dGTP, [¹³C¹⁵N]dCTP, and [¹³C¹⁵N]TTP. Calibration curves were calculated using the ratio of the analyte area to the internal standard area by linear regression using a weighting factor of 1/*x*. The samples were centrifuged for 10 min at 20 000g to remove cellular debris, and the supernatant was evaporated until dry under a stream of air. Prior to analysis, each sample was reconstituted in 100 μL/10⁶ cells of mobile phase A and centrifuged at 20 000g to remove insoluble particulates.

Instrumentation. The HPLC system was a Dionex Packing Ultimate 3000 modular LC system and comprised of two ternary pumps, a vacuum degasser, a thermostatted autosampler, and a thermostatted column compartment (Dionex Corp., Sunnyvale, CA). A TSQ Quantum Ultra triple quadrupole mass spectrometer (Thermo Electron Corp., Waltham, MA) was used for detection. Thermo Xcalibur software version 2.0 was used to operate the HPLC and the mass spectrometer and to perform data analysis.

Chromatography Columns. Three columns were evaluated: PFP (pentafluorophenyl) propyl, 50 mm × 1 mm, 3 μm particle size, (Restek, Bellefonte, PA); Hypersil GOLD-AQ (aqueous), 100 mm × 1 mm, 3 μm particle size; and Hypersil GOLD-C18, 100 mm × 1 mm, 3 μm particle size (Thermo Electron Corp., Waltham, MA).

Table 1. Parent Compounds *m/z*, Product Compounds *m/z*, Collision Energy, and Tube Lens Values for All Nucleosides, Nucleotides, NRTI, and NRTI-TP

	parent <i>m/z</i>	product <i>m/z</i>	collision energy (V)	tube lens (V)	ionization mode
3TC	230	112	15	70	+
3TC-MP	310	112	27	70	+
3TC-TP	470	112	27	90	+
DXG	254	152	15	70	+
DXG-MP	334	152	26	90	+
DXG-TP	494	152	30	130	+
TFV	288	176	20	70	+
TFV-DP	448	270	27	130	+
ZDV-MP	348	81	35	90	+
ZDV-TP	506	380	18	90	–
(–)-FTC-TP	488	130	30	130	+
CBV-TP	488	152	35	130	+
dATP	492	136	20	116	+
dGTP	508	152	30	110	+
dCTP	468	112	30	90	+
TTP	483	81	20	90	+
[¹³ C ¹⁵ N]dATP	507	146	20	116	+
[¹³ C ¹⁵ N]dGTP	523	162	30	110	+
[¹³ C ¹⁵ N]dCTP	480	119	30	90	+
[¹³ C ¹⁵ N]TTP	495	134	20	90	+

Ion-Pair Method Development Using Hypersil GOLD-C18 Column. Ammonium phosphate buffer (1 and 2 mM) and ammonium hydrogen carbonate (10 and 20 mM) were assayed by preparation of four separate buffers containing 3 mM HMA. The pH 7, 8, 9.2, and 10 were tested using four separate buffers containing 10 mM ammonium hydrogen carbonate and 3 mM HMA. To obtain pH 7 and 8 and pH 10, the buffer was adjusted with formic acid and ammonium hydroxide, respectively. No adjustments were required to obtain pH 9.2. Finally, the HMA concentration at 0, 3, 6, 9, and 12 mM was optimized using a buffer consisting of 1 mM ammonium phosphate. Standard calibration solutions prepared at 50 nM were used. The factors that were considered to discriminate the general quality of the chromatography for all analogues were the tailing factor ($Tf = A_{5\%} + B_{5\%}/2A_{5\%}$, where *A* and *B* are the left and the right peak width at 5% of height, respectively), the peak capacity ($k' = t_r - t_o/t_o$, where *t_r* is the retention time of the compound of interest and *t_o* is the retention time of an unretained compound), the effective plate number [$Ne = 5.54(t_r - t_o/w_{1/2})$, where *w_{1/2}* is the peak width at half height] and the peak area.

Optimized Ion-Pair Method Used for Partial Validation.

A linear gradient separation was performed on the Hypersil GOLD-C18 column (Thermo Electron, Waltham, MA). The mobile phases A and B consisted of 2 mM ammonium phosphate buffer containing 3 mM HMA and acetonitrile, respectively. The flow rate was maintained at 50 μL/min, and a 45 μL injection volume was applied. The autosampler was maintained at 4 °C and the column at 30 °C. The gradient used for separation started with 9% acetonitrile and reached 60% in 15 min. The return to initial conditions was achieved without the ramp, and the equilibration time was 14 min.

Mass Spectrometry Conditions. The mass spectrometer was operated in the positive or negative ionization mode with spray voltages of 3.0 and 4.5 kV, respectively, and at a capillary temperature of 390 °C; sheath gas was maintained at 60 (arbitrary units), ion sweep gas at 0.3 (arbitrary units), auxiliary gas at 5 (arbitrary units). The collision cell pressure was maintained at

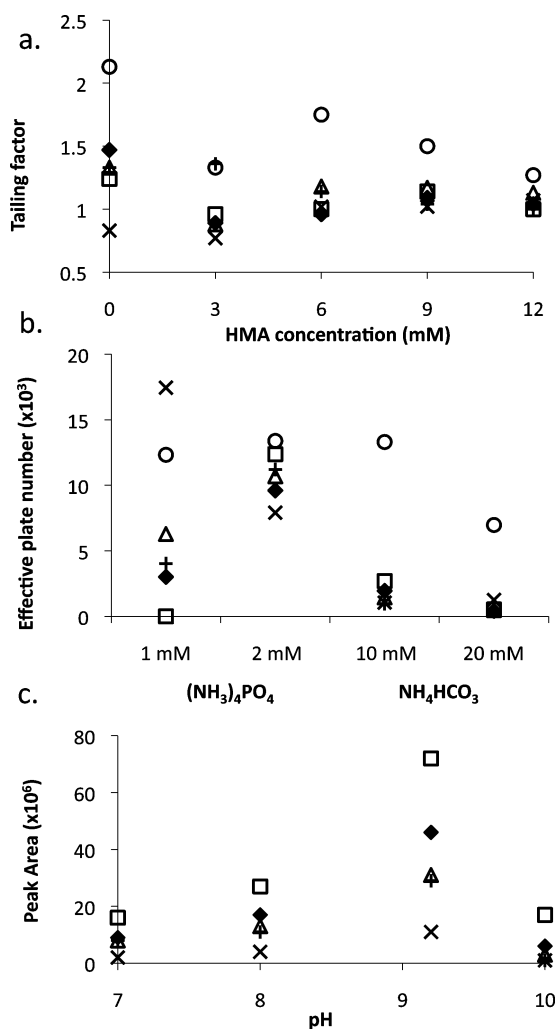


Figure 1. Chromatography parameters of NRTI-TP represented by the symbols: +, 3TC-TP; x, DXG-TP; ◆, TFV-DP; □, CBV-TP; Δ, (-)-FTC-TP; and ○, ZDV-TP: (a) tailing factor (Tf) at five different HMA concentrations; 0, 3, 6, 9, and 12 mM. (b) Effective plate number (Ne) at four different buffer compositions; 1 and 2 mM ammonium phosphate; 10 and 20 mM ammonium hydrogen carbonate. (c) Peak area at pH 7.0, 8.0, 9.2, and 10.0.

1.5 mTorr with a 0.01 s scan time, 0.1 scan width ($\Delta m/z$) and 0.7 full width half-height maximum resolution (unit mass) for both quadrupoles (Q1 and Q3) at all transitions. The intensity of selected product ion in the MS/MS spectrum of each compound was optimized using direct infusion of the analytes in the corresponding mobile phase at a concentration of 25 $\mu\text{g/mL}$, which was loaded separately into the instrument using a syringe pump at 5 $\mu\text{L/min}$. These selected reaction-monitoring (SRM) transitions were further optimized for each compound at the exact proportion of mobile phase/acetonitrile in the source using LC-MS/MS injection. The following scan parameters were utilized: precursor ion m/z , product ion m/z , collision energy, tube lens offset, and ionization mode (Table 1). All nucleosides and nucleotides were analyzed in positive mode from 2 to 11 min, except for ZDV-TP, which was analyzed between 11 and 13 min in negative mode. The chromatography method developed had optimal separation between the last two eluted nucleotides, namely, CBV-TP and ZDV-TP to enable a switch in polarity (from positive to negative) at 11 min. Before 2 min and after 13 min,

the effluent from the column was diverted to waste and a cleaning solution was sprayed on the ion source to avoid loss of signal. Multiple cleaning solutions were assessed with different percentages of acetonitrile (20%, 25%, and 50%) and with different percentages of formic acid (0%, 0.1%, and 0.4%). The combination of acetonitrile/water: 80/20 (v/v) without formic acid demonstrated the greatest sensitivity over time.

Partial Method Validation. Interday reproducibility was assessed by four injections each at low, medium, and high concentrations at 1, 10, and 100 nM of DXG, DXG-MP, DXG-TP, (-)-FTC-TP, TFV, TFV-DP, CBV-TP and 10, 100, and 1 000 nM of ZDV-MP, ZDV-TP, [¹³C¹⁵N]dATP, [¹³C¹⁵N]dGTP, [¹³C¹⁵N]dCTP, and [¹³C¹⁵N]TTP in a matrix containing 10⁶ cells/100 μL of mobile phase on four consecutive days. Intraday reproducibility was evaluated by five consecutive injections each of the same concentrations noted above. The accuracy was calculated as a percentage of the difference between the theoretical value and the calculated value from the experiment against the theoretical value. Precision was expressed as % relative standard deviation (RSD).

RESULTS AND DISCUSSION

Column Selection. The methodology using the column Hypersil GOLD-C18 with ion-pair reagent displayed the highest performance. The PFP propyl and the Hypersil-AQ columns designed for the separation of polar compounds with the use of volatile buffers that are compatible with mass spectrometry detection failed to discriminate the components of interest without the use of an ion pair reagent. Several buffers were assessed, such as ammonium formate and ammonium acetate, with concentrations ranging from 5 to 50 mM adjusted to a pH range from 4 to 8. At pH 4 and 8, no retention was achieved: all nucleoside triphosphates were eluted into the void volume. At pH 5 and 6, retention and separation were observed but the symmetry of the peaks obtained, the retention capacity, and the sensitivity were not sufficient for quantification purposes. Neither an increase in organic phase nor in ammonium salt improved these parameters. Thus, the development of an ion-pair methodology using the most efficient Hypersil GOLD-C18 column became the main focus.

Temperature Selection. The column compartment temperature was evaluated between 20 and 35 °C, and a significant improvement was observed at 30 °C, which was chosen as the optimal column temperature.

Ion-Pair Method Development. The values of chromatography parameters (Ne, k' , Tf, and area) for 3TC, 3TC-MP, 3TC-TP, DXG, DXG-MP, DXG-TP, TFV, TFV-DP, ZDV-TP, (-)-FTC-TP, and CBV-TP were used as a guide to select the optimal pH, HMA concentration, and buffer composition (Table S1 in the Supporting Information).

HMA Concentration Effect. HMA at 12 mM gave the lowest peak tailing (Figure 1a), the highest effective plate number, and the greatest peak area among all concentrations assessed; however, the ion source was clogged following 10 injections and the sensitivity was decreased without significant improvements even after source cleaning for 15 min between each injection. Interestingly, the decrease in peak tailing observed at 9 or 12 mM HMA suggests that HMA might possess a silanol-masking activity. Generally, phosphorylated metabolites and pairing ions (HMA) undergo a partition mechanism between the mobile phase and

Table 2. Intraday and Interday Accuracy and Precision for DXG, DXG-MP, DXG-TP, TFV, TFV-DP, ZDV-MP, ZDV-TP, (-)-FTC-TP, CBV-TP, and [¹³C¹⁵N]dNTP

	concn (nM)	interday (n = 4)		intraday (n = 5)	
		precision (%)	accuracy (%)	precision (%)	accuracy (%)
DXG	1	3.4	96.1	8.7	94.7
	10	5.3	91.7	3.4	93.7
	100	6.8	108.5	2.4	93.0
DXG-MP	1	10.9	105.4	11.2	102.0
	10	11.9	96.8	4.1	98.7
	100	0.2	102.2	5.4	96.8
DXG-TP	1	3.6	99.6	16.4	113.3
	10	7.5	109.7	3.6	110.4
	100	5.9	109.9	2.0	103.3
TFV	1	6.8	101.8	4.9	96.5
	10	3.6	100.6	2.4	88.7
	100	6.3	106.4	6.0	102.4
TFV-DP	1	14.3	108.8	6.8	96.5
	10	6.9	99.8	6.2	94.7
	100	9.5	93.2	3.3	97.0
ZDV-MP	10				
	100	14.1	105.1	13.1	110.1
	1 000	6.5	98.8		
ZDV-TP	10	19.8	91.1	13.6	89.2
	100	19.2	86.5	19.4	92.8
	1 000	6.2	104.8	11.4	98.3
(-)-FTC-TP	1	10.7	91.7	7.4	98.7
	10	13.5	99.9	13.0	112.9
	100	12.9	95.7	3.6	110.8
CBV-TP	1	12.3	94.5	6.0	111.2
	10	9.8	115.4	8.1	99.2
	100	20.0	97.7	4.2	95.8
[¹³ C ¹⁵ N]dATP	10	16.9	87.0	19.2	89.4
	100	13.6	106.6	6.6	102.6
	1 000	5.4	97.5	3.9	95.6
[¹³ C ¹⁵ N]dGTP	10	11.9	100.9	11.4	99.1
	100	10.5	108.4	5.1	103.7
	1 000	2.6	97.8	2.9	96.0
[¹³ C ¹⁵ N]dGTP	10	10.1	108.6	10.6	108.3
	100	16.4	101.6	5.3	74.8
	1 000	5.9	103.1	2.9	108.8
[¹³ C ¹⁵ N]TTP	10				
	100	16.4	114.1	5.3	103.8
	1 000	6.0	104.0	3.0	125.0

the stationary phase.³⁵ This mechanism can be described by an equation: HMA⁺ (mobile) + P⁻ (mobile) ↔ HMA⁺P⁻ (stationary), where hexylamine (HMA⁺) is the cation and the phosphorylated nucleotides (P⁻) are the anions. Thus, enough HMA should be available in the mobile phase for this reaction to occur. Optimized HMA concentration at 3 mM was sufficient to obtain a symmetric peak, while avoiding clogging the source and maintaining ionization over time.

Buffer Effect. Ammonium phosphate at 1 and 2 mM and ammonium hydrogen carbonate at 10 and 20 mM were compared. Ammonium hydrogen carbonate caused an increase in peak tailing, a decrease in effective plate numbers for all analytes except for ZDV-TP (Figure 1b) at both 10 and 20 mM, and worsened the peak symmetry of all analytes at 20 mM. Ammonium phosphate at 2 mM, but not 1 mM, increased the effective plate number of all the analytes tested, except for DXG-TP (Figure 1b) and appeared to be a superior buffer for running samples over several days, without the peak shift observed with the ammonium

hydrogen carbonate buffers. The improved properties obtained by the use of 2 mM ammonium phosphate versus ammonium hydrogen carbonate could be explained by its rank in the Hofmeister series, where the carbonate ions are placed lower than phosphate ions.^{36,37} Carbonate ions would have a lower propensity to retain protonated amines, such as HMA, than phosphate ions, explaining the necessity to raise the concentration of ammonium hydrogen carbonate. Carbonate ions would also increase the chaotropic effects, which could destabilize folded proteins, decrease their solubility, and give rise to salting-out behavior inside the column.³⁷ This was consistent with our observations with 20 mM ammonium hydrogen carbonate wherein a loss in chromatography quality was seen possibly due to clogging of the column (Figure 1b). In addition, ammonium hydrogen carbonate decomposes, which results in higher variability of the buffer composition and is not suitable for high-throughput analysis.³⁸ Finally, ammonium phosphate buffer is a silanol masking agent and is a potent buffer at high pH especially when a high volume of samples are injected and when the pK_a of the compound is ≥ 8,³⁸ which is often the case for nucleotides,³⁹ producing a better peak shape and making it the optimal buffer for nucleotide analysis.

pH Effect. With the application of pH 7, 8, 9.2, and 10, there was no noticeable change in the number of effective plates. The peak tailing decreased as the pH increased, and the peak capacity was stable from pH 7 to 9.2 but dropped at pH 10. The peak area and the signal intensity were decreased at pH 7, 8, and 10 and were increased at pH 9.2, making pH 9.2 optimal for all nucleotides (Figure 1c). Also, it was found that increasing the HMA concentration (pK_a 10.56) raised the pH and produced an improvement of signal intensity. Interestingly, when the pH was adjusted to 10 with ammonium hydroxide, a decrease in the signal intensity occurred (Figure 1c). Thus, both the pH and the silanol-masking effect of HMA might enhance the positive ionization of nucleotides. Furthermore, the addition of ammonium hydroxide or formic acid to the mobile phase could lower the sensitivity as first described by Vela et al.²⁷ Additionally, the pH influenced the ionization of the nucleotides. At low pH and up to 9.5, ZDV-TP was better ionized in the negative mode than in the positive mode, due to the inability of the thymine base to accept an extra proton unless conditions are extremely basic (thymidine nucleoside and nucleotide pK_a > 9.5).³⁹ The pH chosen, 9.2, justifies the use of negative mode ionization for ZDV-TP along with a specific transition *m/z* 506 → 380.²³

Internal Standards Selection. It was critical to choose three internal standards compatible with the chemistries and the retention time of each of the three classes of compounds measured, nucleoside, MP, and TP. 3TC, 3TC-MP, and 3TC-TP were assessed. However, dCTP was measured by monitoring the ion transitions *m/z* 468 → 112, which slightly differed from the one for 3TC-TP *m/z* 470 → 112. Thus, an additional peak was detectable on the 3TC-TP reconstituted ion chromatogram, which represented the dCTP isotopic distribution. The separation of the two compounds by over 2 min alleviated the risks of dCTP

(36) Roberts, J. M.; Diaz, A. R.; Fortin, D. T.; Friedle, J. M.; Piper, S. D. *Anal. Chem.* **2002**, *74*, 4927–4932.

(37) Zhang, Y.; Cremer, P. S. *Curr. Opin. Chem. Biol.* **2006**, *10*, 658–663.

(38) McCalley, D. V. *J. Chromatogr., A* **2003**, *987*, 17–28.

(39) Nordhoff, E. K. F.; Roepstorff, P. *Mass Spectrom. Rev.* **1996**, *15*, 67–138.

(35) Fritz, J. S. *J. Chromatogr., A* **2005**, *1085*, 8–17.

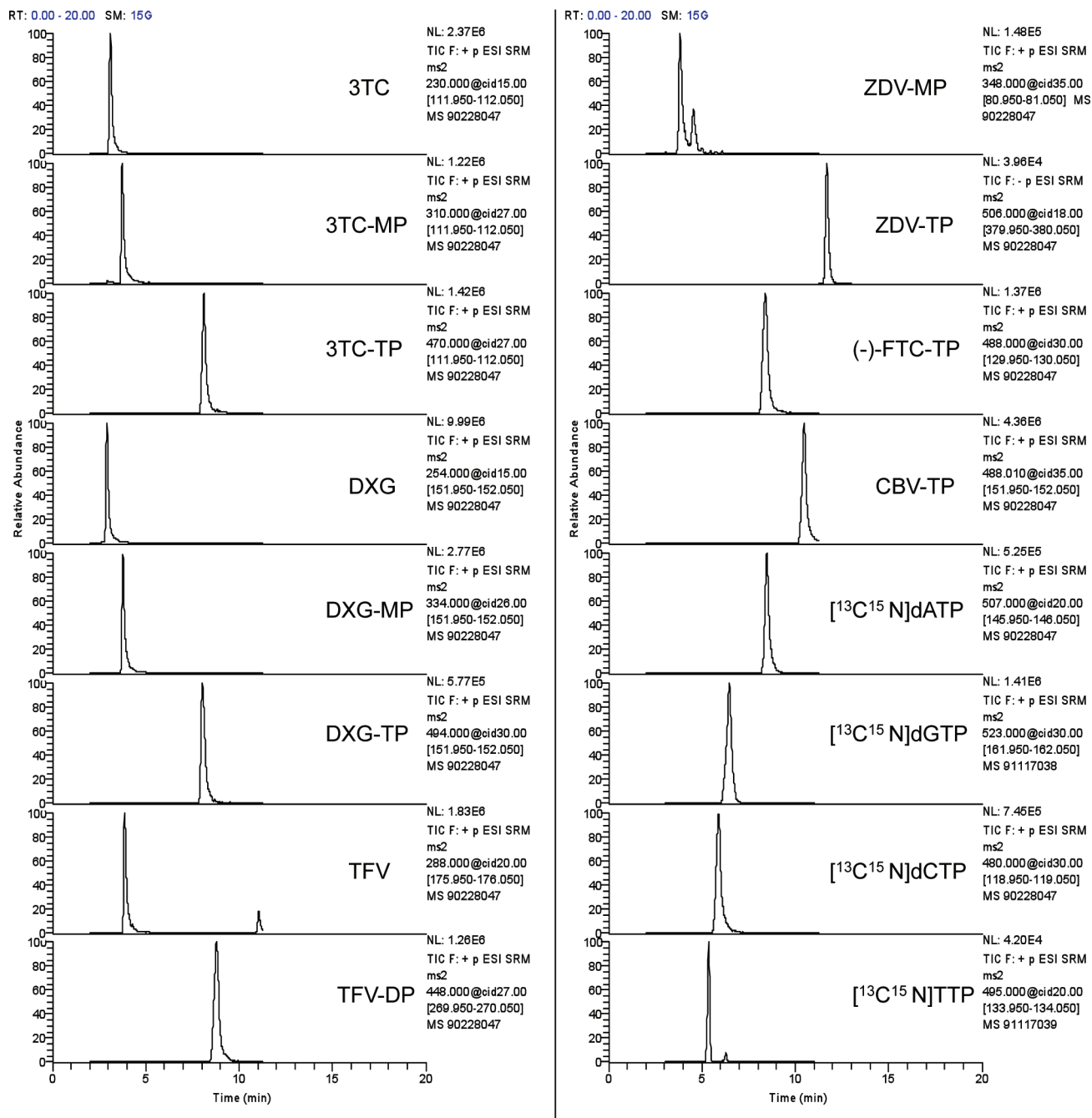


Figure 2. Typical chromatograms displaying all the standards used for the partial validation spiked in a PBM cells matrix containing 1×10^6 cells/100 μ L of mobile phase. The RIC shows the peaks obtained for DXG, DXG-MP, DXG-TP, TFV, TFV-DP, ZDV-MP, ZDV-TP, (-)-FTC-TP, CBV-TP, [¹³C¹⁵N]dATP, [¹³C¹⁵N]dGTP, and [¹³C¹⁵N]dCTP at 100 nM and [¹³C¹⁵N]TTP at 500 nM. Internal standards, 3TC, 3TC-MP, and 3TC-TP were at 100 nM.

interference over the peak area of 3TC-TP. 3TC, 3TC-MP, and 3TC-TP demonstrated a symmetrical peak shape and a lack of interference with endogenous compounds by injections of cell blanks compared with spiked standards and standards in reconstitution solvent.

Method Sensitivity and Partial Validation. Intraday and interday criteria for all nucleosides and nucleotides studied were within the range of acceptance, precision <20%, and $100 \pm 25\%$ accuracy (Table 2). A reconstituted ion chromatogram illustrates the separation obtained for all the calibration standards (Figure 2). ZDV-MP was eluted 1 min after an

interfering peak, which could be dGMP, AMP, or a coelution of both. Lower limits of quantification were 1 nM for DXG, DXG-MP, DXG-TP, TFV, TFV-DP, (-)-FTC-TP, and CBV-TP and 10 nM for [¹³C¹⁵N]dATP, [¹³C¹⁵N]dGTP, [¹³C¹⁵N]dCTP, and ZDV-TP, and 100 nM for [¹³C¹⁵N]TTP and ZDV-MP, which was sensitive enough to quantify all NRTI-TP in PBM cells and in macrophages (Figure 3) as well as endogenous dNTP. Sensitivity and specificity of the method developed was achieved by the intensity and the specificity of the MS/MS product formed in the positive ionization mode.²⁴ This method was subsequently applied for quantitative analysis of intracel-

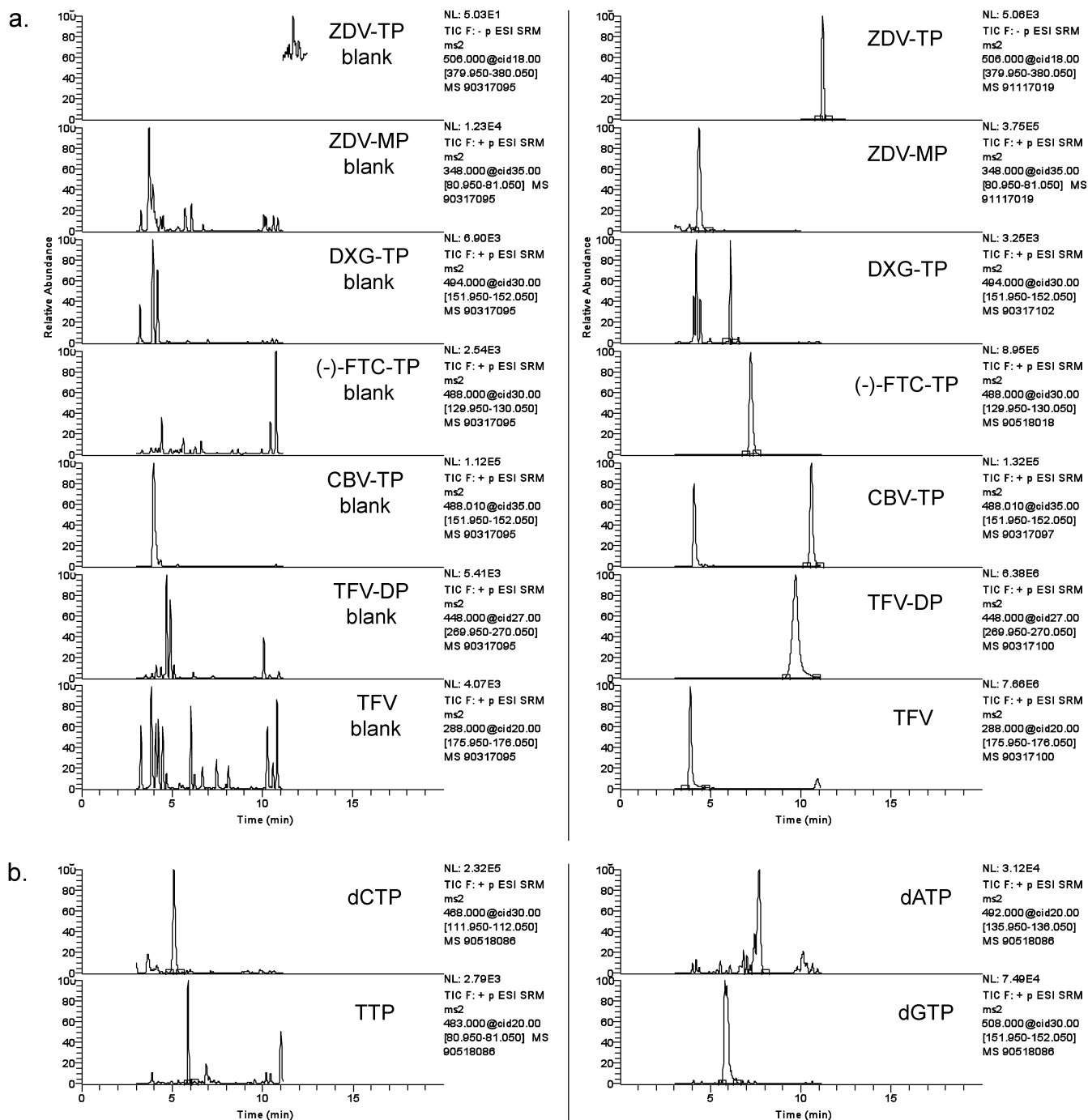


Figure 3. (a) Typical chromatograms for NRTI-TP, obtained from macrophages. Five drugs (ZDV, ABC, TDF, (-)-FTC, and DXG) were incubated separately at 10 μ M for 4 h and analyzed in five different LC-MS/MS runs. The left chromatograms represent five background signals obtained from a single injection of untreated macrophage extract; these chromatograms are marked as “blank”. The right chromatograms represent the five signals obtained from five separate injections of treated macrophage extracts. The sample incubated with TDF was diluted 20 times. (b) Typical chromatograms of endogenous dNTP obtained from a single macrophage extract.

lular NRTI-TP and endogenous dNTP levels in human PBM cells and in macrophages. The values found following NRTI incubations were in the expected range for ZDV-TP, CBV-TP, TFV-DP, and DXG-TP. However, the (-)-FTC-TP levels were 4-fold higher than those previously reported, which may be due to variable assay condition (Table 3).^{40,41} Endogenous dNTP levels were within the range of 0.33–11.9 and 0.08–5.8 pmol/ 10^6 cells in PBM cells and in macrophages, respectively. These values are within the previously reported range.¹⁵

CONCLUSIONS

This novel analytical method provides an accurate, rapid, and selective quantification of most clinically relevant nucleoside and nucleotide analogues simultaneously with successful application in primary human PBM cells and macrophages. This highly sensitive LC-MS/MS method was developed for simultaneous quantification of intracellular nucleotide concentrations of DAPD, TDF, ZDV, (-)-FTC, ABC, and endogenous dNTP but also provides a flexible foundation that can allow for the quantification

Table 3. NRTI-TP Levels (Picomoles/10⁶ Cells) in 72 h-PHA Stimulated Human PBM Cells, Following a 4 h Incubation of 10 μ M NRTI, in Comparison with Previously Published Data Using Similar Assay Conditions

	NRTI-TP levels	previous publications
ZDV-TP	1.13 \pm 0.27	\sim 1.1 ⁴²
CBV-TP	0.16 \pm 0.002	0.12 \pm 0.07 ⁴³
TFV-DP	0.05 \pm 0.03	0.038–0.11 ⁴⁰
(–)-FTC-TP	\sim 16	2.74–4.14 ⁴⁰
DXG-TP	0.05 \pm 0.03	\sim 0.015 ⁴⁴

of other NRTI with slight modifications. The developed method can also be applied for the accurate simultaneous determination of nucleosides and their intracellular metabolites from human samples in the context of pharmacokinetic evaluations since combination treatments are used for the treatment of HIV-1 infection.

ACKNOWLEDGMENT

This research was supported by the U.S. Public Health Service Grant 5P30-AI-50409 (CFAR), Grants 5R37-AI-041980, 4R37-AI-025899, and 5R01-AI-071846 and by the Department of Veterans Affairs. This work was partly presented with the pharmacological data in lymphocytes and macrophages at the HIV DART Conference in Puerto Rico, December 9–12, 2008. We thank Selwyn J.

Hurwitz and Judy Mathew for helpful discussions and critical reading of the manuscript. We thank RESTEK (Bellefonte, PA) for providing the PFP propyl column. Dr. Raymond F. Schinazi has received or may receive future royalties from the sale of DAPD/DXG, 3TC, and (–)-FTC as recognition for his contribution to the discovery and development of these drugs.

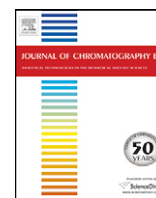
SUPPORTING INFORMATION AVAILABLE

Values of chromatography parameters (Ne, k' , T_R, and area) for 3TC, 3TC-MP, 3TC-TP, DXG, DXG-MP, DXG-TP, TFV, TFV-DP, ZDV, TP, (–)-FTC-TP, and CBV-TP. This material is available free of charge via the Internet at <http://pubs.acs.org>.

Received for review December 1, 2009. Accepted January 25, 2010.

AC902737J

- (40) Borroto-Esoda, K.; Vela, J. E.; Myrick, F.; Ray, A. S.; Miller, M. D. *Antiviral Ther.* **2006**, *11*, 377–384.
- (41) Gavegnano, C.; Fromentin, E.; Schinazi, R. F. In *Global Antiviral Journal*; IHL Press: St. Martin, West Indies, 2009; Vol. 5, p 43.
- (42) Qian, M.; Chandrasena, G.; Ho, R. J.; Unadkat, J. D. *Antimicrob. Agents Chemother.* **1994**, *38*, 2398–2403.
- (43) Ray, A. S.; Myrick, F.; Vela, J. E.; Olson, L. Y.; Eisenberg, E. J.; Borroto-Esoda, K.; Miller, M. D.; Fridland, A. *Antiviral Ther.* **2005**, *10*, 451–457.
- (44) Feng, J. Y.; Parker, W. B.; Krajewski, M. L.; Deville-Bonne, D.; Veron, M.; Krishnan, P.; Cheng, Y. C.; Borroto-Esoda, K. *Biochem. Pharmacol.* **2004**, *68*, 1879–1888.



Simultaneous quantification of 9-(β -D-1,3-dioxolan-4-yl)guanine, Amdoxovir and Zidovudine in human plasma by liquid chromatography–tandem mass spectrometric assay

Emilie Fromentin, Ghazia Asif, Aleksandr Obikhod, Selwyn J. Hurwitz, Raymond F. Schinazi*

Center for AIDS Research, Laboratory of Biochemical Pharmacology, Department of Pediatrics, Emory University School of Medicine, and Veterans Affairs Medical Center, Decatur, GA 30033, USA

ARTICLE INFO

Article history:

Received 20 February 2009

Accepted 11 August 2009

Available online 27 August 2009

Keywords:

Nucleoside analogs

Pharmacokinetics

ABSTRACT

A sensitive method was developed and validated for simultaneous measurement of an investigational antiviral nucleoside, Amdoxovir (DAPD), its deaminated metabolite 9-(β -D-1,3-dioxolan-4-yl)guanine (DXG), and Zidovudine (ZDV) in human plasma. This method employed high-performance liquid chromatography–tandem mass spectrometry with electrospray ionization. DXG and DAPD separation with sufficient resolution was necessary since they differ in only one mass to charge ratio, which increases the risk of overlapping MS/MS signals. However, the new method was observed to have functional sensitivity and specificity without interference. Samples were purified by ultrafiltration after protein precipitation with methanol. The total run time was 29 min. A linear calibration range from 2 to 3000 ng mL⁻¹ and 2 to 5000 ng mL⁻¹ was achieved for DAPD and DXG, and ZDV, respectively. Precisions and accuracies were both $\pm 15\%$ ($\pm 20\%$ for the lower limit of quantification) and recoveries were higher than 90%. Matrix effects/ion suppressions were also investigated. The analytes were chemically stable under all relevant conditions and the method was successfully applied for the analysis of plasma samples from HIV-infected persons treated with combinations of DAPD and ZDV.

Published by Elsevier B.V.

1. Introduction

Nucleoside reverse transcriptase inhibitors (NRTI) currently constitute the backbone of combinatorial regimens for the treatment of HIV infections and are usually combined with protease (PI), non-nucleosides reverse transcriptase (NNRTI), integrase, or entry/fusion inhibitors. The dosing of antiretroviral agent can be complex due to a significant potential for drug interactions, adverse effects and adherence challenges [1]. Resistance is still a major concern for NRTI, as is true for all classes of HIV drugs. Therefore, new compounds with improved safety, effectiveness and with a high genetic barrier to resistance are warranted. A clinical study was conducted evaluating the combination of Amdoxovir, [(–)- β -D-2,6-diaminopurine dioxolane, DAPD, AMDX], an investigational NRTI at 500 mg twice daily (bid) with standard and reduced doses of 3'-azido-3'-deoxythymidine (Zidovudine, ZDV, AZT) at 200 or 300 mg bid, respectively [2].

DAPD, a prodrug of 9-(β -D-1,3-dioxolan-4-yl)guanine (DXG), is currently in phase 2b clinical testing for the treatment of HIV-1 infection, and has been safely administered to nearly 200 patients [3]; www.rfspharma.com, last consulted on June 15, 2009). DXG has potent anti-HIV activity with a high genetic barrier to resistance, but is limited by its aqueous solubility. Therefore, DAPD was developed as a prodrug, which is rapidly deaminated by the ubiquitous enzyme adenosine deaminase (ADA) to DXG, followed by intracellular phosphorylation of DXG to its active metabolite DXG-5'-triphosphate which is a potent inhibitor of HIV-1 reverse transcriptase (HIV-1 RT) [4]. Therefore, it is important to accurately measure the concentrations of both compounds in human plasma, to assess the bioconversion efficiency of DAPD to DXG *in vivo* [4].

DAPD is currently the only guanosine nucleoside analog in clinical development, and has activity *in vitro* against wild type and drug-resistant forms of HIV-1, including viruses that are resistant to ZDV (mutations M41L, D67N, K70R, L210W, T215Y/F and K219Q/E) and 3TC (mutation M184V/I) [5–8]. ZDV, a thymidine nucleoside analog, was the first antiretroviral drug approved by the FDA, initially as a monotherapy regimen and subsequently as a component of HAART regimens [9,10]. The current approved oral dose of ZDV is 300 mg bid. ZDV undergoes intracellular phosphorylation, similar to other NRTI, to form the active ZDV-5'-triphosphate, which inhibits wild-type HIV-1 RT [11]. However, ZDV treatment is lim-

* Corresponding author at: Veterans Affairs Medical Center, 1670 Clairmont Rd, Medical Research 151H, Decatur, GA 30033, USA. Tel.: +1 404 728 7711; fax: +1 404 728 7726.

E-mail address: rschina@emory.edu (R.F. Schinazi).

ited by adverse effects, which may include nausea and malaise, as well as serious bone marrow cytotoxicity, including anemia and neutropenia [12–14]. A recent *in silico* study using population enzyme kinetic and pharmacokinetic data, suggested that decreasing the dose of ZDV from 300 to 200 mg, bid may decrease the amount of cellular ZDV-MP associated with hematological toxicity, without significantly reducing the cellular amount of ZDV-TP associated with antiviral efficacy [2]. Furthermore, a cellular pharmacology study demonstrated no drug–drug interaction at the phosphorylation level between ZDV and DXG [15]. Additionally, the development of HIV-1 resistant to DXG emerges slowly *in vitro* and viruses resistant to DXG had one of two mutations (K65R or L74V) within the viral polymerase gene [8,16–18]. ZDV has anti-K65R activity and therefore, could be potentially incorporated as a ‘resistance repellent’ for the K65R mutation that may result from prolonged treatment with DAPD and other K65R selecting drugs such as tenofovir disoproxil fumarate [2,16,18]. Furthermore, DXG demonstrated antiviral synergy in combination with ZDV in human peripheral blood mononuclear cells, and the combination of DAPD and ZDV completely prevented the development of DAPD or ZDV-associated resistance mutations through Week 28 [7,30].

A proof-of-concept randomized, placebo-controlled, single site study was conducted in HIV-infected persons to evaluate the safety, efficacy and pharmacokinetics of DAPD 500 mg po bid, in combination with ZDV 200 or 300 mg po bid. The study was conducted in Argentina and was approved by the site institutional review board/ethics review committee. The overall mean CD4⁺ cell count was 417 cells/mm³ (range 201–1071), HIV-1 RNA was 4.5 log₁₀ copies/mL (range 3.6–6.0) at baseline, and the median age was 33 (range 21–52) with an equal gender distribution (50% male, 50% female). Both combinations were safe and well tolerated [31], and produced a similar 2-log₁₀ decrease in mean plasma HIV-1 RNA from baseline at Day 10, supporting the earlier *in silico* ZDV study [2]. It was essential to develop a robust and validated LC–MS/MS method to measure the drug concentrations of DAPD, DXG and ZDV in plasma obtained from the pharmacokinetic component of the clinical study described above [32].

LC–MS/MS methodologies, such as reverse-phase chromatography tandem mass spectrometry and electrospray ionization, have been used for the last decade, have demonstrated improved specificity and sensitivity, and are capable of measuring very low concentrations of nucleosides in plasma and other tissues. Recently, levels of quantification as low as 0.5 ng mL⁻¹ of ZDV in plasma were reported [19]. The extraction of the nucleosides from the plasma for these assays typically involve, either solid phase extraction [19–23], or simple sample clean-up using a robotic system and disposable Centricon 30 ultra-filtration units [24].

Simultaneous measurement of ZDV, DAPD and its major metabolite, DXG was accomplished, despite polarity differences between ZDV and the two guanosine analogs, and the similarity of DAPD and DXG differing by only one functional group (Fig. 1).

A previously unpublished method for DAPD and DXG quantification [32] developed by Triangle Pharmaceuticals Inc. (acquired by Gilead Sciences in 2003) was modified to allow simultaneous quantification of ZDV in plasma. Herein, we present an optimized and improved method for extracting and simultaneously quantifying DAPD, DXG and ZDV in human plasma, as well as evidence of the reproducibility, accuracy and precision of this method.

2. Experimental

2.1. Material and reagent

2.1.1. Chemicals

Reference standards for DAPD and DXG were obtained from RFS Pharma, LLC (Tucker, GA). ZDV was obtained from Samchully Pharmaceuticals Co. Ltd. (Seoul, Korea). 2,6-Diaminopurine-2'-deoxyribose (DPD) and 2'-deoxyadenosine (2'-dA) were purchased from Sigma (St Louis, MO, USA) and 2'-deoxycoformycin (DCF), a potent adenosine deaminase inhibitor, from Waterstone Technology LLC (Carmel, IN).

2.1.2. Liquid chromatography

Human blood from healthy subjects was obtained from the American Red Cross (Atlanta, USA) and used as control human plasma. Eppendorf centrifuge model 5417C (Eppendorf North America, NY, USA) was used for plasma preparation. HPLC-grade methanol was obtained from Thermo Fisher Scientific Inc. (Waltham, MA), ultrapure water from an ELGA Ultrapure equipped with US filters, formic acid from Fluka (St Louis, MO, USA) and ammonium formate (purity 99%) from Acros Organics (NJ, USA). High-pressure nitrogen and ultra high purity and high-pressure argon were purchased from Nexair (Suwanee, GA). Eppendorf 1.5 mL safe lock cones were used to preserve the samples.

The HPLC system was a Dionex Packing Ultimate 3000 modular LC system comprising of a quaternary pump, vacuum degasser, thermostated autosampler, and thermostated column compartment (Dionex, CA). A TSQ Quantum Ultra triple quadrupole mass spectrometer (Thermo Scientific, Waltham, MA, USA) was used for detection. Thermo Xcalibur software version 1.3 was used to operate HPLC, the mass spectrometer and to perform data analyses.

2.1.3. Stock standard solutions

Standard stock solutions were freshly prepared in ultrapure MeOH:H₂O (1:1) to achieve the following concentrations: 0.2 mg mL⁻¹ for DAPD, 0.1 mg mL⁻¹ for DXG, 0.5 mg mL⁻¹ for ZDV and 1 mg mL⁻¹ for DCF (for conversion to μM, refer to Tables 2 and 3). Standards were serially diluted to 100, 10 and 1 μg mL⁻¹. Calibration standards covering the range from 2 to 5000 ng mL⁻¹ were prepared by adding appropriate volumes of serially diluted stock solutions to human plasma containing 10 μL of DCF at 1 mg mL⁻¹ (final volume 5 mL). Eight calibration concen-

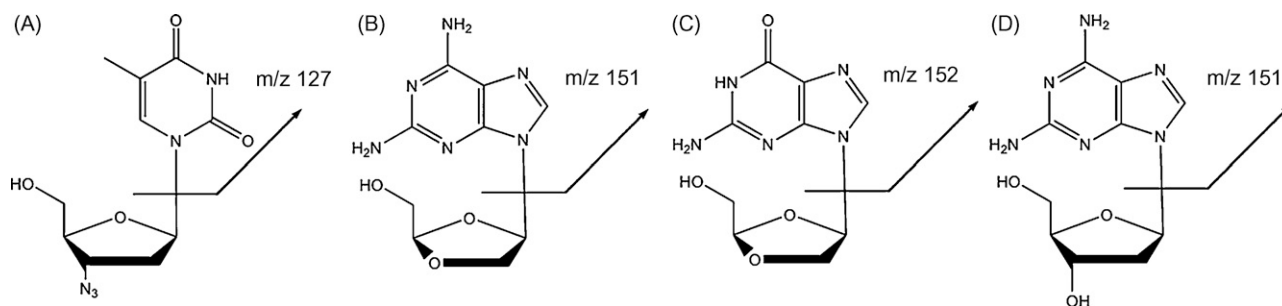


Fig. 1. Chemical structure of (A) Zidovudine, ZDV, (B) Amdoxovir, DAPD, (C) 9-(β-D-1,3-dioxolan-4-yl)guanine, DXG, (D) 2,6-diaminopurine-2'-deoxyribose, DPD and the representation of the fragment used in the Selected Reaction Monitoring (SRM).

trations (2, 5, 10, 50, 100, 500, 1000 and 3000 ng mL⁻¹) were used to define the calibration curve for all three analytes and an additional concentration, 5000 ng mL⁻¹ was used to ZDV calibration. Five quality control (QC) standards were also used (2, 5, 10, 500 and 3000 ng mL⁻¹) for assay validation. Aliquots of about 1 mL of calibration standards and QC samples were transferred to 1.5 mL polypropylene snap-cap tubes and stored frozen at -20 °C until analysis. All stock standard solutions were stored at -20 °C.

A stock solution of the internal standard, DPD was prepared at 1 mg mL⁻¹ in methanol, and was diluted to a 250 ng mL⁻¹ solution in methanol for use during sample preparation. A stock solution of 100 mM ammonium formate was prepared and adjusted once to pH 4.8 using formic acid followed by filtration under vacuum with nylon discs 0.2 µm (Whatman, New Jersey, USA) and was stored at 4 °C. A stock solution of 4 mM 2'-dA was prepared and filtered under vacuum using nylon discs 0.2 µm (Whatman, New Jersey, USA) and was stored at 4 °C.

2.2. Preparation of plasma samples and extraction procedure

DAPD and DXG were extracted from human plasma using a methanol-based protein precipitation procedure, followed by LC-MS/MS analysis. Prior to analysis, calibration standards, quality controls (QC) and clinical samples (collected at Aclires-Argentina SRL, Buenos Aires, Argentina), were thawed and allowed to equilibrate at room temperature. One hundred µL of plasma (calibration, QC and subject samples) were transferred to a 1.5 mL polypropylene snap-cap tubes and spiked with 400 µL of methanol-based solution containing internal standard (DPD, 250 ng mL⁻¹). The microcentrifuge vials were capped and vortex mixed for 1–2 s. The samples were allowed to sit for 15 min before being mixed under vortex at high speed for 30 s to inactivate any HIV present in the samples. The vials were centrifuged at 14,000 × g for 5 min followed by the removal of 200 µL of the supernatant to two microcentrifuge tubes, which was evaporated to dryness under a stream of air. The residue was reconstituted in 125 µL of 2 mM ammonium formate, pH 4.8 and 0.04 mM 2'-dA and briefly centrifuged at high speed. The supernatant was transferred to a Costar Spin-X microcentrifuge tube filter and centrifuged at 14,000 × g for 5 min. Fifty µL of the filtrate were transferred to 1.5 mL vials containing an insert of 200 µL, and 5 µL were injected directly into the chromatographic system.

2.3. LC-MS/MS conditions

2.3.1. Reverse-phase chromatography

Chromatographic separation was performed using a Betabasic-C18 column (100 × 1 mm, 3 µm particle size; Thermo Scientific, Waltham, MA, USA). This column was protected from remaining particles by a pre-column filter with 0.2 µm particle size (Thermo Scientific, Waltham, MA, USA). The mobile phase A consisted of 2 mM ammonium formate buffer, pH 4.8 containing 0.04 mM 2'-dA prepared daily from stock solutions. The mobile phase B consisted of methanol. The initial conditions were 94% A and 6% B at 50 µL min⁻¹. DXG, DAPD and DPD were eluted by this isocratic method during the first 7 min of analysis. From 7.5 min to 8.5 min, the flow rate was increased to 100 µL min⁻¹, from 8.5 min to 13 min, B was increased from 6% to 90% and immediately

decreased to 6% at 14.3 min allowing ZDV elution. The flow rate was maintained at 100 µL min⁻¹ until 25 min to accelerate the column re-equilibration and was decreased to 50 µL min⁻¹ in 1 min. The total run time was 29 min, including time for column regeneration, which was optimized in order to maintain an efficient separation of DAPD and DXG on the following run. However, a shorter re-equilibration time led to a co-elution of DAPD and DXG and no benefit was achieved using longer re-equilibration times. The column temperature was kept constant at 30 °C. The column effluent was directed to waste via the divert valve of the mass spectrometer at 0–3 min, 8–13 min and 15–29 min. During these intervals, a cleaning solution containing 80% methanol and 0.4% formic acid in water was used at 50 µL min⁻¹. This cleaning of the ion source improved the sensitivity of detection. A solution consisting of 80% methanol and 0.1% formic acid in water was used for autosampler loop and syringe cleaning following injection.

2.3.2. MS/MS conditions

Analytes were protonated by electrospray ionization (ESI) in positive mode. Selected Reaction Monitoring (SRM) mode was used for the acquisition. The intensity of selected product ion in the MS/MS spectrum of each compound was optimized using direct infusion of the analytes in the corresponding mobile phase at 25 µg mL⁻¹ and individually into the instrument using a syringe pump at 5 µL min⁻¹. The sheath and auxiliary gas (nitrogen) were set at 45 and 0.5 arbitrary units (au), respectively without ion sweep gas. The collision gas (argon) pressure was set at 1.3 mTorr. The spray voltage was 4000 V. The capillary was heated at 280 °C and 0.1 s scan time was used. The collision-induced dissociation (CID) was at -6 V. Scan parameters were as follows: precursor ion *m/z*, product ion *m/z*, collision energy, tube lens offset and the full width half mass (FWHM) resolution (unit resolution) for both quadrupole (Q1 and Q3) and are listed in Table 1. A representation of the hypothesized fragmentation for all nucleosides is shown in Fig. 1.

2.4. Validation

2.4.1. Limit of quantification

The limit of quantification (LOQ) was defined as the smallest quantity of analyte likely to be quantified accurately with a precision within ±20%. For each of the three analytes, QC and calibration standards were prepared at the lower limit of quantification (2 ng mL⁻¹).

2.4.2. Linearity

Ten calibration standards (2, 5, 10, 50, 100, 500, 1000, 3000 and 5000 ng mL⁻¹) and four QCs (2, 10, 500 and 3000 ng mL⁻¹) were prepared in control blank plasma pretreated with DCF, prior to processing the clinical samples. Standards were processed simultaneously with the patient samples and were assayed prior to patient samples. QCs were run along with the clinical samples to ensure confidence in the sample stability during the sequence and in the accuracy of the quantification. Calibration curves were calculated by linear regression using a weighting factor of 1/*x*. Linearity was evaluated by means of back-calculated concentrations of the calibration standards; these values should be within 15% of the nominal concentration and 20% of the nominal concentration at LLOQ to

Table 1
Scan parameters of the Thermo TSQ Quantum Ultra triple quadrupole mass spectrometer.

Analyte	Precursor ion (<i>m/z</i>)	Product ion (<i>m/z</i>)	Collision energy (V)	Tube lens offset (V)	FWHM resolution for Q1	FWHM resolution for Q3
DAPD	253	151	27	59	1.00	0.70
DXG	254	152	20	80	0.70	0.50
ZDV	268	127	24	51	0.70	0.50
DPD	267	151	25	68	0.70	0.70

be accepted. Based on the criteria, less than 25% of the calibration standards were rejected from the calibration curve.

2.4.3. Specificity and selectivity

Two sets of human blank plasma were prepared and analyzed in the same manner as the calibration standards and QCs, but without the internal standard. The objective was to determine whether any endogenous compounds interfere at the mass transition chosen for DAPD, DXG, DPD and ZDV. Interference can occur when co-eluting endogenous compounds, produce ions with the same m/z values that are used to monitor the analytes and internal standard. The peak area of any endogenous compounds co-eluting with the analyte should not exceed 20% of the analyte peak area at LLOQ or 5% of the internal standard area.

2.4.4. Recovery and matrix effect

The amount of analyte lost during sample preparation was calculated from the recovery values. Recoveries of DAPD, DXG and ZDV from plasma following sample preparation were assessed in triplicate by comparing the response of each analyte extracted from plasma with the response of the same analyte at the same concentration spiked in post-extracted blank plasma. It was also important to ensure the absence of a significant matrix effect. Significant ion suppression could occur when non-appropriate solvents are used or when endogenous compounds are simultaneously eluted with the analyte of interest resulting in interference with its ionization. The suitable dilution had to be determined to avoid decreasing the MS signal in the presence of increasing amounts of biological sample. The matrix effect was assessed by comparing the response of the post-extracted blank plasma spiked at known concentration and the response of the same analyte at the same concentration prepared in mobile phase. This value provided information about specific ion suppression in plasma. A low, medium and high-level concentration at 10, 100 and 1000 ng mL⁻¹, respectively was used to assess recovery and matrix effects.

2.4.5. Accuracy and precision

The intra- and inter-day precisions and accuracy were also evaluated at low, medium and high concentrations (10, 100 and 1000 ng mL⁻¹). For intra-assay precision, one control sample from each of the three concentrations was assayed on six runs in one sequence. For inter-day precision, one control sample from each of the three concentrations was assayed on four separate days (corresponding to four runs). The vial containing the control sample was maintained at -20 °C between injections. Inter-day extraction reproducibility was assessed by calculating the precision of five extracted spiked standards in plasma, analyzed on five different days. Intra- and inter-day variations were assessed by comparing means and standard deviations of drug concentrations at the three levels. The precision was evaluated as the relative standard deviation of the mean expressed as a percentage (coefficient variation - %CV) and had acceptance criteria of less than 20%. Accuracy was expressed as the mean absolute percentage deviation from the theoretically determined concentration with acceptance criteria of within 80–120%.

2.4.6. Stability

The stability of extracted standards from plasma in the autosampler was assayed by quantification of each analyte at 1000 ng mL⁻¹ after storage for 40 h and 5 days at 4 °C. The stability of the standards during the extraction was assessed by quantification of each analyte at 1000 ng mL⁻¹ after storage at room temperature for 24 h. The stability of extracted standards after three freeze/thaw cycles was also evaluated. The analyte was considered stable in biological matrix or extracts when 80–120% of the initial concentration was measured. The re-injection reproducibility was assessed to determine

if an analytical run could be re-analyzed in the case of instrument failure.

2.4.7. Carryover

Carryover was evaluated by injecting two matrix blanks immediately following the upper limit of quantification (ULOQ) standard and the lower limit of quantification (LLOQ) standard. Carryover was acceptable as long as the mean carry over in the first blank was less than or equal to 30% of the peak area of the ULOQ and LLOQ and was less than or equal to 20% in the second blank.

3. Results

3.1. LC/MS/MS characteristics

Typical LC-MS/MS chromatograms for extracted DAPD, DXG, ZDV and DPD (internal standard) compared with standard extracted from plasma blank are shown in Fig. 2. The retention times of DAPD, DXG, DPD and ZDV were 5.49, 3.86, 6.10 and 13.65 min, respectively.

An additional peak was observed at 5.45 min on DXG reconstituted ion chromatogram (RIC) in both patient and standard, but not in blank plasma. This interference was observable at the same retention time as DAPD. This peak was approximately 10% of DAPD signal intensity and resulted from the isotope distribution of DAPD. The chromatographic separation was essential in order to accurately quantify DXG. A plasma sample from a patient was also analyzed without internal standard to confirm that no endogenous substances interfered with any of the analytes, including the internal standard.

The highest intensity for protonated ions was found in positive mode for all analytes and internal standard as they have an ability to accept protons. The introduction of a methanol–water–formic acid (80:20:0.4 v/v/v) solution to the electrospray ionization (ESI) source, while the effluent from the column was diverted to waste, increased the intensity and participated in rinsing the source. The optimization of capillary temperature and nitrogen flow was considered important as they both played an important role in minimizing ion suppression and increasing the sensitivity of the method.

3.2. Linearity and limit of quantification

The standard curve was obtained by fitting the ratio of peak height of DAPD, DXG and ZDV to that of the internal standard against the concentrations (2–3000 ng mL⁻¹) of DAPD and DXG and (2–5000 ng mL⁻¹) of ZDV using a 1/x weighted linear regression ($y = Ax + B$). The lower limit of quantification (LLOQ) was 2 ng mL⁻¹, which could be quantified accurately and precisely within ±20% for each analyte. This corresponds to an amount of 3.2 pg of analyte injected on column. The upper limit of quantification (ULOQ) was 3000 ng mL⁻¹ for DAPD and DXG and 5000 ng mL⁻¹ for ZDV.

3.3. Validation results

3.3.1. Recovery and matrix effect

Recovery was determined by measuring an extracted sample against a post-extracted spiked sample. Matrix effect was determined by measuring a post-extracted spiked sample and an un-extracted sample. Three concentrations (10, 100 and 1000 ng mL⁻¹) were used and assayed in duplicates (Table 2). Absolute values were determined by comparing areas and relative values determined by comparing ratios (area of the analyte over the area of the internal standard).

The relative recovery and matrix effect values reflect general analyte loss on both the analyte and the internal standard. The abso-

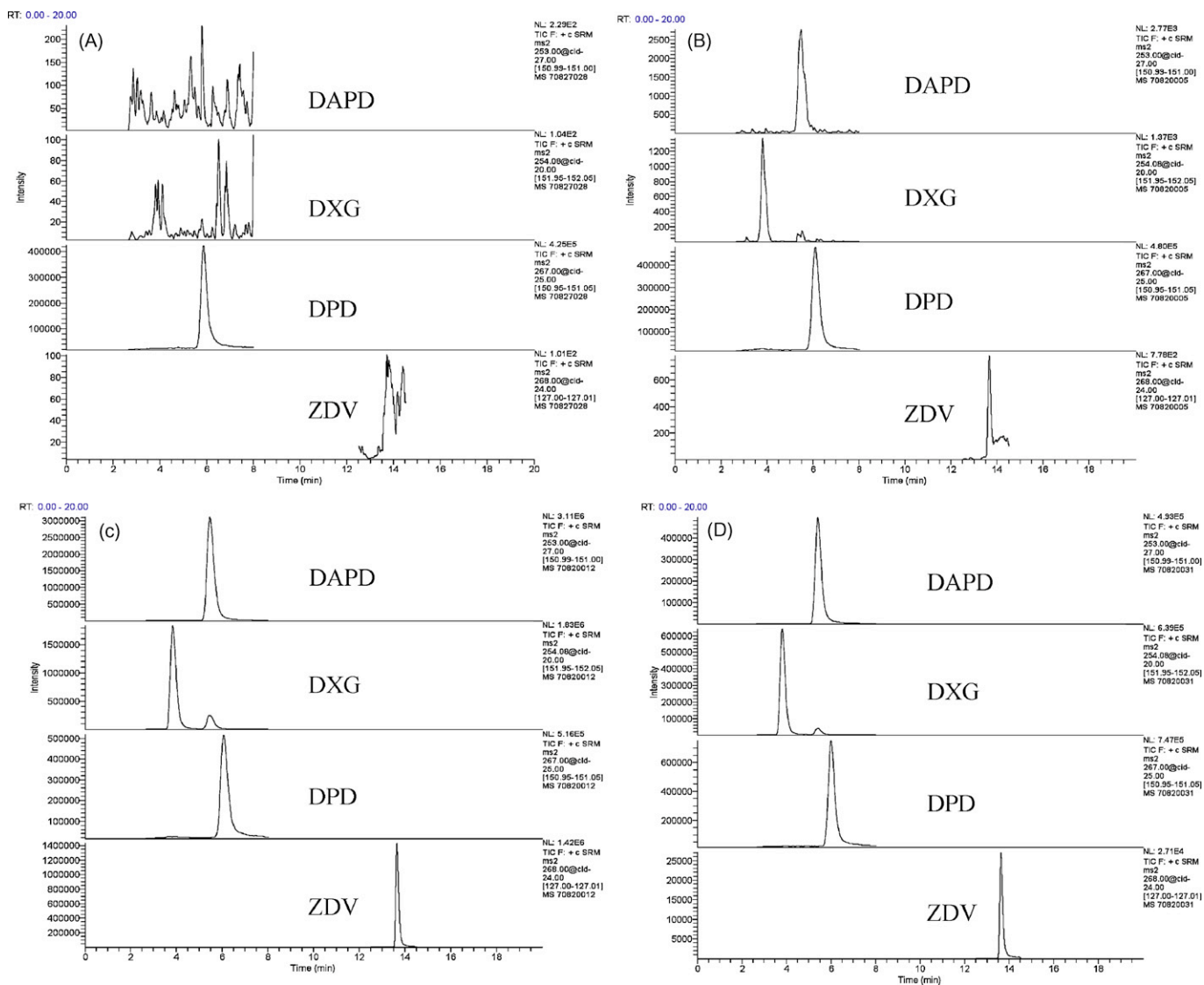


Fig. 2. Reconstituted ion chromatograms (RIC) for (A) patient plasma obtained on first day of treatment before first dose administration, (B) healthy subject plasma at 2 ng mL^{-1} of each standards, (C) healthy subject plasma at 3000 ng mL^{-1} of each standards and (D) patient plasma 4 h after the first dose administration; the calculated analyte concentrations were as follow: 328 ng mL^{-1} , 693 ng mL^{-1} and 43 ng mL^{-1} for DAPD, DXG and ZDV, respectively (all plasma samples from healthy subjects and patient were treated with methanol containing internal standard, DPD). The top trace is the RIC for DAPD, the second trace is the RIC for DXG, the third trace is the RIC for DPD and the bottom trace is the RIC for ZDV. The retention time appears on top of the peak.

lute values represent specific loss occurring during the extraction or specific ion suppression. For all analytes, the recovery values provided confidence in the extraction process. Greater matrix effect was observed for DXG compared with DAPD and ZDV, but the ion suppression did not significantly vary with increasing concentrations of DXG, allowing the linearity of the response.

3.3.2. Accuracy and precision

The results of intra-assay and inter-assay precision for three concentrations (low, medium and high) are summarized in Table 3. Instrument intra-assay imprecision was $<5\%$ and accuracy was $>95\%$ at all concentrations. Instrument inter-assay imprecision was $<10\%$ at all concentrations, accuracy was $>80\%$ at low concentration

Table 2
Recovery and matrix effect ($10, 100$ and 1000 ng mL^{-1}) in duplicate.

Analyte	Conc. (ng mL^{-1}) ^a	Absolute recovery (%)	Relative recovery (%)	Absolute matrix effect (%)	Relative matrix effect (%)
DXG	10	81.8	91.8	33.1	23.0
DAPD		95.3	92.3	9.5	-3.0
ZDV		101.3	97.3	12.6	0.8
DXG	100	97.2	104.9	34.2	16.6
DAPD		89.3	94.5	21.0	-0.6
ZDV		91.4	95.6	22.5	2.5
DXG	1000	92.3	106.5	19.7	15.0
DAPD		86.9	93.2	3.3	-2.6
ZDV		67.4	80.4	5.1	-0.3

^a To convert ng mL^{-1} to nM, the concentration should be divided by 253, 252, 267 for DXG, DAPD and ZDV, respectively.

Table 3
Intra- and inter-assay precision and inter-assay reproducibility for all three analytes.

Analyte	Conc. ^a (ng mL ⁻¹)	Intra-assay precision (n = 6 runs)		Inter-assay precision (n = 4 runs)		Inter-assay extraction reproducibility (n = 5 replicates)	
		Accuracy (%)	CV (%)	Accuracy (%)	CV (%)	Accuracy (%)	CV (%)
DXG	10	104.6	3.4	90.8	2.7	99.1	9.2
DAPD		104.5	4.1	82.7	7.0	97.2	8.1
ZDV		97.2	1.4	85.0	5.1	101.7	10.9
DXG	100	108.2	3.2	107.4	8.5	103.6	10.5
DAPD		106.1	0.4	104.5	9.3	97.9	7.7
ZDV		103.7	3.1	102.4	3.5	103.1	13.5
DXG	1000	106.8	2.5	105.4	4.6	101.3	7.1
DAPD		106.1	1.4	102.9	4.8	94.1	10.3
ZDV		105.7	1.5	99.3	1.9	96.8	9.11

^a To convert ng mL⁻¹ to nM, the concentration should be divided by 253, 252, 267 for DXG, DAPD and ZDV, respectively.

and >99% at high and medium concentrations. Extraction reproducibility was in the range of 94.1–103.6% accuracy and 7.1–13.5% imprecision.

3.3.3. Stability

The analytes were found to be stable under all conditions tested and the variation in concentration was minimal with 84–110% recovery (Table 4).

3.3.4. Carryover

At LLOQ, for ZDV and DXG, the peaks in the blank following the injection at 2 ng mL⁻¹ were in the range of the background noise of the reconstituted ion chromatogram and consequently were not integrated. For DAPD, at LLOQ, the carryover was 8% in the first blank and 4% in the second blank, which were acceptable. For all analytes, at ULOQ, the carryover was below 0.08% in the first blank and below 0.03% in the second.

4. Discussion

An improved method was developed and validated for high throughput simultaneous measurement of DAPD, DXG and ZDV levels in plasma, generating data necessary for clinical and pharmacokinetic analysis. LC-MS/MS methods have been used successfully for the last decade for quantification of antiretroviral agents, including NRTI in biological matrix. Limited work was available for DAPD and DXG. However, ZDV quantification by LC-MS/MS, using reverse phase chromatography, has been described previously [19,22–25]. Short runs were used for ZDV detection with mobile phase containing 0.1% of acetic acid [25] or at neutral pH [19,24]. However, at pH 4.8, which improved DAPD and DXG separation, ZDV retention was increased, which could be explained by the work of Bezy et al., who demonstrated that at a pH between 5 and 7, ZDV was neutral and its retention was increased, whereas at pH 9, ZDV became negatively charged with a low retention [23]. ZDV was detected either in positive [26,27] or negative mode [19,22–25], depending on the mobile phase used. In our case, the positive mode was found to have greater sensitivity for all analytes. The challenge was to obtain a discriminating and rapid separation of DAPD and DXG, which have similar molecular weights and fragmentation patterns, while still achiev-

ing simultaneous detection of ZDV, which is less polar than DAPD and DXG.

A binary method was developed, consisting of an isocratic elution of DAPD, DXG and DPD in the first 8 min of the run followed by a fast gradient for ZDV elution, because of its strong affinity for the stationary phase. Following the gradient, it became essential to optimize the equilibration time of the column with 6% methanol in order to maintain consistent retention times for DAPD and DXG for the subsequent injection, since these retention times were very sensitive to slight variations in methanol concentration. The peak shape of all analytes was improved by the addition of 0.04 mM of 2'-dA, creating a shift in baseline signal of the reconstituted ion chromatogram, and decreasing background noise. 2'-dA may act as a silanol-masking agent, which would prevent the non-specific binding of the analytes to the column. It may also produce an ion-pairing effect with other nucleosides, enhancing the shape of the peaks. The peak shape was also greatly improved by using a microbore column, with 3 μm particle size, which allowed the use of lower flow rates than wider columns with bigger particle size, while increasing the backpressure. Increasing the particle size to 5 μm and using a different column: Hypersil GOLD-C18 (100 × 1 mm, 5 μm particle size; Thermo Scientific, Waltham, MA, USA), caused a peak broadening. However, the use of shorter column to reduce the run time decreased the resolution between DXG and DAPD inducing quantification error due to signal overlap. Several gradients were tested, but the steepest slope was necessary to shorten the re-equilibration time. The use of this column improved the assay sensitivity by decreasing the need for sample dilution. Furthermore, a reduction in mobile phase volume introduced to the ion source provided the added benefit of decreasing the ion suppression over time, rendering high throughput analysis of the clinical trial samples possible. In addition, reducing the amount of mobile phase, and therefore the amount of organic solvent, was advantageous, since it reduced the cost of the analysis, and was also more ecological. For the clinical trial, 43 clinical samples were successfully assayed in sequences of 26 h, including standards and QCs.

In this method, the extraction was performed manually, which was time consuming and could be further adapted to allow for high throughput application. Kenney et al. used a robotic system, which decrease bias and imprecision, as well as increase the throughput [24]. The extraction imprecision and inaccuracy did not

Table 4
Stability of the analytes extracted from plasma spiked at 1000 ng mL⁻¹ under temperature variation conditions.

Analyte	24 h at room temperature (% recovery)	40 h at 4 °C (% recovery)	5 days at 4 °C (% recovery)	4 freeze/thaw cycles at -20 °C (% recovery)
DXG	101	104	91	110
DAPD	92	100	95	99
ZDV	96	91	84	104

exceed 15% for 5 days, meeting the limits required to validate the method.

5. Conclusions

A sensitive and robust LC–MS/MS method was developed and validated for simultaneous measurement of DAPD, DXG and ZDV in plasma. The results obtained [32,34] using this optimized method were in accordance to previous reported studies [28–30,33] and the lower limit of quantification was sufficient to perform the pharmacokinetic analysis on clinical samples [34]. This new method should be useful to simultaneously measure DAPD, DXG and ZDV in clinical samples and will allow further assessment of potential drug–drug interactions.

Acknowledgments

This work was supported in part by NIH Grant 4R37-AI-025899, 5R37-AI-041980, 5P30-AI-50409 (CFAR), and by the Department of Veterans Affairs. We would like to thank Judy Mathew for helpful discussions and critical reading of the manuscript. Dr. Schinazi was a founder of Triangle Pharmaceuticals Inc., and the founder of RFS Pharma LLC which is developing DAPD clinically. He is also an inventor of DAPD, DXG and 3TC and may receive future royalties from the sale of these drugs.

References

- [1] N. Plipat, P.K. Ruan, T. Fenton, R. Yogev, *J. Virol.* 78 (2004) 11272.
- [2] S.J. Hurwitz, G. Asif, N.M. Kivel, R.F. Schinazi, *Antimicrob. Agents Chemother.* 52 (2008) 4241.
- [3] A.H. Corbett, J.C. Rublein, *Curr. Opin. Investig. Drugs* 2 (2001) 348.
- [4] P.A. Furman, J. Jeffrey, L.L. Kiefer, J.Y. Feng, K.S. Anderson, K. Borroto-Esoda, E. Hill, W.C. Copeland, C.K. Chu, J.P. Sommadossi, I. Liberman, R.F. Schinazi, G.R. Painter, *Antimicrob. Agents Chemother.* 45 (2001) 158.
- [5] J.L. Jeffrey, J.Y. Feng, C.C. Qi, K.S. Anderson, P.A. Furman, *J. Biol. Chem.* 278 (2003) 18971.
- [6] B. Seignerres, C. Pichoud, P. Martin, P. Furman, C. Trepo, F. Zoulim, *Hepatology* 36 (2002) 710.
- [7] Z. Gu, M.A. Wainberg, N. Nguyen-Ba, L. L'Heureux, J.M. de Muys, T.L. Bowlin, R.F. Rando, *Antimicrob. Agents Chemother.* 43 (1999) 2376.
- [8] J.P. Mewshaw, F.T. Myrick, D.A. Wakefield, B.J. Hooper, J.L. Harris, B. McCreedy, K. Borroto-Esoda, J. Acquir. Immune Defic. Syndr. 29 (2002) 11.
- [9] C.C. Carpenter, D.A. Cooper, M.A. Fischl, J.M. Gatell, B.G. Gazzard, S.M. Hammer, M.S. Hirsch, D.M. Jacobsen, D.A. Katzenstein, J.S. Montaner, D.D. Richman, M.S. Saag, M. Schechter, R.T. Schooley, M.A. Thompson, S. Vella, P.G. Yeni, P.A. Volberding, *JAMA* 283 (2000) 381.
- [10] M.A. Fischl, D.D. Richman, D.M. Causey, M.H. Grieco, Y. Bryson, D. Mildvan, O.L. Laskin, J.E. Groopman, P.A. Volberding, R.T. Schooley, et al., *JAMA* 262 (1989) 2405.
- [11] J.E. Reardon, W.H. Miller, *J. Biol. Chem.* 265 (1990) 20302.
- [12] A.C. Collier, S. Bozzette, R.W. Coombs, D.M. Causey, D.A. Schoenfeld, S.A. Specator, C.B. Pettinelli, G. Davies, D.D. Richman, J.M. Leedom, et al., *N. Engl. J. Med.* 323 (1990) 1015.
- [13] M.G. Spiga, D.A. Weidner, C. Trentesaux, R.D. LeBoeuf, J.P. Sommadossi, *Antiviral Res.* 44 (1999) 167.
- [14] D.D. Richman, M.A. Fischl, M.H. Grieco, M.S. Gottlieb, P.A. Volberding, O.L. Laskin, J.M. Leedom, J.E. Groopman, D. Mildvan, M.S. Hirsch, et al., *N. Engl. J. Med.* 317 (1987) 192.
- [15] B.I. Hernandez-Santiago, A. Obikhod, E. Fromentin, S.J. Hurwitz, R.F. Schinazi, *Antivir. Chem. Chemother.* 18 (2007) 343.
- [16] K.L. White, N.A. Margot, T. Wrinn, C.J. Petropoulos, M.D. Miller, L.K. Naeger, *Antimicrob. Agents Chemother.* 46 (2002) 3437.
- [17] H.Z. Bazmi, J.L. Hammond, S.C. Cavalcanti, C.K. Chu, R.F. Schinazi, J.W. Mellors, *Antimicrob. Agents Chemother.* 44 (2000) 1783.
- [18] U.M. Parikh, D.L. Koontz, C.K. Chu, R.F. Schinazi, J.W. Mellors, *Antimicrob. Agents Chemother.* 49 (2005) 1139.
- [19] S. Compain, D. Schlemmer, M. Levi, A. Pruvost, C. Goujard, J. Grassi, H. Benech, *J. Mass Spectrom.* 40 (2005) 9.
- [20] J.L. Wiesner, F.C. Sutherland, M.J. Smit, G.H. van Essen, H.K. Hundt, K.J. Swart, A.F. Hundt, *J. Chromatogr. B: Analyt. Technol. Biomed. Life Sci.* 773 (2002) 129.
- [21] A. Volosov, C. Alexander, L. Ting, S.J. Soldin, *Clin. Biochem.* 35 (2002) 99.
- [22] A. Loregian, M.C. Scarpa, S. Pagni, S.G. Parisi, G. Palu, *J. Chromatogr. B: Analyt. Technol. Biomed. Life Sci.* 856 (2007) 358.
- [23] V. Bezy, P. Morin, P. Couerbe, G. Leleu, L. Agrofoglio, *J. Chromatogr. B: Analyt. Technol. Biomed. Life Sci.* 821 (2005) 132.
- [24] K.B. Kenney, S.A. Wring, R.M. Carr, G.N. Wells, J.A. Dunn, *J. Pharm. Biomed. Anal.* 22 (2000) 967.
- [25] A.K. Gehrig, G. Mikus, W.E. Haefeli, J. Burhenne, *Rapid Commun. Mass Spectrom.* 21 (2007) 2704.
- [26] B.L. Robbins, P.A. Poston, E.F. Neal, C. Slaughter, J.H. Rodman, *J. Chromatogr. B: Analyt. Technol. Biomed. Life Sci.* 850 (2007) 310.
- [27] C. Estrela Rde, M.C. Salvadori, G. Suarez-Kurtz, *Rapid Commun. Mass Spectrom.* 18 (2004) 1147.
- [28] J.F. Marier, M. Dimarco, R. Guilbaud, C. Dodard, G. Morelli, S.K. Tippabhotla, A.K. Singla, N.R. Thudi, T. Monif, *J. Clin. Pharmacol.* 47 (2007) 1381.
- [29] A.C. Cremieux, C. Katlama, C. Gillotin, D. Demarles, G.J. Yuen, F. Raffi, *Pharmacotherapy* 21 (2001) 424.
- [30] H. Chen, R.F. Schinazi, P. Rajagopalan, Z. Gao, C.K. Chu, H.M. McClure, F.D. Boudinot, *AIDS Res. Hum. Retroviruses* 15 (1999) 1625.
- [31] K.L. Rapp, M. Ruckstuhl, R.F. Schinazi, *Antivir. Ther.* 12 (2007) S130 (Abstract 117).
- [32] G. Asif, S.J. Hurwitz, P.M. Tarnish, R.L. Murphy, R.F. Schinazi, HIV DART 2008, Puerto Rico, December 9–12, 2008, p. 78 (Abstract 71).
- [33] L.H. Wang, J.W. Bigley, M. Brosnan-Cook, N.D. Sista, F. Rousseau and the DAPD-101 Clinical Trial Group, Conference of Retroviruses and Opportunistic Infections, Chicago, IL, February 4–8, 2001, Abstract 752, www.retroconference.org/2001.
- [34] R.L. Murphy, C. Zala, C. Ochoa, P.M. Tharnish, J. Mathew, E. Fromentin, G. Asif, S.J. Hurwitz, N.M. Kivel, R.F. Schinazi, Conference of Retroviruses and Opportunistic Infections, Boston, MA, February 3–6, 2008, p. 360 (Abstract 794).

Summary

Our laboratory is specialized in drug discovery and development, more specifically in nucleoside analogue research as potential antiviral agents. The laboratory is organized in several teams, including, chemists, virologists, molecular biologists and pharmacologists. The pharmacologists study the metabolism of both FDA approved and new drugs *in vitro* and in humans. amdoxovir™ is in development in our laboratory as anti-human immunodeficiency virus (HIV) and is in phase I/II clinical trial. The analytical team studies antiviral agents from cell culture work to clinical trials. To accomplish this goal, we used high performance liquid chromatography tandem mass spectrometry, which is sensitive and specific enough to detect analytes in the ppb range, in a complex biological matrix.

Since only the triphosphate forms of the nucleoside analogues are active intracellularly, it was necessary to develop a method to analyze these polar compounds. The method, presented in the first chapter, was successfully used for the simultaneous quantification of the nucleotide (phosphate forms) metabolites of approved nucleoside, amdoxovir as well as for endogenous natural nucleotides in human lymphocytes and macrophages. The limits of quantification were low enough to measure nucleotide levels in the ppb range.

In the second chapter, we extended our knowledge on amdoxovir metabolism in primary human lymphocytes cells. To do so, we incubated amdoxovir with nucleosides susceptible of inhibiting its phosphorylation. Then, we established the lack of interaction between amdoxovir and three other nucleosides analogues. Finally, deeper studies on endogenous natural nucleotides provided an understanding of the antiviral synergistic effects between amdoxovir and zidovudine that was demonstrated *in vitro* and in humans.

The development and validation of a methodology to quantify amdoxovir, its metabolite and the approved drug zidovudine in plasma is presented in the first chapter. This method was applied to a proof-of-concept study conducted in 24 HIV-infected individuals.

Résumé

Notre laboratoire, Laboratory of Biochemical Pharmacology (LOBP), dirigé par Dr R.F. Schinazi, est spécialisé dans la recherche sur les nucléosides analogues et plus particulièrement les inhibiteurs de la transcriptase inverse. Au sein de ce laboratoire, l'équipe de pharmacologie a pour rôle d'étudier le métabolisme des molécules en développement ainsi que des molécules déjà commercialisées dans des cellules humaines en culture. Les résultats obtenus guident les chimistes vers une synthèse de composés plus actifs et moins toxiques. Pour les molécules les plus avancées, comme l'amdoxovir™, les études réalisées au laboratoire relèvent du stade II d'essai clinique. Le rôle de l'équipe analytique est de réaliser toutes les mesures liées aux essais cliniques et cellulaires. Pour cela, nous avons choisi d'utiliser des instruments permettant des mesures spécifiques avec une sensibilité suffisante pour mesurer des quantités de l'ordre du ppb. Notre choix s'est donc porté sur la chromatographie haute performance en phase liquide couplée à un spectromètre de masse de type triple quadrupôle.

Puisque seuls les métabolites phosphorylés des nucléosides analogues sont actifs dans les cellules, il fut nécessaire de développer une méthode pour analyser ces composés polaires. Cette méthode, présentée dans le premier chapitre, permet l'analyse simultanée de la plupart des métabolites de nucléosides analogues commercialisés, ceux de l'amdoxovir et des nucléotides naturels présents dans les cellules. Les limites de détections sont telles que de très faibles niveaux de triphosphates ont pu être quantifiés dans les macrophages. Ces résultats sont présentés à la fin du second chapitre.

Dans le deuxième chapitre, nous avons voulu approfondir nos connaissances sur le métabolisme de l'amdoxovir dans les lymphocytes. Pour cela, nous avons testé l'amdoxovir en présence de nucléosides susceptible d'inhiber sa phosphorylation. Puis nous avons établi l'absence d'interaction directe entre l'amdoxovir et trois autres nucléosides analogues commercialisés. Finalement, des études plus poussées sur les nucléotides naturels donnent une indication pour expliquer les effets synergiques entre l'amdoxovir et la zidovudine.

Dans le dernier chapitre, nous présentons le développement et la validation d'une méthodologie permettant de mesurer simultanément les niveaux d'amdoxovir, de son métabolite principal et de la zidovudine dans des échantillons de plasma humain. Cette méthode a été appliquée à une étude clinique dont les résultats sont brièvement décrits.

Key Words: Nucleosides, nucleotides, HIV, liquid chromatography, mass spectrometry, lymphocytes, macrophages, pharmacokinetic

Mots Clés: Nucléosides, nucléotides, VIH, chromatographie en phase liquide, spectrométrie de masse, lymphocytes, macrophages, pharmacocinétique